Numerieke studie van rookafvoer
bij brand in grote complexe gebouwen

Numerical Study on Fire Smoke Extraction
in Large Complex Buildings

Nele Tilley

Promotor: prof. dr. ir. B. Merci
Proefschrift ingediend tot het behalen van de graad van
Doctor in de Ingenieurswetenschappen: Werktuigkunde-Elektrotechniek

Vakgroep Mechanica van Stroming, Warmte en Verbranding
Voorzitter: prof. dr. ir. J. Vierendeels
Faculteit Ingenieurswetenschappen en Architectuur
Academiejaar 2011 - 2012

UNIVERSITEIT
GENT

ISBN 978-90-8578-463-0
NUR 978
Wettelijk depot: D/2011/10.500/67

Supervisor

Prof. dr. ir. Bart Merci

Research facility

Department of Flow, Heat and Combustion Mechanics
Ghent University
Sint-Pietersnieuwstraat 41
B – 9000 Gent
Belgium

Members of the exam committee:

dr. ir.-arch. Emmanuel Annerel
Ghent University

ir. Christian Gryspeert
Brandweervereniging Vlaanderen

prof. Bart Merci
supervisor
Ghent University

dr. ir. Pieter Rauwoens
Ghent University

prof. Arnaud Trouvé
University of Maryland

prof. Rik Van de Walle
chairman
Ghent University

prof. Jan Vierendeels
secretary
Ghent University

prof. Stephen Welch
The University *of* Edinburgh

The research presented in this dissertation was supported by a Ph.D grant of the Institute for the Promotion of Innovation through Science and Technology in Flanders (IWT-Vlaanderen).

Preface

First and above all I want to thank my supervisor, Prof. Bart Merci, to give me the opportunity to start this Ph.D and to keep on encouraging my work.

Beside my supervisor, I want to thank everyone who stood beside me while making this Ph.D: my family at home, colleagues at work and other friends everywhere.
They have always been a great support for me for personal and work-related issues, they encouraged me never to give up, were always available when I needed them, showed interest in the work I was doing and never stopped believing in me.
But also, they have all been there for the distractions I needed, to put countless numbers of smiles on my face, discuss the most pointless topics and just to have a great time.

Many thanks to all of you, not only for being there when I needed it, but also for making me who I am today.

Dank je wel iedereen, om er voor mij te zijn wanneer ik het nodig had, en voor alles wat jullie voor mij al betekend hebben.

Nele

Summary

In modern architecture, large and open spaces are often included in buildings that are developed to be used by a large number of occupants, like shopping malls, hotels, office buildings,… When a fire occurs in such a building, the smoke is able to travel over long distances, unhindered by any compartmentation. However, fire safety in such a space can be designed in such a way that the smoke is not allowed to spread throughout the entire space, causing a harmful environment for the building occupants. Therefore, smoke and heat exhaust ventilation systems are a common type of fire safety measure to prevent smoke spread in large open spaces inside these complex buildings. The present study focuses on smoke extraction in large closed car parks and atria.

As computer power still keeps on increasing and reliable models have been developed in the past for fire and smoke modelling, the approach in the present study is to use numerical simulations as so-called 'numerical experiments'. This way, possible effects of the different numerically studied parameter variations can be discovered in a relatively cheap way.

However, before using the numerical simulations, their validity for the configurations at hand needs to be studied. The N-percent rule is introduced as a reliable criterion to define the smoke layer interface in the simulations. Good agreement is shown between reduced-scale experiments from literature and numerical simulations, performed with the program Fire Dynamics Simulator. Both in the atrium and tunnel configuration, the trends of the required ventilation parameters are well predicted in the simulations. Thus, confidence exists to use numerical

simulations as ‘numerical experiments’ in similar smoke flow configurations.

Smoke extraction in car parks can thus be studied with the same modelling program. Limitation is made to car parks with a flat ceiling, centrally placed car fire and a uni-directional smoke flow pattern. Four parameters are varied in the car park: the fire heat release rate per unit area, fire source area, car park height and car park width. Three formulae are developed based on this parameter variation. The first formula defines the relation between he critical inlet velocity in the car park and the four varied parameters. This critical ventilation velocity is defined as the minimum required velocity for all smoke to flow in the downstream direction of the fire, i.e. for all the smoke to stay at the same side of the fire. The difference between inlet and outlet velocity due to the heat inserted into the smoke is theoretically derived based on fire dynamics theory as a second formula. This theoretically derived relation is confirmed by all simulations. When smoke backlayering (smoke movement in the upstream direction) in the car park is allowed, a quantification is made as a third formula for the difference between critical and actual ventilation velocity corresponding to a certain backlayering distance. Comparison with full-scale experiments shows good agreement with the suggested formulae.

In the atrium configuration, a 2D adhered spill plume is studied with the origin of the fire in a room adjacent to the atrium. First, scaling of experimental and numerical setups from reduced-scale to full-scale is discussed. Scaling based on Froude number alone is confirmed to be allowed as long as the flow is sufficiently turbulent, i.e. the Reynolds number is sufficiently high.
As this turbulence requirement is fulfilled in the reduced-scale atrium setup simulations, the parameter variation can be performed in this configuration. Smoke extraction at the ceiling of the atrium is studied. When the extraction mass flow rate is increased beyond a certain threshold value, a multi-dimensional effect is noted in the atrium. This

multi-dimensional effect relates to a downward smoke flow movement and resulting vortex at the opposite atrium side from the rising smoke plume caused by the horizontal momentum of the ceiling jet in the atrium. As a result, the interface height of the smoke layer in the atrium varies with horizontal position. This effect had not been quantified yet as it only appears beyond the range of extraction rates studied in experiments before.

By performing a parameter variation of the fire heat release rate and the dimensions of the atrium (atrium width at the spill edge, atrium height above the spill edge and atrium length), a formula is proposed for extraction mass flow rate in the atrium necessary to obtain a certain average smoke free height in case of a multi-dimensional atrium smoke layer. The threshold value for the transition from a one-dimensional to a multi-dimensional smoke layer is presented.

A variation study of ventilation parameters – size and position of makeup air inlet opening and position of smoke extraction outlet – is performed starting from a basic configuration setup. The variation of the position of inlet and outlet shows no significant effect on the smoke layer pattern in the atrium, especially considering the fact that the origin of the fire usually cannot be predicted, making it impossible to ensure the best location of the ventilation system in the design beforehand. The size of the makeup air inlet opening, however, has a large influence on the smoke layer pattern in the atrium. It appears that when the inlet opening is not large enough, the high velocity of the incoming air will cause a major disturbance of the smoke flow field in the atrium, resulting in a reduced performance of the smoke extraction system. It is thus important in atrium design to ensure sufficiently large makeup air inlet openings.

To summarise, formulae are developed for the design of the smoke extraction system in two large, complex configurations. Both a car park configuration with flat ceiling, centrally placed car fire and uni-directional smoke flow pattern; and the 2D adhered spill plume in an atrium configuration are studied.

Samenvatting

Volgens de hedendaagse architectuur bevatten gebouwen die bedoeld zijn voor een groot aantal aanwezigen vaak grote open ruimtes. Winkelcentra, hotels of kantoorgebouwen zijn daar typische voorbeelden van. Wanneer brand uitbreekt in een dergelijk gebouw, kan de rook zich over een grote afstand verspreiden, door geen enkele vorm van compartimentering gehinderd. De brandveiligheid van een dergelijke ruimte kan ontworpen worden op een zodanige manier dat de rook wel verhinderd wordt om zich door de hele ruimte te verspreiden. Op die manier wordt een schadelijke omgeving voor de aanwezigen vermeden. Om hieraan tegemoet te komen, zijn rook en warmteafvoersystemen een veel gebruikte maatregel om rookverspreiding doorheen grote open ruimtes te verhinderen in dergelijke complexe gebouwen. Deze studie richt zich op mechanische rookafvoer in grote gesloten parkeergarages en atria.

Omdat de huidige computerkracht steeds toeneemt en in het verleden reeds betrouwbare modellen zijn ontwikkeld voor het modelleren van brand en rook, wordt in deze studie daarvan gebruik gemaakt. Numerieke simulaties worden daarbij als zogenoemde 'numerieke experimenten' gebruikt. Zo kunnen mogelijke effecten van de numeriek bestudeerde parametervariaties op relatief goedkope manier gevonden worden.

Voordat de numerieke simulaties gebruikt kunnen worden, moet eerst hun geschiktheid aangetoond worden voor de bestudeerde configuraties. De N-percent regel wordt vooropgesteld als een betrouwbaar criterium om de grens van de rooklaag te bepalen in de

simulaties. Goede overeenkomst wordt aangetoond tussen de kleinschalige experimenten uit de literatuur en de numerieke simulaties die uitgevoerd worden in het programma Fire Dynamics Simulator. Zowel voor een atrium als voor een tunnel, worden de trends van de ventilatieparameters goed voorspeld in de simulaties. Daaruit volgt het vertrouwen om de numerieke simulaties te gebruiken als 'numerieke experimenten' in configuraties met een gelijkaardige rookbeweging.

Rookafvoer in parkeergarages kan dus bestudeerd worden met hetzelfde simulatieprogramma. De studie wordt beperkt tot parkeergarages met vlak plafond, waarbij de brand in het midden van de garage is geplaatst en een uni-directioneel patroon van de rooklaag aanwezig is. Vier parameters worden gevarieerd in de parkeergarage: het brandvermogen per eenheid oppervlakte, de oppervlakte van de brand en de hoogte en breedte van de parkeergarage. Drie formules worden ontwikkeld, gebaseerd op deze parametervariatie. De eerste formule definieert het verband tussen de kritische inlaatsnelheid in de parkeergarage en de vier bestudeerde parameters. Deze kritische ventilatiesnelheid is gedefinieerd als de minimaal nodige snelheid die ervoor zorgt dat alle rook in de stroomafwaartse richting van de brand blijft. Het verschil tussen inlaat- en uitlaatsnelheid dat veroorzaakt wordt door de warmte die door de rook wordt opgenomen, wordt theoretisch afgeleid op basis van branddynamica als tweede ontwikkelde formule. Dit theoretisch afgeleide verband wordt bevestigd in alle simulaties. Wanneer backlayering van de rook toegelaten is in de parkeergarage (beweging van de rook in de stroomopwaartse richting), wordt een verband tussen kritische en benodigde snelheid voor een zekere backlayering afstand vooropgesteld als derde formule. Goede overeenkomst tussen de opgestelde formules en grootschalige experimenten wordt aangetoond.

In de atriumconfiguratie wordt de 2D aangehechte rookpluim bestudeerd waarbij de brand zich in een aanpalende kamer van het atrium bevindt. Eerst wordt het opschalen van zowel numerieke als

experimentele kleinschalige tot grootschalige opstellingen besproken. Opschalen gebaseerd op enkel Froudegetal is toegestaan zolang de stroming voldoende turbulent is, namelijk wanneer het Reynoldsgetal voldoende hoog is.

Omdat deze voorwaarde voor turbulentie vervuld is in de simulaties van de kleinschalige atriumconfiguratie, kan de parameterstudie in deze opstelling uitgevoerd worden. Daarin wordt tookafvoer in het plafond van het atrium bestudeerd. Wanneer het extractie-massadebiet stijgt boven een bepaalde drempelwaarde, wordt een multidimensionaal effect opgemerkt in het atrium. Dit multidimensionaal effect gaat gepaard met een neerwaartse rookbeweging en resulterende wervel in het atrium aan de overzijde van de stijgende rookpluim en wordt veroorzaakt door de horizontale impuls van de *ceiling jet* in het atrium. De rookvrije hoogte onder de rooklaag in het atrium zal als gevolg daarvan veranderen met horizontale positie. Dit effect is nog niet eerder gekwantificeerd aangezien het zich pas manifesteert bij een extractiedebiet groter dan de eerder in experimenten bestudeerde debieten.

Door het uitvoeren van een parametervariatie van het brandvermogen en de afmetingen van het atrium (breedte van het atrium aan de *spill edge*, hoogte van het atrium boven de *spill edge* en lengte van het atrium) kan een formule voorgesteld worden voor extractiedebiet in het atrium. Het nodige massadebiet om een bepaalde gemiddelde vrije rooklaaghoogte te voorzien in het geval van een multidimensionale rooklaag kan hiermee berekend worden. De drempelwaarde voor de overgang van ééndimensionale naar multidimensionale rooklaag wordt voorgesteld.

Een studie van de variatie van bepaalde ventilatieparameters – grootte en positie van de opening voor inkomende lucht en positie van de extractie uitlaat – wordt uitgevoerd startende van een basisconfiguratie. De variatie van de positie van zowel uitlaat als inlaat vertoont geen significant effect op de rooklaag in het atrium, voornamelijk omdat de exacte positie van de brand niet voorspeld kan worden, waardoor het onmogelijk is de beste locatie voor rookafvoer te voorzien in het

ontwerp van het atrium. De grootte van de inlaatopening voor toegevoerde lucht heeft echter wel een grote invloed op de vorm van de rooklaag in het atrium. Uit de studie blijkt dat wanneer de inlaatopening niet groot genoeg is, de grote snelheid van de inkomende lucht een behoorlijke verstoring van het stromingsveld van de rook in het atrium veroorzaakt, waardoor het rookafvoersysteem niet meer voldoende zal presteren. Het is dus van belang om in het atriumontwerp te verzekeren dat de inlaatopeningen voor toevoer van lucht voldoende groot zijn.

Samengevat werden formules ontwikkeld voor het dimensioneren van het rookafvoersysteem in twee grote complexe configuraties. Zowel studie van grote gesloten parkeergarages met vlak plafond, centraal geplaatste brandhaard en uni-directioneel patroon van de rooklaag; als een 2D aangehechte rookpluim configuratie in een atrium, is uitgevoerd.

Contents

Preface v
Summary ix
Samenvatting xiii
Contents xvii
List of Figures xix
List of Tables xxiii
List of Symbols xxv
Chapter 1 Introduction 1
1.1 Context 1
1.2 Considerations 2
1.3 Research goal 3
1.4 Outline 3
Chapter 2 Fire dynamics and fire modelling 5
2.1 Fire, smoke and fire safety engineering 5
2.2 Fire dynamics 9
2.3 Fire and smoke modelling 14
2.4 CFD modelling 16
2.5 References 19
Chapter 3 Literature review 21
3.1 Car parks 21
3.2 Atria 27
3.3 References 35
Chapter 4 Confirmation of the validity of small-scale simulation results 39
4.1 Introduction 39
4.2 Atrium 40
4.3 Tunnel 51

4.4 Conclusions 58
4.5 References 59
Chapter 5 Smoke extraction in closed car parks 61
5.1 Introduction 61
5.2 Setup of the simulations 65
5.3 Results 69
5.4 Range of validity 83
5.5 Comparison with large scale experiments 84
5.6 Conclusion 87
5.7 References 89
Chapter 6 Extrapolation of data from reduced-scale set-ups to full-scale atria 91
6.1 Introduction 91
6.2 Governing equations – scaling laws 93
6.3 Results 98
6.4 Conclusion 105
6.5 References 106
Chapter 7 Smoke extraction in atria, the 2D adhered spill plume 107
7.1 Introduction and setup 107
7.2 Basic configuration and multi-dimensional smoke layer 111
7.3 Variation of fire and atrium configuration 114
7.4 Variation of ventilation parameters 127
7.5 Conclusion 138
7.6 References 140
Chapter 8 Conclusions 141
Chapter 9 Recommendations for future work 145
References 147

List of Figures

Figure 2.1 Mass flow, temperature and velocity in the ideal plume. 7
Figure 2.2 The ceiling jet. 8
Figure 2.3 Representation of zone modelling. 15
Figure 2.4 Representation of field modelling. 16
Figure 2.5 RANS, LES and DNS modelling of turbulence 18

Figure 3.1 Car park configuration. 22
Figure 3.2 Backlayering in a car park. 22
Figure 3.3 Fire in an adjacent room to an atrium: spill edge, downstand and balcony. 27
Figure 3.4 Adhered and free spill plumes. 28
Figure 3.5 Two- and three-dimensional spill plumes. 29
Figure 3.6 Smoke and heat extraction system in an atrium. 30

Figure 4.1 Atrium configuration. 41
Figure 4.2 Temperature variation on a vertical line (x = 3.75 m) in the atrium. 44
Figure 4.3 Second derivative of temperature in the atrium (left) and N-percent rule in atrium (right). 46
Figure 4.4 Interface height in the atrium. 47
Figure 4.5 Experimental and CFD results of smoke mass flow extraction rate as function of rise height. 50
Figure 4.6 Comparison of FDS 4 and FDS 5 numerical results with experiments. 51
Figure 4.7 Extrapolation to determine critical velocity in tunnel D with heat release rate 22.5 kW (with standard FDS radiation modelling). 53
Figure 4.8 Experimental and numerical results for v_{cr} in tunnel D. The squares represent the possible effect of heat loss in the experiments by cooling of the ceiling near the fire. 56

Figure 5.1 Difference in aspect ratios between tunnels ($w \approx h < l$) and car parks ($h < w, l$). 62
Figure 5.2 Principle of critical horizontal velocity in a car park..... 62
Figure 5.3 Grid refinement in car park: temperatures at z = 2.3 m. Cell sizes in [cm x cm x cm]. 67
Figure 5.4 Grid refinement in car park: temperatures at x = 8 m. Cell sizes in [cm x cm x cm]. 68
Figure 5.5 Backlayering distance variation with the value of N in the N-percent rule on centerline temperature data..... 70
Figure 5.6 Linear extrapolation of backlayering distance to calculate the critical inlet velocity..... 71
Figure 5.7 Critical inlet velocity with variable convective heat release rate per unit area..... 72
Figure 5.8 Critical inlet velocity with variable fire source area..... 73
Figure 5.9 Critical inlet velocity with variable car park width..... 73
Figure 5.10 Critical inlet velocity with variable height difference between fire source area and ceiling..... 75
Figure 5.11 Critical inlet velocity with variable car park height..... 76
Figure 5.12 Critical inlet velocity from simulations and from Eq. (5.6)..... 77
Figure 5.13 Difference between outlet and inlet velocity from Eq. (5.10) and as obtained from the simulations. 79
Figure 5.14 Relation between backlayering distance and ventilation velocity: factor *a*..... 80
Figure 5.15 V-shaped smoke pattern in a top view of the car park near critical ventilation conditions..... 82
Figure 5.16 Effect of difference in inlet opening configuration on the smoke pattern in a car park..... 83
Figure 5.17 Effect of difference in inlet opening configuration on the smoke pattern in a car park..... 85
Figure 5.18 Extrapolation (—) of measured temperatures (•) to the interface temperature (--) for estimation of the backlayering distance..... 87

Figure 6.1 Schematic representation of smoke filling in an atrium configuration (fire in adjacent room). 91
Figure 6.2 Averaged temperature fields in the vertical symmetry plane at corresponding times of simulations 1-6..... 102
Figure 6.3 Temperature simulation data on a vertical line in the atrium. 103

Figure 6.4 Averaged temperature fields between t = 141 s – 162 s of simulations 7, 8, 1 and 3. Ordering from left to right: laminar → turbulent. 104
Figure 6.5 Temperature simulation data on a vertical line in the atrium. 104

Figure 7.1 Atrium and adhered spill plume, basic configuration. 108
Figure 7.2 Confirmation of the validity of the coarser-grid simulations.....109
Figure 7.3. One-dimensional (left) versus multi-dimensional (right) smoke layer pattern in atrium. Temperature fields at y = 0.45 m, time-averaged quasi steady-state data for 20s. 112
Figure 7.4 Basic configuration simulation results. 113
Figure 7.5 Simulation results for heat release rate variation: $\dot{Q}_{conv} = 5.4\,\text{kW}$ ...114
Figure 7.6 Simulation results for heat release rate variation: $\dot{Q}_{conv} = 8.8$ kW . 115
Figure 7.7 Variation of outlet extraction area: simulation results.....116
Figure 7.8 Natural ventilation in atrium: simulation results. 117
Figure 7.9 Mass flow rate and outlet velocity for natural ventilation in atrium. 118
Figure 7.10 Simulation results for the variation of width: W_s = 0.6 m.....118
Figure 7.11 Simulation results for the variation of width: W_s = 0.75 m. 119
Figure 7.12 Simulation results for the variation of width: W_s = 1.2 m.....119
Figure 7.13 Simulation results for $\dot{Q}_{conv} = 5.377\,\text{kW}$ and W_s = 0.6 m.....120
Figure 7.14 Simulation results for the variation of height: H_s = 2.4 m.....121
Figure 7.15 Simulation results for the variation of height: H_s = 4.2 m.....121
Figure 7.16 Simulation results for the variation of height: H_s = 5.4 m.....122
Figure 7.17 Simulation results for the variation of length: L_a = 1.25 m. 123
Figure 7.18 Simulation results for the variation of length: L_a = 2 m.....123
Figure 7.19 Simulation results for the variation of length: L_a = 3 m.....124
Figure 7.20 Simulation results for the variation of length: L_a = 3.75 m. 124
Figure 7.21 Smoke free height above spill edge from Eq. (7.16) and as obtained from the simulations. 127
Figure 7.22 Extraction outlet position. 128
Figure 7.23 Simulation results of left-hand-side positioned outlet.....129
Figure 7.24 Simulation results of right-hand-side positioned outlet. 130
Figure 7.25 Position of the makeup air inlet openings. 131
Figure 7.26 Simulation results for inlet opening B+C. 132
Figure 7.27 Repetition of Fig. 7.4: Basic configuration simulation results. 132
Figure 7.28 Simulation results for inlet opening B.....133

Figure 7.29 Average temperature field between t = 80 s and t = 100 s in plane x = 2.5 m for only inlet opening B present. 134
Figure 7.30 Simulation results for inlet opening A+B+C 134
Figure 7.31 Simulation results for inlet opening height h_o = 1.5 m. 135
Figure 7.32 Simulation results for inlet opening height h_o = 1.0 m. 136
Figure 7.33 Simulation results for inlet opening height h_o = 0.6 m. 136
Figure 7.34 Simulation results for inlet opening height h_o = 0.3 m. 137
Figure 7.35 Temperature fields and flow patterns at y = 0.45 m in atrium. Time-averaged quasi steady-state data for 20 s. 138

List of Tables

Table 4.1 Begin (t_1) and end (t_2) times for the calculation of time-averaged simulation results. 44
Table 4.2 Simulation results in the small-scale atrium. 49
Table 4.3 Critical velocities with corresponding heat release rates (default settings, χ_r obtained from simulations). 54
Table 4.4 Critical velocities with corresponding heat release rates (adiabatic simulations, χ_r = 0.43 assumed for calculation of $\dot{Q}$) 55
Table 4.5 Maximum temperatures near the ceiling found in the numerical simulations. 57

Table 5.1 Variation limits of the four parameters. 66
Table 5.2 Experimental input data. 86
Table 5.3 Backlayering distances from experiments and simulations. 86

Table 6.1 Important dimensionless numbers in the eight simulations. Scaling factor a = 9. 100
Table 6.2 Scaling of the imposed parameters in the eight simulations. Scaling factor a = 9. 101
Table 6.3 Initial values of the imposed parameters in 'basic' simulation 1. 101
Table 6.4 Numbering and specific features of all eight performed simulations. 101

List of Symbols

A	area	m^2
a	factor in backlayering distance formula	s
A_F	fire source area	m^2
b	balcony length	m
C	coefficient in spill plume relation	$kg/(m.s.kW^{1/3})$
C_m	coefficient in spill plume relation	$m^{4/3}/(s.kW^{1/3})$
c_p	heat capacity	kJ/kg K
C_s	Smagorinsky constant	–
d	backlayering distance	m
D	mass diffusivity	m^2/s
D^*	characteristic length scale	m
D_F	fire source diameter	m
D_H	hydraulic diameter	m
d_s	thickness of emerging smoke layer	m
g	gravitational acceleration	m/s^2
h	car park height	m
h	convection coefficient	W/m^2K
H_a	atrium height above the floor	m
h_o	height of makeup air inlet opening	m
H_R	compartment height	m
h_s	sensible enthalpy	J/kg
H_s	atrium height above the spill edge	m
I_b	radiation intensity source term	kW/m^2
k	thermal conductivity	W/(m.K)
k	turbulent kinetic energy	m^2/s^2
K_g	grade correction factor	–

L	length scale	m
l	car park length	m
L_a	length of atrium	m
l_F	flame length	m
$\dot{m}$	mass flow rate	kg/s
$\dot{m}_s$	emerging mass flow rate at spill edge	kg/s
M_w	molecular weight	g/mol
N	value in N-percent rule	–
p	pressure	Pa
$\dot{q}''$	heat release rate per unit area	kW/m^2
$\dot{q}'''$	heat release rate per unit volume	W/m^3
$\dot{Q}$	fire heat release rate	kW
$\dot{Q}''$	dimensionless form of heat release rate	–
$\dot{Q}^*$	dimensionless form of heat release rate	–
r	distance from fire plume axis	m
S	rate of strain	1/s
T	temperature	K
t	time	s
$T_{av,s}$	average temperature of the smoke layer	K
T_f	temperature of hot gases	K
T_l	minimum temperature on vertical line	K
u	velocity	m/s
v	velocity	m/s
V''	dimensionless form of velocity	–
V^*	dimensionless form of velocity	–
$\dot{V}$	volume flow rate	m^3/s
w	car park width	m
W_a	atrium width	m
W_s	atrium width at the spill edge	m
x	distance in horizontal direction	m
Y	mass fraction	–
y	distance in horizontal direction	m

z	distance in vertical direction	m
z_o	virtual origin height	m
z_s	smoke free height above the spill edge	m
Δ	grid cell size	m
ΔH_c	heat of combustion	kJ/kg
χ	combustion efficiency	–
χ_r	radiative fraction	–
δ	Kronecker delta	–
ε	emissivity	–
ϕ	configuration factor	–
ν	kinematic viscosity	m^2/s
μ	dynamic viscosity	Pa s
ρ	density	kg/m^3
σ	Stefan-Boltzman constant	W/m^2K^4
τ	stress tensor	Pa

Species

C	soot
C_3H_8	propane
CO	carbon monoxide
CO_2	carbon dioxide
H_2O	water (vapour)
N_2	nitrogen
O_2	oxygen

Dimensionless numbers

Ec	Eckert
Eu	Euler
Fr	Froude
Pr	Prandtl
Ra	Rayleigh
Re	Reynolds
Sc	Schmidt

Abbreviations

1D	one-dimensional
2D	two-dimensional
3D	three-dimensional
CFD	Computational Fluid Dynamics
DNS	Direct Numerical Simulations
FDS	Fire Dynamics Simulator
HRR	heat release rate
LES	Large Eddy Simulations
NIST	National Institute of Standards and Technology
PUA	per unit area
RANS	Reynolds-Averaged Navier Stokes
SHC	Smoke and Heat Control

Subscripts

0	ambient conditions
cr	critical
cs	cross-sectional
F	fire
in	inlet (cold air)
int	interface
max	maximum
min	minimum
out	outlet (hot smoke)
ox	oxygen

Chapter 1
Introduction

1.1 Context

In modern building trends, a tendency exists to use available land as effectively as possible by placing high buildings, or build underground facilities. Especially facility buildings, like shopping malls, office buildings, hotels, museums or hospitals, often contain multiple storeys and / or underground areas like car parks or storage basements.

Although the available ground area is thus used very effectively, modern architecture likes to include large open spaces. An example of such an open space is an atrium inside a high-rise building, occupying multiple floors that are thus not entirely separated from each other.

When a fire occurs in such an open space, the smoke from the fire is thus not contained in a confined room and is able to spread within the building when no fire safety measures are present. In those types of buildings, compartmentation would not be an acceptable solution to prevent smoke spread, as it does not match with the architectural design. Therefore, smoke and heat extraction systems are usually installed in large complex buildings. Those systems extract smoke from the space. This way, the presence of smoke is limited to a specified zone and smoke spread is somehow prevented. The extraction system (partly) clears the space by means of one or more ventilators that actively extract the hot smoke from the building into the surroundings.

The present research focuses on smoke extraction in atria and car parks. Both are large complex buildings and contain a large open space without compartmentation that could contain the smoke or prevent it from spreading. Although the principle of extracting hot smoke is the same in both configurations, they essentially differ in design as smoke clearance is horizontal in car parks, while vertical in atria.

1.2 Considerations

Although such smoke extraction systems are already frequently installed in atrium and car park configurations, the design of these systems can still be improved.

In car parks, not so much research has been reported yet on the design of smoke extraction systems. A number of studies have been presented for tunnel ventilation, but this is quite different in nature from car park ventilation, as will be explained later in the present study. Present regulations in car parks are mostly based on limited research and rule-of-thumb values.

A larger number of studies report research on smoke extraction in atria. Most of these studies, however, concern a (large) set of reduced-scale experiments, and report a smoke extraction design calculation method from extrapolation of these experiments. However, only limited parameter variations are addressed in these studies, and they often present results for only a relatively small range of validity.

Therefore, a continuous need exists to study smoke extraction systems, both in car parks and atria. Extensive parameter variations need to be performed, to be able to account for the entire building configuration in designing the smoke and heat control system.

1.3 Research goal

In the present research, car park and atrium configurations are studied by performing simulations of the fire environment and smoke movement. The results of these simulations are used as so-called "numerical experiments" to derive and/or confirm existing semi-empirical equations for the design of the smoke and heat extraction ventilation system in both configurations.

By using simulations for parameter variation, the possibly interesting parameter combinations can be found in a relatively cheap way, so that afterwards these results can be coupled back to experimental research and these possibly important effects can be confirmed.

1.4 Outline

First, the validity of the simulations needs to be confirmed (Chapter 4). Afterwards, parameter variations are performed with the simulations, and derived formulae are constructed both for car parks (Chapter 5) and atria (Chapter 7). As the atrium results are based on reduced-scale configurations, the considerations to be taken into account in scaling the results are also discussed (Chapter 6).

2 Chapter 2
Fire dynamics and fire modelling

In this chapter, the principles of fire, smoke management and (performance-based) fire safety engineering are introduced, and some background on fire dynamics is provided. Fire modelling and the way it is used in the present study are explained. The models used in the research performed are presented.
Only some basic theory on fire science and fire modelling is introduced. The reader is referred to e.g. [1-3], for further reading on fire dynamics. More detail on heat and mass transfer is available in e.g. [4]. In e.g. [5-8], flow modelling and commonly used submodels are discussed in more detail.

2.1 Fire, smoke and fire safety engineering

Fire

The phenomenon of fire is a combination of physical and chemical processes, occurring in and around a fuel. The fuel can be solid, liquid or gaseous. While the combustion of the fuel is a chemical process, heat transfer from and to the fuel or flame and the flow mechanics of the fire smoke are physical processes.
Controlled fires are often used, both in domestic and industrial applications, for the generation of heat and power. However, uncontrolled fires can cause significant damage and lead to the loss of lives, goods and buildings.

Three elements are needed to create a fire. The so-called fire triangle says that fuel, oxygen and ignition need to be present at the same time – and in the correct form – to start a fire. After ignition, the fire can spread depending on oxygen and fuel availability.

Two types of fire are distinguished. In ventilation-controlled fires, a large amount of fuel is present, but only a limited amount of oxygen. The fire size will depend on the presence of oxygen. Fuel-controlled fires occur when a sufficient amount of oxygen is present, in which case the fire size depends on the availability of the fuel.

The present study deals with design fires. It is assumed that the fire has somehow ignited and that the heat release from the fire is equal to what can be expected to occur in the specific situation that is studied. Ignition and fire growth are not taken into account. The expected fire size is usually derived from experimental studies or from fire scene investigations.

Heat from the fire flames is transferred to the fuel and the surroundings. For the fires under consideration, it can be assumed that about 35% of the heat release rate from the fire is transferred to the walls of the configuration by radiative heat transfer. The remaining 65% is mostly convective heat, transferred from the fire to the smoke. Conductive heat transfer is only a very small portion of the fire heat release rate and is usually not considered.

Smoke

In the flames, a number of toxic and non-toxic gases are produced by the combustion chemistry. These are mainly H_2O, CO_2 and CO. Solid particles in the form of mainly soot are also produced. As these gases are hot, they will rise in the cold environment, entraining cold air. This way, fire smoke mainly consists of heated air (O_2 and N_2).

In an ideal fire plume, three regions are distinguished [9]:
- the continuous flame region, in the near field of the fire, where there is acceleration of the gases,
- the intermittent flame region, with intermittent flaming and
- the buoyant plume, where both velocity and temperature decrease with height.

The mass flow rate of the smoke plume will increase with height, as more air is entrained into the plume, and the plume temperature decreases (Fig. 2.1).

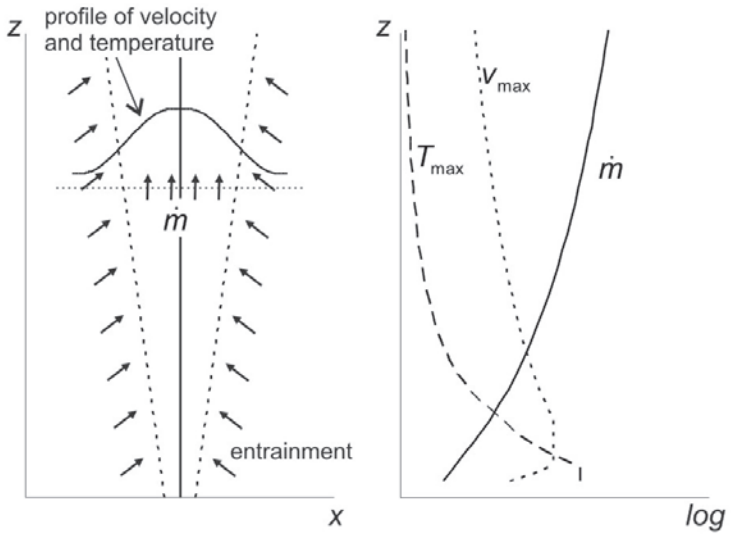

Figure 2.1 Mass flow, temperature and velocity in the ideal plume.

When the flow of the free plume is obstructed by the presence of a ceiling, a ceiling jet is created (Fig. 2.2). Underneath the ceiling, the smoke will flow radially outward from the fire plume axis, until again some obstruction or opening is met. The further away from the axis, the lower the velocity and temperature of the ceiling jet become. In the ceiling jet, almost no entrainment of air takes place.

When discussing the atrium configuration in Chapter 3, another type of plume – the spill plume – is introduced.

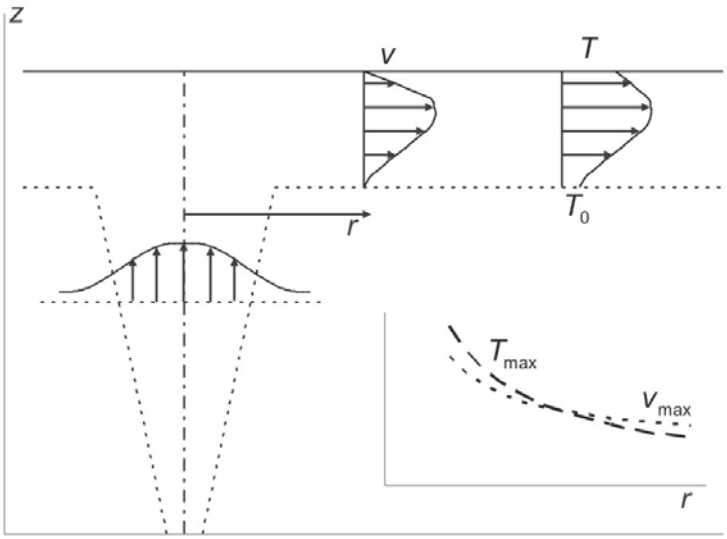

Figure 2.2 The ceiling jet.

Fire safety engineering

Fire safety engineering is an engineering discipline where the main focus is on fulfilling three goals:

- safety of occupants, both in protection (limiting temperatures and toxic gases) and in evacuation,
- safety of firemen, to ensure the safest possible conditions for their interaction,
- protection of structures, ensuring that buildings can still be used after occurrence of a fire.

Preventing as well as limiting and fighting of fires are part of the fire safety engineering strategy. The focus in the present study is on smoke and heat control systems, a form of active fire safety engineering, where the three goals are met by lowering inside temperatures and removing toxic gases by actively extracting smoke from (a part of) a building.

A recent form of fire safety engineering is performance-based design where design criteria are specified, rather than exact measures. The fire safety engineer's task in this kind of design is to ensure that the design criteria are met, but no specific ways to meet them are prescribed.

2.2 Fire dynamics

2.2.1 Fuel, combustion and heat release rate

Fuels can be in a solid, liquid or gaseous form. The density ρ of the fuel is the mass per unit volume. Fuels considered in the present study are of liquid or solid form. For such a fuel to be involved in the fire process, it has to be brought in gaseous form. Heating the fuel will result in evaporation (liquid) or pyrolysis (solid) of the fuel into gas. These combustible volatiles mix with air to form a flammable mixture.

Air consists of 21 vol% oxygen (O_2) and 79 vol% nitrogen (N_2). Thus, for every mol of O_2, 3.76 mol of N_2 is present in air. It is assumed to be an ideal gas, for which the ideal gas law states at constant pressure:

ρT = constant. (3.1)

The density of air at ambient temperature (T_0 = 293 K) is ρ_0 = 1.2 kg/m^3. Smoke – mainly consisting of air – is assumed to show the same behaviour and to have similar properties as air itself. The ideal gas law is therefore also assumed valid for hot smoke from a fire.

As smoke is assigned the same properties as air, the value of heat capacity can (for the present study) be assumed constant, independent of temperature within the range considered and equal to

c_p = 1 kJ/kg K. (3.2)

The heat release rate that is thus absorbed by smoke passing through an area is equal to

$$\dot{Q}_{conv} = \dot{m} c_p \Delta T \,, \quad (3.3)$$

where $\dot{m}$ is the mass flow rate of the smoke, and ΔT the temperature difference between the hot smoke passing through that area and the cold surroundings.

Combustion of the flammable gas mixture results in the formation of combustion products and the production of heat. For example, the stoichiometric oxidation equation for propane in air is:

$$C_3H_8 + 5\ O_2 + 5 \cdot 3.76\ N_2 \rightarrow 3\ CO_2 + 4\ H_2O + 18.8\ N_2. \quad (3.4)$$

Stoichiometry means that exactly enough oxygen is present for the available fuel to burn completely and to form only the combustion gases carbon dioxide (CO_2) and water vapour (H_2O). However, if the combustion is incomplete, other products will be also formed in the reaction. The oxidation equation for propane in oxygen that is used in the simulations presented in the following chapters is [10]:

$$C_3H_8 + 4.1285\ O_2 \rightarrow 2.0637\ CO_2 + 4\ H_2O + 0.1296\ CO + 0.8067\ C. \quad (3.5)$$

The heat of combustion of the volatiles (ΔH_c) is the energy that is released in the oxidation of a unit of mass or volume of the fuel. For propane, this heat of combustion has a value ΔH_c = 46 MJ/kg.
The produced heat release rate can thus be calculated as

$$\dot{Q} = \chi \dot{m}''_F A_F \Delta H_c , \quad (3.6)$$

with χ: a factor to account for incomplete combustion
A_F: the fuel surface area (m²)
$\dot{m}''_F$: the burning rate of the fuel (kg/(s m²))

However, another heat of combustion can be defined as the energy released per unit mass of oxygen in the oxidation reaction. For most common volatiles from hydrocarbon type fuels, this heat of combustion has a more or less constant value of $\Delta H_{c,ox} \approx 13$ MJ/kg(O_2) [11]. With this definition, the produced heat release rate is

$$\dot{Q} = \dot{m}_{ox} \Delta H_{c,ox} , \quad (3.7)$$

where $\dot{m}_{ox}$ (kg/s) denotes the consumed oxygen in the combustion process.

2.2.2 Heat transfer

The three basic mechanisms of heat transfer are conduction, convection and radiation. In fire, all three mechanisms occur.

Conduction

Although it also occurs in fluids, conduction is mainly known as heat transfer within solids, where the heat transfers from a hot to a cold zone. In fire situations, conduction heat transfer is mostly important within the fuel. As the fuel heats up, it can be ignited, and fire can spread along the fuel. As the present study focuses on design fires, the mechanism of conduction within the fuel is not considered here.

In the case of an enclosure fire, conduction occurs through the walls of the enclosure, where heat is transferred from the hot inner side of the wall to the cold outer side, thus losing heat of the fire to the surroundings.

Conductive heat transfer can be described as a heat flux, quantified by Fourier's Law, which in one direction is written as:

$$\dot{q}''_x = -k\frac{dT}{dx}, \tag{3.8}$$

where k is the thermal conductivity (W/m.K), dependent on material and temperature.

Convection

Heat transfer to or from a solid, where movement of the surrounding fluid is involved, is convective heat transfer. Exchange of heat takes place between the fluidum and the solid. When the fluid is heated up or cooled down, it starts to move due to buoyant forces (density difference).

Newton's relationship for convection states:

$$\dot{q}'' = h\Delta T\,. \tag{3.9}$$

In this relation, h (W/m^{2}K) is the convective heat transfer coefficient. Unlike thermal conductivity, it is not a material or fluidum property. The

convective heat transfer coefficient depends also on the system, geometry, the properties of the flow and fluid and the temperature difference.

Radiation

The third mechanism of heat transfer, radiation, differs from conduction and convection in the sense that no contact is needed between the source and the receiver of the heat transfer. Radiation is the transfer of energy by electromagnetic waves. Radiation from a flame is emitted mostly by soot particles in the flame. Radiative heat transfer will cause the fuel to heat up which is important in spread and growth of the fire. More important in the present research, however (as design fires are assumed and fire spread is not discussed) is the radiative heat transfer from the flames to the surroundings, heating up the walls of e.g. an enclosure.

By using the Stefan-Boltzmann equation for the energy emitted by a body, the intensity of radiant energy is found to be

$$\dot{q}'' = \phi\varepsilon\sigma\left(T^4 - T_0^4\right). \qquad (3.10)$$

Here, ϕ is the configuration factor, taking into account the geometrical relationship between the emitter and the receiver. ε is the emissivity of the surface and σ the Stefan-Boltzmann constant (σ = 5.67 10^{-8} W/m^2K^4). Radiative heat transfer thus scales with the fourth power of temperature.

As mentioned in paragraph 2.1, most fire design scenarios assume that 35% of the heat release rate of the fire is radiation to the surroundings. Conduction heat transfer is usually of limited importance and the remaining 65% is thus mainly convective heat transfer to the fire smoke.

2.2.3 Fluid mechanics: conservation equations

The movement of smoke in the surrounding air, and the entrainment of air into the rising plume, can be described by fluid mechanics. The

conservation equations are coupled equations that describe the flow of a fluid, and are the main equations that will have to be solved in simulating the fire environment (see paragraph 2.3).

Conservation of mass

For a single phase flow, this reads:

$$\frac{\partial \rho}{\partial t} + \nabla \cdot \rho \mathbf{v} = 0 \tag{3.11}$$

Thus, the net mass that flows out of a control volume equals the mass generated inside this volume at any given time. If no mass is generated inside the volume, this means that the incoming and outgoing mass flow rates are equal.

Conservation of momentum

$$\frac{\partial}{\partial t}\left(\rho \mathbf{v}\right) + \nabla \cdot \left(\rho \mathbf{v}\mathbf{v}\right) = -\nabla\left(p + \rho_0 g \mathbf{z}\right) + \left(\rho_0 - \rho\right)\mathbf{g} + \nabla \cdot \boldsymbol{\tau} \tag{3.12}$$

$$\text{with } \boldsymbol{\tau} = \mu\left(2\mathbf{S} - \frac{2}{3}\boldsymbol{\delta}\left(\nabla \cdot \mathbf{v}\right)\right) \tag{3.13}$$

$$S_{ij} = \frac{1}{2}\left(\frac{\partial v_i}{\partial x_j} + \frac{\partial v_j}{\partial x_i}\right) \tag{3.14}$$

The conservation of momentum is described by Newton's second law of motion. This states that the time rate of change of momentum of a system is equal to the net force acting on the system and takes place in the direction of the net force. The forces that act on the control volume are those due to normal stress and shear stress, and body forces such as the force due to gravity.

Conservation of energy

$$\frac{\partial}{\partial t}\left(\rho h_s\right)+\nabla\cdot\left(\rho h_s \mathbf{v}\right)=\frac{\partial p}{\partial t}+\dot{q}'''-\nabla\cdot\dot{\mathbf{q}}''+\tau_{ij}\nabla\mathbf{v} \tag{3.15}$$

With $\dot{\mathbf{q}}''=-k\nabla T-\sum_a h_{s,a}\rho D_a\nabla Y_a+\dot{\mathbf{q}}_r''$ (3.16)

$$h_s=\sum_a Y_a h_{s,a}=\sum_a\left(Y_a\int_{T_0}^{T}c_{p,a}T'dT'\right) \tag{3.17}$$

The law of conservation of energy states that the total amount of energy in a system is conserved over time. Thus, energy can neither be created nor destroyed. It can only be transformed from one state to another, for instance chemical energy can become kinetic energy.

2.3 Fire and smoke modelling

Modelling of fire and smoke is often used by fire safety engineers to ascertain that a developed fire safety design meets the specified performance-based criteria. Modelling is usually cheaper than experiments, can be performed before actually constructing a building and does not cause any damage to the building.
To verify the performance of a smoke and heat exhaust ventilation system in an existing building, smoke tests are sometimes performed. However, tests using hot smoke can damage the building. Tests using cold smoke, on the other hand, are not representative for fire smoke, as the cold smoke does not contain the correct momentum. Therefore, smoke modelling is often preferred over smoke tests.

Three categories of fire modelling can be distinguished: hand calculations, zone models and field models.

Hand-calculations

Hand-calculations are based on empirical models. With these calculations, some basic features of the fire can be calculated, like the mass flow and temperature of a fire plume (see paragraph 2.1).

Zone models

A first type of computer modelling is zone modelling. Most commonly, a compartment is divided by the zone model into two zones, an upper hot layer and a lower cold layer (Fig. 2.3). Conservation equations (paragraph 2.2) are applied to each zone. Additional empirical correlations are present in the zone model, for the fire source term, smoke plume mass flow, interactions with ventilation openings etc.

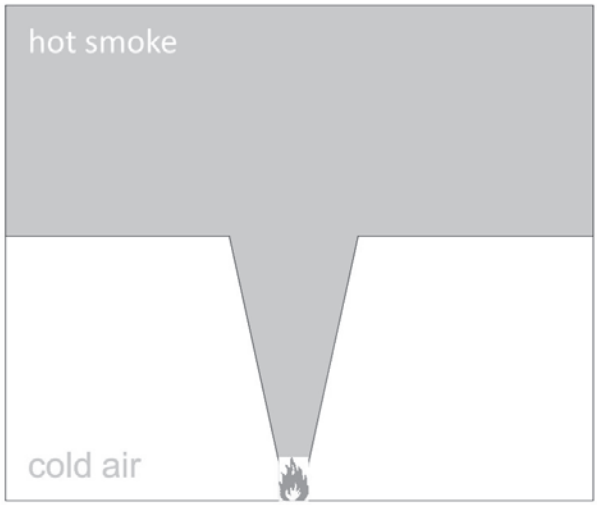

Figure 2.3 Representation of zone modelling.

Field models

With increasing available computer power, deterministic field models become increasingly interesting. The most commonly used type of field models is Computational Fluid Dynamics (CFD). In these models, the environment studied is divided into a large number of small volumes. In each of these cells, the quantities are constant at a specific time (Fig. 2.4). They vary, however, for each cell and each time step.

Conservation equations are applied to each of these cells. As the environment is divided into much smaller cells than in zone modelling, the field models provide more precise results, but require larger computational time and power. Submodels are still necessary in field modelling, as some processes (e.g. combustion, turbulence,...) occur on

even smaller time or length scales than can be resolved by the cell partitioning.

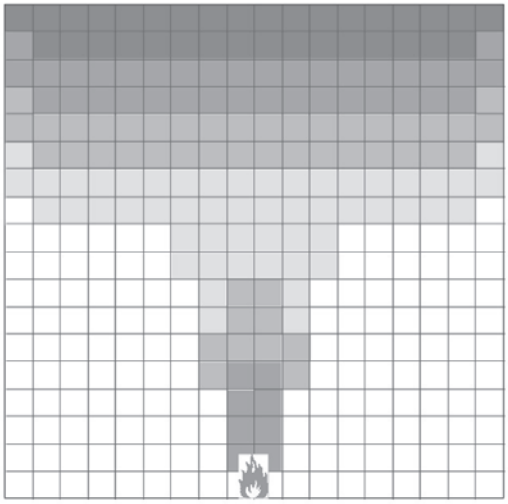

Figure 2.4 Representation of field modelling.

Another way to benefit from fire modelling, in contrast to evaluating a specific individual fire safety engineering design for a certain building, is by using numerical simulations of fire and smoke spread as so-called 'numerical experiments'. From a large set of simulations with parameter variations, the results can be used in the same way as experimental results, in the sense that empirical correlations can be derived from the numerical results. In the present study, this approach is adopted.

2.4 CFD modelling

As the present study deals with fire modelling with CFD, some more insight is given here first. The focus in the present paragraph is on the submodels that are used in the present study. For further reading on other submodels, the reader is referred to specific literature e.g. [5,8].

Combustion modelling

As the grid cell size is not fine enough to resolve the diffusion of fuel and oxygen to capture all details of the combustion process, a flame sheet model for combustion is used. This so-called 'mixed is burnt' model

assumes that the reaction of fuel and oxygen occurs rapidly and completely upon mixing. The combustion in this model occurs so rapidly that fuel and oxygen cannot co-exist in a cell. They both simultaneously vanish at a flame surface, consuming at least one of them completely within the cell, leaving behind the combustion products and the remaining oxygen or fuel. If more oxygen is present in a cell than what is needed to burn the fuel in the cell completely, then some part of that oxygen will remain in the cell. If not enough oxygen is present to burn all fuel in the cell, some of the fuel will remain.
More information on combustion modelling can be found in e.g. [8].

Turbulence modelling
Three types of turbulence modelling are available: RANS (Reynolds Averaged Navier Stokes), LES (Large Eddy Simulation) and DNS (Direct Numerical Simulations).
In RANS modelling, only the average flow field is calculated, and all turbulent motions are modelled, so that the information on time-dependent behaviour of the flow is less reliable.
In LES modelling, the conservation equations are filtered, and these filtered equations are solved. This way, the large eddies are explicitly taken into account in a calculation. Small eddies are implicitly accounted for by using a subgrid-scale model. This method will provide more reliable results in geometries with strong time-dependent turbulent motions. Therefore however, LES modelling requires three-dimensional and time-accurate calculations.
In DNS, the grid and time resolution are so fine that the conservation equations can be numerically solved without any turbulence model.
Fig. 2.5 schematically shows the difference between these three types of turbulence modelling.

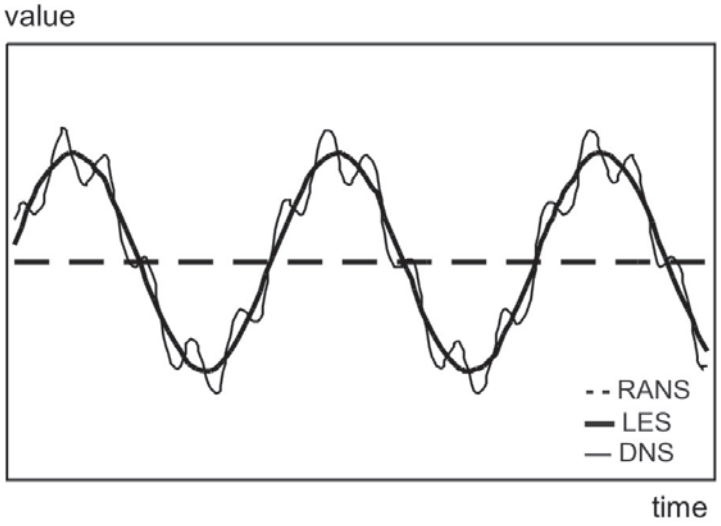

Figure 2.5 RANS, LES and DNS modelling of turbulence.

In the present work, the LES modelling technique is used.
Mathematically, the conservation equations are filtered, in order to obtain a filtered velocity field when solved. The velocity field is thus decomposed into a filtered part, which is resolved on the computational grid, and a subgrid velocity field that cannot be represented on the grid. For compressible flows, the Favre filtering is used to decompose the turbulent fields. This density weighted variable **v** is represented as:

$$\tilde{\mathbf{v}} = \overline{\rho \mathbf{v}} / \bar{\rho} \tag{3.18}$$

Using this Favre filtering, the momentum conservation equation (Eq. (2.12)) becomes

$$\frac{\partial(\bar{\rho}\tilde{\mathbf{v}})}{\partial t} + \nabla \cdot (\bar{\rho}\tilde{\mathbf{v}}\tilde{\mathbf{v}}) = -\nabla(\bar{p} + \rho_0 g \mathbf{z}) + (\rho_0 - \bar{\rho})\mathbf{g} + \nabla \cdot (\bar{\boldsymbol{\tau}} - \boldsymbol{\tau}^*) \tag{3.19}$$

where the turbulent stress is expressed as

$$\boldsymbol{\tau}^* = -\bar{\rho}\left(\widetilde{\mathbf{vv}} - \tilde{\mathbf{v}}\tilde{\mathbf{v}}\right). \tag{3.20}$$

With the eddy viscosity hypothesis, this subgrid scale stress tensor can be written as

$$\boldsymbol{\tau}^* = 2\mu_T \left(\tilde{S} - \frac{1}{3}\boldsymbol{\delta}\nabla\cdot\tilde{\mathbf{v}} \right) - \frac{2}{3}\boldsymbol{\delta}\bar{\rho}\tilde{k}\,. \tag{3.21}$$

In this representation, the turbulent dynamic viscosity is modelled as

$$\mu_T = \bar{\rho}\left(C_s\Delta\right)^2 \left|\tilde{\mathbf{S}}\right| \tag{3.22}$$

and it was suggested [12] that for commonly encountered flows the isotropic part $\left((2/3)\boldsymbol{\delta}\bar{\rho}\tilde{k}\right)$ of Eq. (2.21) can be neglected.

The Smagorinsky model used in the present study [13] uses a value C_s = 0.2 for the Smagorinksy constant.

2.5 References

[1] Drysdale D, An Introduction to Fire Dynamics, John Wiley and Sons, Chichester (1998)

[2] Quintiere JG, Fundamentals of Fire Phenomena, John Wiley and Sons, Chichester (2006)

[3] Karlsson B, Quintiere JG, Enclosure Fire Dynamics, CRC Press, Boca Raton, FL (2000)

[4] Welty JR, Wicks CE, Wilson RE, Rorrer G, Fundamentals of Momentum, Heat, and Mass Transfer, John Wiley and Sons, New York NY (2001)

[5] Pope SB, Turbulent flows, Cambridge University Press, Cambridge (2000)

[6] Chung TJ, Computational Fluid Dynamics, Cambridge University Press, Cambridge (2002)

[7] Pope SB, Ten questions concerning the large-eddy simulation of turbulent flows. New J. of Physics 6: 1–24 (2004)

[8] Peters N, Turbulent Combustion, Cambridge University Press, Cambridge (2000)

[9] McCaffrey BJ, Purely Buoyant Diffusion Flames: Some Experimental Results, NBSIR 79-1910, National Bureau of Standards (1979)

[10] McGrattan K, Hostikka S, Floyd J, Baum H, Rehm R, Mell W, McDermott R, Fire Dynamics Simulator (Version 5) Technical Reference Guide, NIST 1018-5, National Institute of Standards and Technology (2008)

[11] Huggett C, Estimation of Rate of Heat Release by Means of Oxygen Consumption Measurements, Fire and Materials 4: 61-65 (1980)

[12] Erlebacher G, Hussaini MY, Speziale CG, Zang TA, Toward the Large-Eddy Simulation of Compressible Turbulent Flows, J. of Fluid Mechanics 238: 155-185 (1992)

[13] Smagorinsky J, General Circulation Experiments with the Primitive Equations. I. The Basic Experiment, Monthly Weather Review 91: 99-164 (1963)

3 Chapter 3 Literature review

3.1 Car parks

For smoke and heat extraction in large, closed car parks, two options are available: longitudinal and transversal ventilation. In the latter case, the smoke is extracted from the ceiling of the car park through several openings. However, in the present study, focus is on the more common longitudinal ventilation, where smoke is extracted from one or more points at a side of the car park.

Without any form of ventilation present, the smoke from the fire initially flows upwards until the plume reaches the ceiling. The ceiling jet that is then formed will spread radially outwards from the fire axis (Fig. 2.2) until the car park boundaries are met.

When a horizontal (longitudinal) ventilation system is present, however, the smoke will be pushed towards the hot smoke extraction outlet. In the present study, the “front” side of the car park (right hand side in Fig. 3.1) is entirely open, so the makeup air can enter the car park freely.

Fig. 3.1 shows a situation where the extraction velocity is large enough to ensure that all the smoke from the fire is in the downstream direction. The minimum velocity that produces this situation is called the critical velocity.

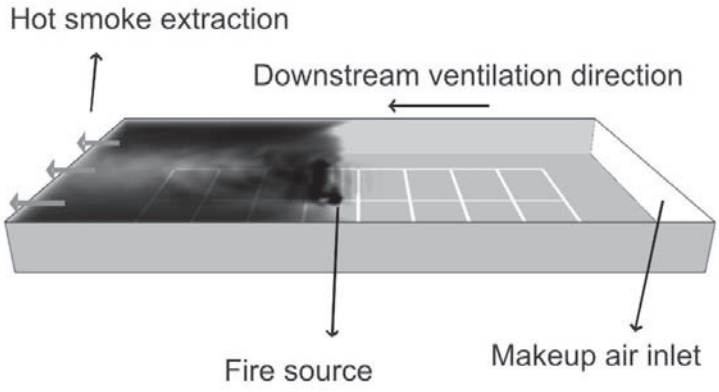

Figure 3.1 Car park configuration.

If the extraction velocity decreases below the critical value, however, the smoke will also flow in the upstream direction, against the incoming air flow. In this situation, a so-called backlayering distance can be defined as the horizontal distance from the fire to the start of the smoke layer in the car park (Fig. 3.2).

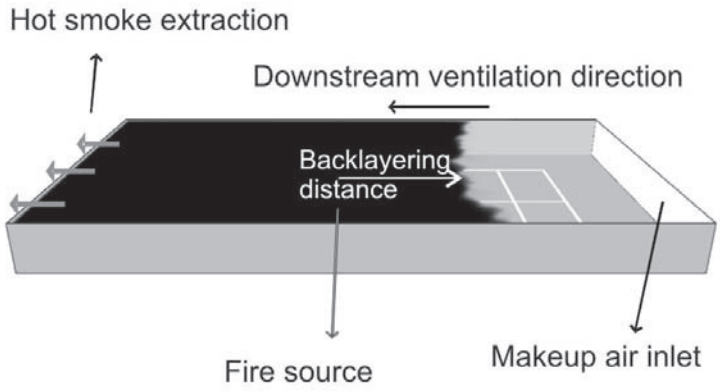

Figure 3.2 Backlayering in a car park.

The present study deals with – as mentioned – closed car parks where the inlet side is open. Thus, no recirculation effects are present here (see Chapter 5) and the smoke is not able to exit the structure at other places

than the open front side or through the exhaust ventilation system. Furthermore, the fire is placed in the middle of the car park, and both floor and ceiling are flat, inclination is not studied. As design fires are imposed in the simulations, the influence of the ventilation on the heat release or spread of the fire is also outside the scope of the present research.

In previous studies, focus was mostly on tunnel fires and ventilation. Several authors have defined analytical or semi-empirical formulae to define the critical inlet velocity in tunnels.
Thomas [1] performed a purely analytical derivation of smoke flow in a tunnel. Posing that the critical Froude number equals 1, a theoretical formula for critical velocity in tunnels was proposed:

$$v_{cr,in} = \left(\frac{g \dot{Q}_{conv} h}{\rho_0 c_p T_0 A_{cs}} \right)^{1/3} . \tag{3.1}$$

Here, $v_{cr,in}$ denotes the critical velocity of the incoming air flow. $\dot{Q}_{conv}$ is the convective heat release rate of the fire, h the tunnel height and A_{cs} the cross-sectional area of the tunnel. g, ρ_0, c_p and T_0 are ambient environmental properties.

Based on the approach of Thomas, Danziger and Kennedy [2] proposed a similar formula for critical inlet velocity in tunnels:

$$v_{cr,in} = K_g \left(\frac{g \dot{Q}_{conv} h}{c_p \rho_0 T_f A_{cs} \, \mathrm{Fr}_{cr}} \right)^{1/3} \tag{3.2}$$

$$\text{with } T_f = \left(\frac{\dot{Q}_{conv}}{c_p \rho_0 A_{cr} v_{cr,in}} \right) + T_0 . \tag{3.3}$$

The factor K_g is a grade correction that accounts for a certain slope of the tunnel and T_f represents the temperature of the hot gases. Danziger and Kennedy proposed a value $\mathrm{Fr}_c = 4.5$ for the critical modified Froude number, based on experiments performed by Lee et. al [3].

By performing reduced-scale experiments with an isothermal buoyant helium jet, representing a fire in a rectangular cross-section tunnel of fixed dimensions (height h = 237 mm and width w = 400 mm), Vauquelin [4] presented the following semi-empirical formula:

$$v_{cr,in} = 1.42\left(\frac{g\dot{Q}_{conv}}{\rho_0 c_p T_0}\right)^{1/3} . \tag{3.4}$$

A thermal study with a fuel burner in a fixed reduced-scale tunnel setup was performed by Oka and Atkinson [5]. They presented an experimental correlation in terms of dimensionless critical velocity and heat release rate:

$$V_{cr}^* = \frac{v_{cr,in}}{\sqrt{gh}}, \tag{3.5}$$

$$\dot{Q}^* = \frac{\dot{Q}_{conv}}{\rho_0 c_p T_0 \sqrt{gh^5}}, \tag{3.6}$$

$$\begin{cases} V_{cr}^* = 0.35\left(\dfrac{\dot{Q}^*}{0.124}\right)^{1/3} & \text{for } \dot{Q}^* < 0.124 \\ V_{cr}^* = 0.35 & \text{for } \dot{Q}^* > 0.124 \end{cases} \tag{3.7}$$

The derivation of all the above proposed formulae, however, did not take into account the variation of tunnel dimensions. The dependence on tunnel height and width that is seen in Eqs. (3.1), (3.2), (3.4) and (3.7) is solely based on the choice of the form of dimensionless velocity and heat release rate.

In the experimental study of Wu and Bakar [6], a variation of the tunnel width and fire heat release rate was conducted to study the influence on the critical velocity. Similar to the approach of Oka and Atkinson [5], they performed reduced-scale thermal experiments and proposed new

forms of the dimensionless velocity and heat release rate, now based on the hydraulic diameter of the tunnel section:

$$V_{cr}'' = \frac{v_{cr,in}}{\sqrt{gD_H}} \text{ and} \tag{3.8}$$

$$\dot{Q}^* = \frac{\dot{Q}_{conv}}{\rho_0 c_p T_0 \sqrt{gD_H^5}}, \tag{3.9}$$

where the hydraulic diameter D_H is defined as four times the tunnel cross-section area divided by the perimeter. The following relations for dimensionless critical velocity were proposed:

$$\begin{cases} V_{cr}^* = 0.40\left(\dfrac{\dot{Q}^*}{0.20}\right)^{1/3} & \text{for } \dot{Q}^* < 0.20 \\ V_{cr}^* = 0.40 & \text{for } \dot{Q}^* > 0.20 \end{cases} \tag{3.10}$$

During the thermal experiments with fuel burner, however, the reduced-scale tunnel configuration was cooled for high heat release rates, to limit the temperatures of the walls. This occurred in both mentioned studies with a fuel burner [5,6]. As the cooling is not quantified, some uncertainty on the experimental results is present.

Based on physical models for rising plumes, ceiling jets and existing models for the backlayering region, Kunsch [7] proposed an analytical solution for the critical velocity in tunnels, with dependency on the tunnel aspect ratio h/w. The following equation was derived:

$$V_{cr}^* = 1.48 \frac{\sqrt{1 + 3.11\dot{Q}^{*2/3}}}{1 + 6.13\dot{Q}^{*2/3}} \dot{Q}^{*1/3} \tag{3.11}$$

for aspect ratio h/w = 0.5. The constants 1.48 and 3.11 in Eq. (1.11) vary with tunnel aspect ratio, but within a relatively small range.

A more recent study by Vauquelin [8] presented again the results of a large number of isothermal helium jet experiments. No correlation was proposed, but it was shown that the critical velocity in tunnels is dependent on the geometrical parameters of the tunnel (width and height) and of the fire source (helium jet diameter D_F), as well as on the heat release rate of the fire:

$$v_{cr,in} = f\left(D_F, h, w, \dot{Q}_{conv}\right). \tag{3.12}$$

Not all of these parameters have been introduced yet in existing relations for critical velocity in tunnels.

A recent study by Li et. al [9] reports experimental tests with a porous bed burner fire source in a reduced-scale tunnel setup. The experimental results show slightly higher values for critical velocity than obtained in previous thermal studies [5,6], due to the cooling present in these earlier studies. The proposed trends of [6], however, are confirmed with the experimental data of [9].

Beside experimental studies, some numerical research has been performed on horizontal ventilation in tunnels, in which existing correlations for critical velocity have mainly been confirmed by CFD simulations (e.g. [10,11]).

Research on smoke and heat extraction in car park configurations, however, is limited compared to tunnel configurations. Most work on car park ventilation concerns continuous extraction of toxic car exhaust gases. Forced mechanical ventilation for fire smoke exhaust is – although widely used in car parks – not very often studied. Other work outside the scope of the present study is on fire spread in car parks, and the influence of ventilation on spread and heat release rate of a fire.

A study performed by Chow [12] presents a zone model simulation study on smoke filling in car parks with transversal natural and mechanical ventilation. However, transversal ventilation is of totally

different nature than longitudinal ventilation, concerning the smoke pattern in the car park.

Other work on car parks by Viegas [13] concerns the use of impulse jet fans, which is also outside the scope of the present research.

3.2 Atria

Shopping malls, hotel lobbies and office buildings are common types of atrium configurations. A fire could occur on the atrium floor, or in a room next to the atrium, like a shop, hotel room or office. The present research focuses on fire in an adjacent room to the atrium, where often more combustible material is present.

In the room where the fire starts, the smoke from the fire will first rise, and then form a ceiling jet, until the opening between the fire room and the atrium is reached. The edge of this opening is called the spill edge (Fig. 3.3).

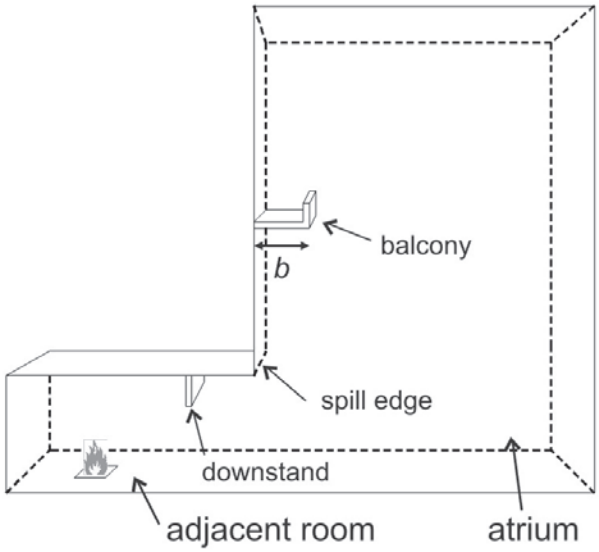

Figure 3.3 Fire in an adjacent room to an atrium: spill edge, downstand and balcony.

In the opening between adjacent room and atrium, a downstand can be present, and in the atrium, a balcony can be located next to the room opening.

When the smoke plume turns around the spill edge, a so-called spill plume is formed in the atrium. This type of plume is sometimes also referred to as a line plume, as at the spill edge, the plume is relatively narrow and long. Two types of spill plumes are known, depending on the geometry of the atrium (Fig. 3.4).

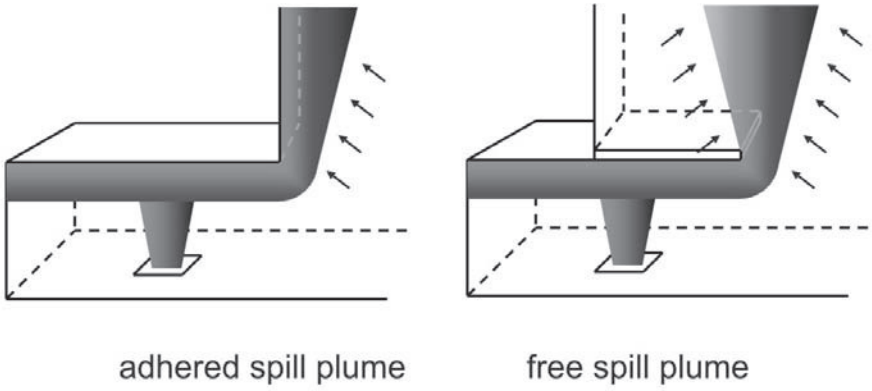

Figure 3.4 Adhered and free spill plumes.

To form a free spill plume, an extended balcony or upper floor level to the adjacent room must be present in the atrium. In the free spill plume, the smoke can rise in an unobstructed manner in the atrium, and air is entrained into both sides of the plume.
An adhered plume, on the other hand, is formed when the vertical wall of the atrium starts at the spill edge of the adjacent room. The rising plume then attaches to the wall of the atrium, so entrainment is only possible into one side of the plume.

Both of these plume types can be subdivided into two more types: two- and three-dimensional spill plumes [14]. Two-dimensional (2D) plumes, are contained within the atrium walls, while in three-dimensional (3D)

plumes, entrainment into the free ends of the plume is possible, and higher plume mass flow rates are present (Fig. 3.5).

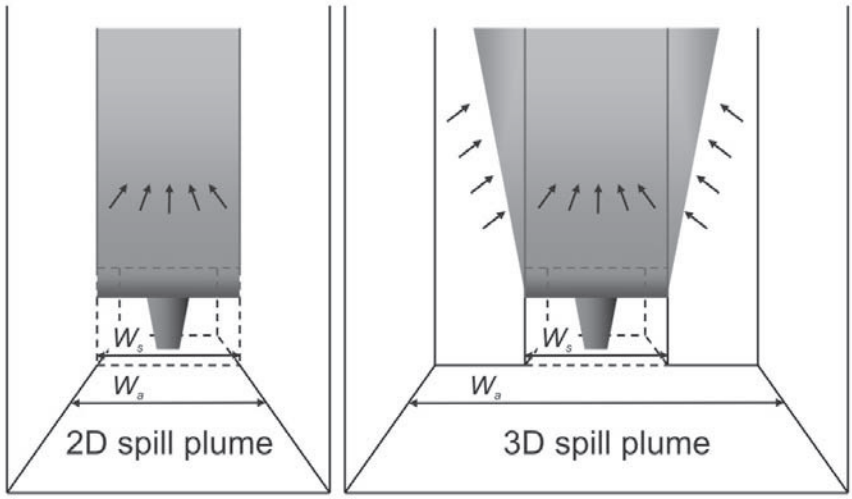

Figure 3.5 Two- and three-dimensional spill plumes.

The focus in the present study is on two-dimensional adhered spill plumes.

Active fire protection in the atrium is often anticipated by installation of a smoke and heat extraction ventilation system at ceiling level in the atrium. Such a system can mechanically extract smoke at a specified flow rate, or it can simply be an open vent that allows natural ventilation of the smoke.

Underneath the smoke layer in the atrium, a so-called smoke free height can be determined, where no smoke is present and possible occupants of the atrium can see and breathe unhindered. A ventilation system in the atrium is usually designed to ensure a certain minimum smoke free height to allow for safe evacuation of the atrium occupants.

To design the ventilation system, it is thus necessary to specify a relation between the height and the mass flow rate of the smoke plume. As the mass flow into the atrium smoke layer is equal to the extracted

mass flow rate, the mass flow rate at the requested smoke free height needs to be known to design the ventilation system (Fig. 3.6).

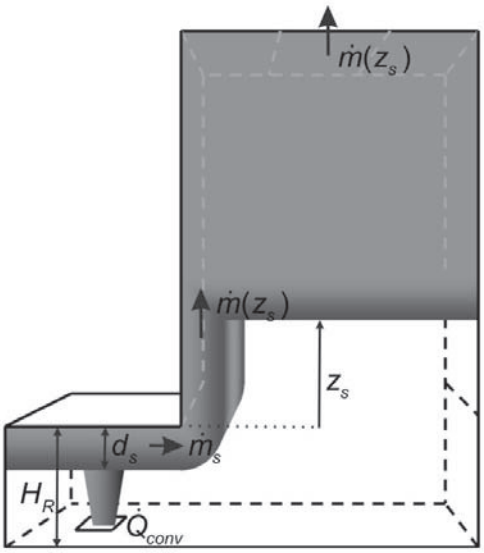

Figure 3.6 Smoke and heat extraction system in an atrium.

A number of previous studies have been performed to define such a formula for extraction mass flow rate in an atrium. Most of these are based on reduced-scale experiments.
Based on the approach of Yokoi [15], and using 1/10th reduced-scale experimental data by Morgan, Marshall and Goldstone [16, 17, 18], Law developed a relation for mass flow rate of a 2D free spill plume [19]:

$$\dot{m}\left(z_s\right)=0.34\left(\dot{Q}W_s^{\,2}\right)^{1/3}\left(z_s+0.15H_R\right), \tag{3.13}$$

with (Fig. 3.6) z_s: the smoke free height above the spill edge,
H_R: the height of the adjacent room,
W_s: the opening width at the spill edge, (Fig. 3.5)
$\dot{Q}$: the total heat release rate of the fire.

Based on the same experimental data [16, 17, 18], Thomas [20] defined an alternative relation for mass flow rate of the smoke plume, where entrainment into the free ends of a 3D spill plume is included:

$$\dot{m}(z_s) = 0.58\rho_0 \left(\frac{g\dot{Q}W_s^2}{\rho_0 c_p T_0} \right)^{1/3} (z_s + z_o) \left(1 + \frac{0.22(z_s + 2z_o)}{W_s} \right). \quad (3.14)$$

In the above equation, z_0 represents a 'virtual origin' of the spill plume: the imaginary line source where the plume would have started had it not come from underneath the spill edge. Thomas defined the virtual origin to be within the range $0.32\ H_R < z_o < 0.66\ H_R$.

Including experimental results by Hansell et. al [21], Law slightly adjusted her previously proposed formula for 2D free spill plumes [22]:

$$\dot{m}(z_s) = 0.31\left(\dot{Q}W_s^2\right)^{1/3} (z_s + 0.25H_R) \quad (3.15)$$

By performing a new set of reduced-scale experiments presented by Marshall and Harrison [23], Poreh et. al adapted the Lee and Emmons 2D thermal line plume model [24] for 2D free spill plumes in atria [25]:

$$\begin{cases} \dfrac{\dot{m}(z_s)}{\dot{Q}_{conv}^{1/3}} = C(z_s + z_o) \\ \text{with } C = 0.3C_m\rho_0 W_s^{2/3} \\ \text{and } z_o = d_s + \dot{m}_s \Big/ \left(C\dot{Q}_{conv}^{1/3}\right) \end{cases} \quad (3.16)$$

By curve fitting to experimental data, the factor C_m was determined to equal C_m = 0.44 in the above presented equation. It was assumed that the entrainment into the curved section of the spilling plume is equal to the entrainment into a vertical free plume rising through the same height, thus defining the value of the virtual origin height z_o. In this definition, d_s represents the depth of the smoke layer emerging from the adjacent room at the spill edge and $\dot{m}_s$ its mass flow.

Eq. (3.16) can be written in a slightly different form to resemble the previously proposed relations:

$$\dot{m}(z_s) = 0.158\left(\dot{Q}_{conv}W_s^2\right)^{1/3} (z_s + d_s) + \dot{m}_s. \quad (3.17)$$

Thomas [26] proposed two new formulae for 2D free spill plumes, using experimental data of [21] and [23]:

$$\begin{cases} \dot{m}(z_s) = 0.16\left(\dot{Q}_{conv} W_s^2\right)^{1/3} z_s + 1.2\dot{m}_s + 0.0027\dot{Q}_{conv} \\ \dot{m}(z_s) = 0.16\left(\dot{Q}_{conv} W_s^2\right)^{1/3} z_s + 1.4\dot{m}_s + 0.0014\dot{Q}_{conv} \end{cases} \quad (3.18)$$

where the second proposed relation is a valid alternative for the first one, providing similar results.

The National Fire Protection Association standard NFPA 92b [27] proposes a new set of formulae for free spill plumes, using full-scale experimental data of Lougheed et. al [28].

$$\begin{cases} z_s < 15\,\text{m}, W_s > 10\,\text{m}: \quad \dot{m}(z_s) = 0.36\left(\dot{Q} W_s^2\right)^{1/3}\left(z_s + 0.25H_R\right) \\ z_s < 15\,\text{m}, W_s < 10\,\text{m}: \quad \dot{m}(z_s) = 0.59\dot{Q}^{1/3} W_s^{1/5}\left(z_s + 0.17 W_s^{7/15} H_R + 10.35 W_s^{7/15} - 15\right) \\ z_s > 15\,\text{m}, 10\,\text{m} < W_s < 14\,\text{m}: \quad \dot{m}(z_s) = 0.2\left(\dot{Q}_{conv} W_s^2\right)^{1/3}\left(z_s + 0.51H_R + 15.75\right) \end{cases} \quad (3.19)$$

A new set of 1/10th reduced-scale spill plume experiments were performed by Harrison, and an adjusted relation for 2D free plumes proposed [29]:

$$\dot{m}(z_s) = 0.2\left(\dot{Q}_{conv} W_s^2\right)^{1/3}\left(z_s + d_s\right) + \dot{m}_s\,. \quad (3.20)$$

In a similar experimental setup as the one used for the derivation of his 2D free plume, Poreh performed a set of experiments on adhered spill plumes [30]. The same relation as Eq. (3.16) was found, with a different value for factor C_m, which, again by means of curve fitting to experimental data, was determined to be equal to C_m = 0.21 for adhered spill plumes. The resulting equation can be written as:

$$\dot{m}(z_s) = 0.076\left(\dot{Q}_{conv} W_s^2\right)^{1/3}\left(z_s + d_s\right) + \dot{m}_s\,. \quad (3.21)$$

In his PhD thesis [14] and article [31], Harrison describes an extensive set of reduced-scale experiments on both 2D and 3D, free and adhered spill plumes. The resulting equations for the mass flow of the spill plume are:

- 2D free spill plume:

$$\dot{m}(z_s) = 0.16\left(\dot{Q}_{conv} W_s^2\right)^{1/3} z_s + 1.34\dot{m}_s \tag{3.22}$$

- 3D free spill plume:

$$\dot{m}(z_s) = 0.16\dot{Q}_{conv}^{1/3}\left[\left(W_s + b\right)^{2/3} + 1.56 d_s^{2/3}\right] z_s + 1.34\dot{m}_s \text{ for } W_s / b > 2\,, \tag{3.23}$$

where b is the balcony length, if present (Fig. 3.3).

- 2D adhered spill plume [31]:

$$\dot{m}(z_s) = 0.08\left(\dot{Q}_{conv} W_s^2\right)^{1/3}\left(z_s + d_s\right) + \dot{m}_s \tag{3.24}$$

- 3D adhered spill plume

$$\dot{m}(z_s) = 0.3\dot{Q}_{conv}^{1/3} W_s^{1/6} d_s^{1/2} z_s + 1.34\dot{m}_s \tag{3.25}$$

Apart from simple one-line equations to calculate the mass flow rate of the spill plume, an extensive method has been proposed by Morgan [32] to calculate the required extraction mass flow rate in the atrium.

The computer modelling studies that have been performed on atria with fire in an adjacent room mainly concern free spill plumes.

Early work by Miles et. al [33] presents a CFD modelling study on a reduced-scale atrium. The simulations indicated good agreement with the proposed relations from Thomas et. al [26] and Poreh et. al [25] for lower extraction mass flow rates, but the simulation results deviated from the suggested formulae for mass flow rate outside the scope of the experiments [23] on which these relations are based.

Another set of CFD simulations on a reduced-scale atrium configuration was presented by Chow et. al [34]. The CFD results showed a similar linear relation between extraction mass flow rate in the free spill plume and smoke free atrium height as presented by Poreh et. al [25].

A zone modelling study on smoke filling in an atrium with a free spill plume, performed by Chow et. al [35] Again, the smoke free height in the atrium simulations corresponds well to the proposed relations by Poreh et. al [25] and Thomas et. al [26].

Both zone and CFD modelling approaches were used in a study by Shi et. al [36]. A new zone model is proposed, including spill plume correlations, and shows good agreement with experiments.

The work of Harrison et. al [14,37] presents a combination of experiments and simulations, on which their proposed formulae for mass flow rates of spill plumes (Eqs. (3.20), (3.22), (3.23), (3.24), (3.25)) are based.

As mentioned before, the present work concerns 2D adhered spill plumes, so the most relevant proposed relations for mass flow rate of the smoke plume are Eqs. (3.21) and (3.24). In their last published study, Harrison et. al [31] showed that Eq. (3.24) also correlates well with the experimental data used by Poreh et. al [30] for their development of Eq. (3.21).

3.3 References

[1] Thomas PH, The movement of smoke in horizontal passages against an air flow, Fire Research Station Note no. 723, Fire Research Station (1968)

[2] Danziger NH, Kennedy WD, Longitudinal ventilation analysis for the Glenwood Canyon tunnels, 4th International Symposium on Aerodynamics and Ventilation of Vehicle Tunnels, BHr Group, 169-186 (1982)

[3] Lee CK, Chaiken RF, Singer JM, Interaction between duct fires and ventilation flow: An experimental study, Combustion Science and Technology 20: 59-72 (1979)

[4] Vauquelin O, Caractérisation expérimentale de l'apparition d'une nappe de retour, Compte Rendus de l'Académie des Sciences, Série II b 321: 15-18 (1995)

[5] Oka Y, Atkinson GT, Control of smoke flow in tunnel fires, Fire Safety J. 25: 305-322 (1995)

[6] Wu Y, Bakar MZA, Control of smoke flow in tunnel fires using longitudinal ventilation systems – a study of the critical velocity, Fire Safety J. 35: 363-390 (2000)

[7] Kunsch JP, Simple model for control of fire gases in a ventilated tunnel, Fire Safety J. 37: 67-81 (2002)

[8] Vauquelin O, Parametrical study of the back flow occurrence in case of a buoyant release into a rectangular channel, Experimental Thermal and Fluid Science 29: 725-731 (2005)

[9] Li YZ, Lei B, Ingason H, Study of critical velocity and backlayering length in longitudinally ventilated tunnel fires, Fire Safety J. 45: 361-370 (2010)

[10] Hwang CC, Edwards JC, The critical ventilation velocity in tunnel fires – a computer simulation, Fire Safety J. 40: 213-244 (2003)

[11] Van Maele K, Merci B, Application of RANS and LES field simulations to predict the critical ventilation velocity in longitudinally ventilated horizontal tunnels, Fire Safety J. 43: 598-609 (2008)

[12] Chow WK, Use of a time constant for designing a smoke control system in car parks, J. of Fire Sciences 13 (5): 357-377 (1995)
[13] Viegas JC, The use of impulse ventilation for smoke control in underground car parks, Tunnelling and Underground Space Technology 25: 42-53 (2010)
[14] Harrison R, Entrainment of Air into Thermal Spill Plumes, Fire Engineering Research Thesis, Christchurch, New Zealand (2009)
[15] Yokoi S, Study on the Prevention of Fire Spread by Hot Upward Current, Report No. 34, Building Research Institute, Japan (1960)
[16] Morgan HP, Marshall NR, Smoke Hazards in Covered, Multi-level Shopping Malls: and Experimentally Based Theory for Smoke Production, BRE CP48/75, Borehamwood (1975)
[17] Morgan HP, Marshall NR, Smoke Control Measures in a Covered Two-storey Shopping Mall having Balconies as Padestrian Walkways, BRE CP11/79, Borehamwood (1979)
[18] Morgan HP, Marshall NR, Goldstone BM, Smoke Hazards in Covered, Multi-level shopping Malls: some Studies using a Model 2-storey Mall, BRE CP45/76, Borehamwood (1976)
[19] Law M, A Note on Smoke Plumes from Fires in Multi-level Shopping Malls, Fire Safety J. 10: 197-202 (1986)
[20] Thomas PH, On the Upward Movement of Smoke and Related Shopping Mall Problems, Fire Safety J. 12: 191-203 (1987)
[21] Hansell GO, Morgan HP, Marshall NR, Smoke flow experiments in a model atrium, Building Research Establishment Occasional Paper, OP 55 (1993)
[22] Law M, Measurements of Balcony Smoke Flow, Fire Safety J. 24: 189-195 (1995)
[23] Marshall NR, Harrison R, Experimental Studies of thermal spill plumes. Building Research Establishment Occasional Paper OP1 (1996)
[24] Lee L, Emmons HW, A study of natural convection above line fires, J. Fluid Mechanics 11: 353-368 (1961)
[25] Poreh M, Morgan HP, Marshall NR, Harrison R, Entrainment by Two-Dimensional Spill Plumes, Fire Safety J. 30: 1-19 (1998)

[26] Thomas PH, Morgan HP, Marshall N, The Spill Plume in Smoke Control Design, Fire Safety J. 30: 21-46 (1998)
[27] NFPA 92B, Smoke Management Systems in Malls, Atria and Large Areas, National Fire Protection Association (2005).
[28] Lougheed GD, McCartney CJ, Gibbs E, Balcony spill plumes, Final Research Project Report 1247. National Research Council, Canada (2006)
[29] Harrison R, Spearpoint M, Entrainment of air into a balcony spill plume, J. of Fire Protection Engineering 16: 211-245 (2006)
[30] Poreh M, Marshall NR, Regev A, Entrainment by adhered two-dimensional plumes, Fire Safety J. 43: 344-350 (2008)
[31] Harrison R, Spearpoint M, Physical scale modeling of adhered spill plume entrainment, Fire Safety J. 45: 149-158 (2010)
[32] Morgan HP, Gosh BK, Garrad G, Pamlitschka R, De Smedt J-C, Schoonbaert LR, Design Methodologies for Smoke and Heat Exhaust Ventilation, BRE Report 368, Building Research Establischment, Watford UK (1999)
[33] Miles S, Kumar S, Cox G, The balcony spill plume – some CFD simulations, Proceedings of the Fifth International Symposium on Fire Safety Science: 237-247 (1997)
[34] Chow WK, Cui E, CFD simulations on Balcony Spill Plume, J. of Fire Sciences 16: 468-485 (1998)
[35] Chow WK, Li J, Simulation on Natural Smoke Filling in Atrium with a Balcony Spill Plume, J. of Fire Sciences 19: 258-283 (2001)
[36] Shi CL, Lu WZ, Chow WK, Huo R, An investigation on spill plume development and natural filling in large full-scale atrium under retail shop fire, Int. J. of Heat and Mass Transfer 50: 513-529 (2007)
[37] Harrison R, Spearpoint M, The Balcony Spill Plume: Entrainment of Air into a Flow from a Compartment Opening to a Higher Projecting Balcony, Fire Technology 43: 301-317 (2007)

4 Chapter 4 Confirmation of the validity of small-scale simulation results

4.1 Introduction

One of the research objectives in fire safety research is the improvement of calculation methods to determine the required smoke extraction rate to meet fire safety objectives (such as smoke free heights or smoke free zones) in different types of buildings; including atria and large closed car parks.

Obviously, a 'conditio sine qua non' is then that the CFD simulation results are reliable, i.e. of sufficient accuracy in 'blind' circumstances. Therefore, as a first step to show that CFD has the potential to be used as 'numerical experiments', two experimentally studied small-scale test cases are extensively investigated in this chapter. The first case concerns fires in a small-scale atrium [1]. A fire in a room, adjacent to the atrium, causes a spill plume to rise in the atrium.

The second test case is a small-scale tunnel experiment [2] with forced mechanical ventilation imposed to avoid the smoke backlayering from the fire. Note that the flow is essentially horizontal, in contrast to the atrium configuration. For the CFD results, the simulation program Fire Dynamics Simulator (FDS, version 5) [3,4], developed by NIST, is used. However, in principle, other CFD packages could be used as well. Indeed, it would be valuable to repeat the study with other CFD packages, investigating their model capability, but this is considered beyond the scope of the present study. The influence on the results of

computational mesh and the thermal boundary conditions will be considered.
The results presented in the present chapter have also been published as a journal paper [5].

4.2 Atrium

In this section, the atrium simulations are discussed. In total, 16 simulations have been performed. Four different heat release rates are studied. For each value of heat release rate, four different extraction rates are imposed. First, the set-up of the original experiments is explained. Afterwards, the numerical set-up of the simulations is discussed. The search for a reliable method to determine the smoke interface height, based on the temperature profile in the atrium, is discussed in a separate section. Finally, the numerical simulation results are presented.

4.2.1 Experimental set-up

In a recently published paper [1], Poreh et al. carried out a series of experiments in a small-scale atrium configuration (Figure 4.1). Four different total fire heat release rates ($\dot{Q}_{conv}$) were created in the room adjacent to the atrium. For each heat release rate, different mass flow rates of smoke ($\dot{m}$) were mechanically extracted at the ceiling of the atrium, corresponding to a certain smoke free height above the spill edge (z_s) in the atrium. The depth (d_s) and mass flow rate ($\dot{m}_s$) of the smoke layer, emerging from the adjacent room, were measured.
The room adjacent to the atrium has size 1.25 m x 0.9 m x 0.6 m, and the atrium itself is 2.5 m x 0.9 m x 3.6 m large.

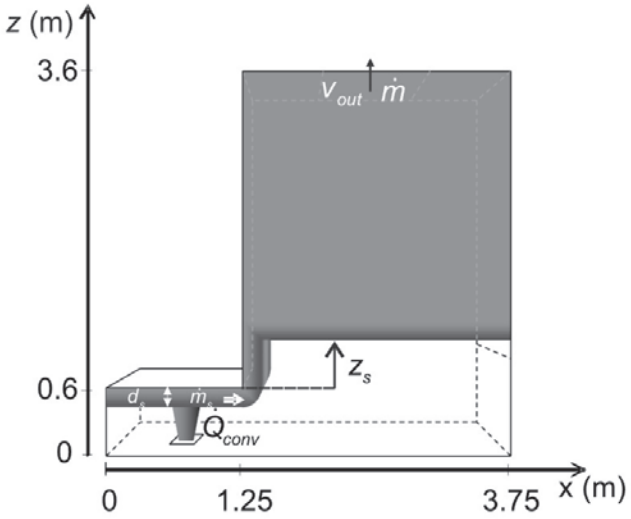

Figure 4.1 Atrium configuration.

From these experiments, Equation (4.1) was deduced in [1] to calculate, for a certain heat release rate, the required smoke extraction mass flow rate, in order to maintain a specific smoke free height above the spill edge in the atrium:

$$\frac{\dot{m}(z_s)}{\dot{Q}_{conv}^{1/3}} = C\left(z_s + z_o\right) \tag{4.1}$$

with $C = 0.3 C_m \rho_0 W_s^{2/3}$ (4.2)

$$z_o = d_s + \frac{\dot{m}_s}{C\dot{Q}_{conv}^{1/3}} \tag{4.3}$$

where z_0 is the virtual origin of the rising spill plume and C_m = 0.21 for adhered spill plumes.

More recent studies of air entrainment in spill plumes in atria include [6,7]. In the present chapter, the intention is not to provide new correlations or insights. The only aim is to illustrate the quality of CFD results, in agreement with the experimental data reported in [1].

4.2.2 Numerical set-up

As mentioned in the introduction, FDS, version 5.2.5 [3,4] is used for the numerical simulations. The standard Smagorinsky LES turbulence

model [8] is incorporated, with Smagorinsky constant C_s = 0.2. The Prandtl number has the constant default value 0.7.
Cubic cells of size 2.5 cm are used, resulting in a grid of 561 600 cells. A grid refinement study has been performed in the adjacent room to the atrium. In this refinement case, cells of size 1.25 cm edge are used in the adjacent room, whereas the cells in the atrium are still of size 2.5 cm edge. A characteristic length scale of the fire can be calculated as

$$D^* = \left(\frac{\dot{Q}}{\rho_0 T_0 c_p \sqrt{g}} \right)^{2/5} . \qquad (4.4)$$

In the refinement case under consideration, the total fire heat release rate is 8.272 kW, resulting in a characteristic length scale D^* = 0.14 m. As stated in [9], a criterion to guarantee reliable LES-results might be that at least ten cells must fit within the characteristic diameter. This is satisfied in the refinement case.

The D^* criterion refers to requirements for the computational grid with respect to global fire scales (in the flaming region). However, it should be noted that other characteristic length scales are also present in the situation at hand. For example, the ceiling jet in the adjacent room with the fire source and the spill plume in the atrium both have characteristic length scales. Therefore, it should be acknowledged that the D^* criterion as presented in Eq. (4.4) is not always sufficient to ensure the quality of the computational grid to capture all phenomena in an accurate manner, as other characteristic length scales can also play important roles in the flow field. On the other hand, the impact of 'missing' certain flow and mixing phenomena need not be crucial per se with respect to the eventual smoke and heat control performance.

A comparative study of simulation results to experimental data is considered here as indicative for the quality of the selected computational grid. Since results obtained on the finer grid hardly differ from results on the coarser grid, the grid with cells of size 2.5 cm is assumed sufficiently fine. Indeed, the detailed configuration of the

smoke plume in the adjacent room is of secondary importance with respect to the main smoke field in the large atrium.
In the simulations, radiation is turned off, so that the fire heat release rate corresponds to $\dot{Q}_{conv}$. The total heat release rate of the fire can be reconstructed as $\dot{Q} = \dot{Q}_{conv} / \left(1 - \chi_r\right)$. This way, uncertainties due to radiation modelling are avoided in the simulations.
All walls are modelled as adiabatic, in agreement with turning off the radiative heat transfer.
In [1], only values of the convective heat release rate are reported, measured in the emerging smoke layer underneath the spill edge. Therefore the convective heat release rate is imposed as fire source in the simulations, with adiabatic walls. The highest temperatures obviously occur in the adjacent room to the atrium, so that by far most of the radiative loss would be found there if radiation modelling were included in the simulations. In the atrium, the plume adheres to the wall. Plume temperatures are relatively low, so radiative losses are negligible within the atrium itself. However, when modelling the walls as adiabatic, no heat is lost by conduction through the walls. The advantage of using non-adiabatic wall conditions would be that convective and conductive heat transfer could be calculated. Yet, the results discussed below, are hardly affected by these heat losses.

It is also important to appreciate that LES are unsteady in nature. Therefore, it is important to discuss the simulation results in terms of 'averages'. The simulations are executed until a quasi-steady-state situation is reached. The data between two time values (t_1 and t_2) in the quasi-steady state are then time averaged. These averages are presented below as the 'simulation results'. The times used for averaging the results depend on the fire heat release rate. Time varies with velocity and length scale as $t \sim L / v$. With Froude scaling, the scaling for velocity is $v \sim \dot{Q} / L^2$, resulting in scaling of time with heat release rate:

$$t \sim L^3 / \dot{Q}. \qquad (4.5)$$

With Eq. (4.5), the averaging period t_1 – t_2 is constructed, the values of which are reported in Table 4.1. These average values are larger than turbulent time scales: from unsteady RANS calculations of the same atrium set-up, the turbulent time scale could be calculated and the maximum value observed was 13 s.

Table 4.1 Begin (t_1) and end (t_2) times for the calculation of time-averaged simulation results.

$\dot{Q}$ (kW)	t_1 (s)	t_2 (s)
4.44	261	335
8.27	140	180
13.5	86	110
18.3	63	81

4.2.3 Determination of the smoke layer interface height

In this CFD study, small-scale atrium experiments are studied, in order to compare the numerical results to the experiments. However, a criterion is first developed to define the height of the smoke layer in the atrium from the simulation results.

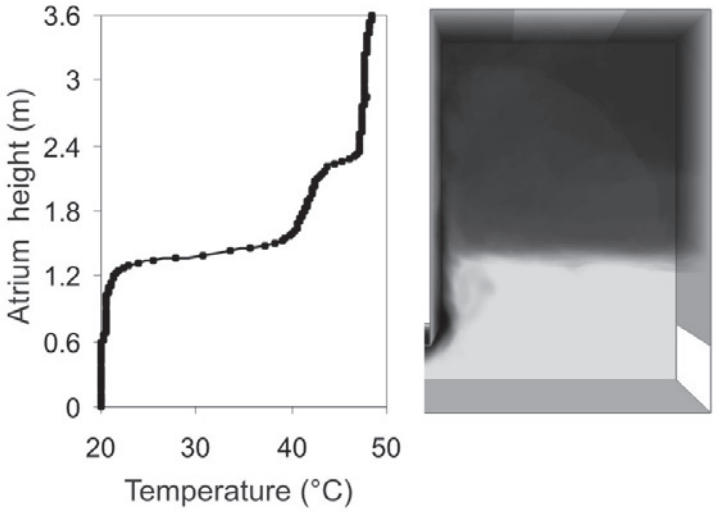

Figure 4.2 Temperature variation on a vertical line (x = 3.75 m) in the atrium.

The left side of Fig. 4.2 depicts a typical temperature profile on a vertical line in the atrium. This profile shows a first (small) increase in temperature at z = 0.6 m, i.e. the height of the right-hand side opening (Fig. 4.1). However, this first temperature rise must not be mistaken for the smoke layer interface, as it is not (Fig. 4.2, right). Therefore, the criterion developed to determine the smoke layer interface should take this into account.

Four different methods for the determination of the smoke layer interface are discussed.
A first method to determine the interface height of the smoke layer is the equation developed by Thomas et al. [10]:

$$H_a - z_{\text{int}} = \frac{\int_0^{H_a} \frac{T - T_0}{T} dz}{\frac{T_{av,s} - T_0}{T_{av,s}}}. \tag{4.6}$$

The integration in this formula is performed using the temperatures from the numerical simulations. However, there is a major disadvantage: the equation implies an iterative procedure. Indeed, the smoke layer interface height is on the left hand side of the equation (z_{int}), but in order to calculate this, the average temperature of the smoke layer is needed ($T_{av,s}$), which can only be calculated if the interface height is already known. This makes the 'Thomas method' a time consuming procedure.

A second method, described in the FDS user guide [4], relies on a calculation method by He et al. [11]. First, the parameters I_1 and I_2 are calculated on a vertical line. The temperature T_l is chosen as the lowest temperature on this vertical line. From this, the value of z_{int} can be calculated:

$$I_1 = \int_0^{H_a} T dz \text{ and } I_2 = \int_0^{H_a} \frac{1}{T} dz \tag{4.7}$$

$$z_{\text{int}} = \frac{T_l\left(I_1 I_2 - H_a{}^2\right)}{I_1 + I_2 T_l^2 - 2H_a T_l} \tag{4.8}$$

The third option relies on the second derivative of the temperature profile. Fig. 4.3 reveals that this might indeed be used to indicate the smoke layer interface height. Using a central scheme to calculate this second derivative at height $z = z_k$ (where k is the index of the computational cell in the vertical direction, $z_k = k\,\Delta z$), divided by the local temperature difference:

$$\frac{\partial^2 T}{\partial z^2 \Delta T} \approx \frac{T_{k-1} - 2T_k + T_{k+1}}{\left(\Delta z\right)^2 \left(T_k - T_0\right)}, \tag{4.9}$$

a local maximum of the second derivative can indeed indicate the smoke layer interface (Fig. 4.3, left). However, this is a local maximum. Indeed, at the first temperature rise in the atrium, around z = 0.6 m (see Fig. 4.1), a much higher value of second derivative is found. Therefore, it is up to the user to define whether the local maximum corresponds to the smoke layer interface height, and it requires a visual detection. Thus, the method of the second derivative is not unambiguous and cannot easily be made automatic.

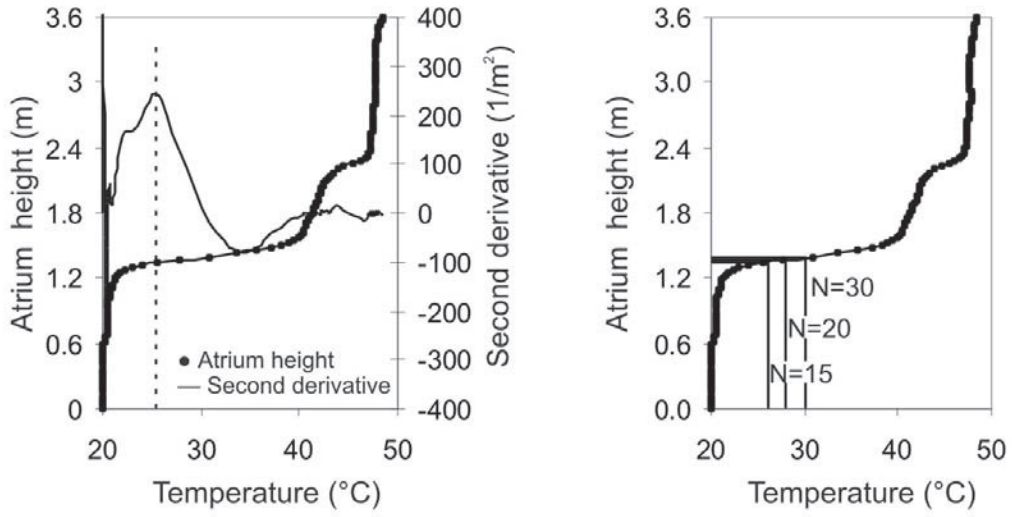

Figure 4.3 Second derivative of temperature in the atrium (left) and N-percent rule in atrium (right).

As final method the determination of the smoke layer interface height by the N-percent rule [12] is considered. An interface temperature is then defined by the following formula:

$$T_{\text{int}} = T_0 + \left(T_{\max} - T_0\right)\text{N}/100 \tag{4.10}$$

In the example of Fig. 4.3, the variation of z_{int} with N is moderate (between 1.3 m and 1.5 m) in the range 10 < N < 65. The value N = 30 is chosen (equivalent to z_{int} = 1.4 m in Fig. 4.3, right). The difference in interface height between values reported elsewhere for N (N = 10, 15, 20 [13]) with N = 30 is very small in the study under consideration. The main reason for choosing the value N = 30 is to avoid that the temperature rise around z = 0.6 m be mistaken for the smoke layer interface height in any of the cases. This method is an easily applicable and unambiguous way to determine the smoke layer interface height in the atrium. An important advantage of this method is that it is not time-consuming and can easily be used in the post-processing of simulation data.

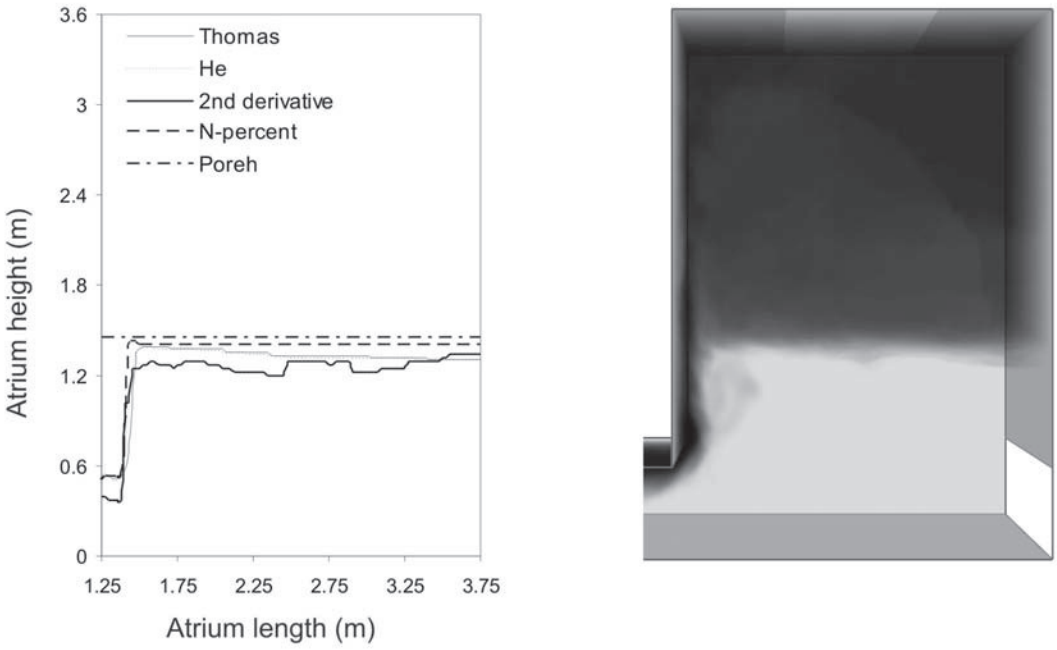

Figure 4.4 Interface height in the atrium.

Fig. 4.4 displays the smoke layer interface height as obtained with each of the four methods. The results are compared to the height, obtained from Eq. (4.1) with the imposed smoke extraction mass flow rate and fire heat release rate. The first three methods result in an underestimation of the smoke-free height in the atrium compared to the experimental value. The N-percent method, with N = 30, provides a better approximation of the calculated interface height. This trend was also observed with other fire heat release rate values and smoke extraction flow rates (not shown). Therefore, the N-percentage method is used from now on to determine the smoke layer interface height in the simulations.

4.2.4 Numerical simulation results

Table 4.2 provides a quantitative overview of the CFD simulation results.

In every simulation, the convective heat release rate ($\dot{Q}_{conv}$) is imposed in the adjacent room, as well as the outlet velocity (v_{out}) at the ceiling of the atrium. The other important values of the simulations are then calculated:

- d_s, the thickness of the smoke layer emerging from the adjacent room, is calculated with the N-percent method in the plane x = 1.25 m, i.e. the vertical plane of the opening between the room and the atrium (Fig. 4.1).
- $\dot{m}_s$, the mass flow rate of the emerging smoke layer, is calculated in the same plane as d_s. A summation is made over all cells in the plane, only taking into account outflow, $v_{x,n} > 0$, not the inflow of air into the adjacent room:

$$\dot{m}_s = \sum_n \max\left(\rho_n \cdot v_{x,n} \cdot A_n ; 0\right) \tag{4.11}$$

- $\dot{m}(z_s)$, the extraction mass flow rate, at the ceiling of the atrium, is calculated in a similar way as $\dot{m}_s$, considering now only the cells in the outlet opening:

$$\dot{m}(z_s) = \sum_n \left(\rho_n \cdot v_{out,n} \cdot A_n \right) \tag{4.12}$$

- z_s, the smoke free height above the spill edge in the atrium, is calculated with the N-percent method in the vertical symmetry plane in the atrium (y = 0.45 m).
- z_o, the virtual origin, is calculated from the above values with Eq. (4.3).

Table 4.2 Simulation results in the small-scale atrium.

$\dot{Q}_{conv}$ (kW)	d_s (m)	$\dot{m}_s$ (kg/s)	z_s (m)	$\dot{m}(z_s)$ (kg/s)	z_o (m)	$z_s + z_o$ (m)	$\dot{m}(z_s) / \dot{Q}_{conv}^{1/3}$ kg/(s kW$^{1/3}$)
2.887	0.12	0.052	0.25	0.094	0.65	1.50	0.06
2.887	0.12	0.052	0.53	0.12	0.65	1.78	0.08
2.887	0.12	0.057	0.68	0.14	0.69	1.97	0.10
2.887	0.12	0.051	0.78	0.15	0.63	2.01	0.11
5.377	0.13	0.067	0.28	0.12	0.68	1.55	0.07
5.377	0.12	0.062	0.50	0.14	0.63	1.73	0.08
5.377	0.12	0.062	0.80	0.18	0.63	2.03	0.10
5.377	0.12	0.060	1.00	0.21	0.62	2.22	0.12
8.792	0.13	0.075	0.23	0.13	0.65	1.48	0.06
8.792	0.12	0.071	0.85	0.22	0.62	2.07	0.11
8.792	0.13	0.072	1.19	0.30	0.63	2.42	0.15
8.792	0.14	0.080	1.59	0.38	0.70	2.89	0.18
11.901	0.13	0.078	0.34	0.15	0.62	1.55	0.07
11.901	0.13	0.078	0.90	0.25	0.62	2.12	0.11
11.901	0.13	0.082	1.42	0.38	0.65	2.66	0.17
11.901	0.14	0.082	1.62	0.42	0.65	2.87	0.18

Figure 4.5 depicts these results in a graph. The numerical results (black dots) are in very good agreement with the experimental data (open

symbols) and with Eq. 4.1 (black line). This is very promising for the use of CFD simulations as 'numerical experiments'.

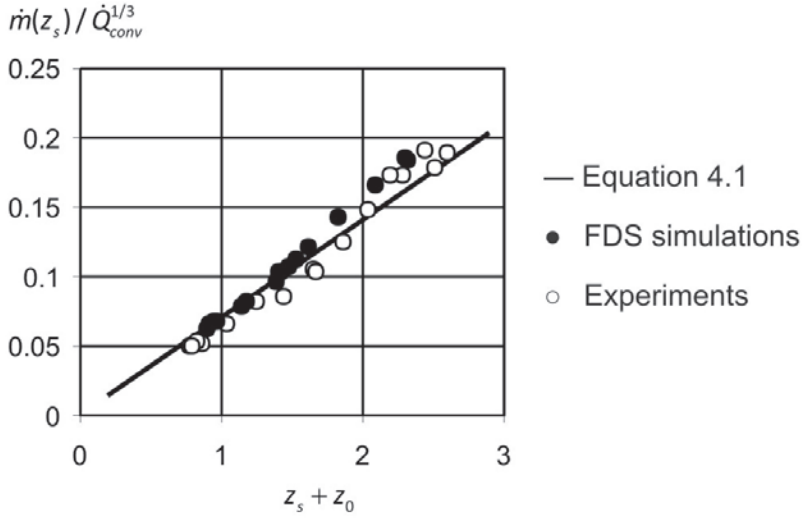

Figure 4.5 Experimental and CFD results of smoke mass flow extraction rate as function of rise height.

As using computational codes to solve fire-related problems is still a quite recent research topic, all available CFD-codes are continuously under development. Each new release of a code therefore contains even better algorithms, new developments and extra included options. Care must be taken that simulation results are not very sensitive to the version of the CFD package used. In the process of the research, FDS was upgraded to version 5. Fig. 4.6 shows that differences with results of FDS, version 4, are very small, so that the argument that CFD simulations can be used as 'numerical experiments', does not depend on the version used here.

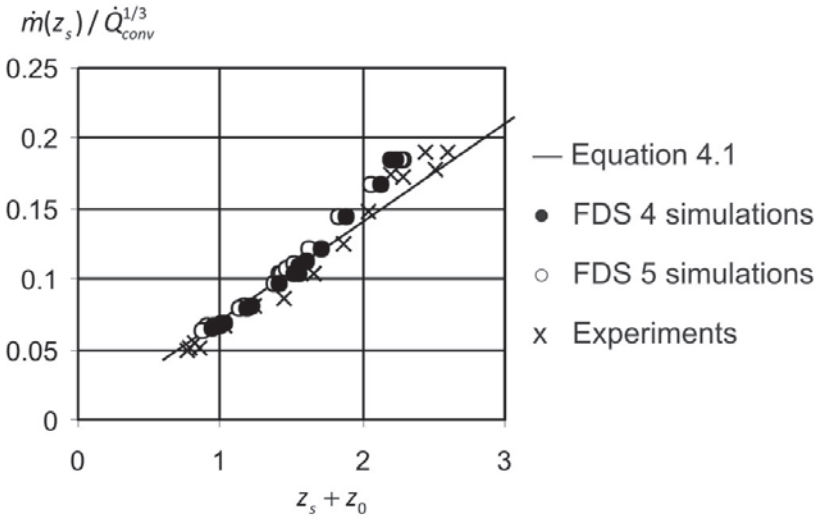

Figure 4.6 Comparison of FDS 4 and FDS 5 numerical results with experiments.

4.3 Tunnel

4.3.1 Introduction

In tunnel configurations with mechanically forced longitudinal ventilation, a key parameter is the critical velocity. This is the minimum velocity required to prevent backlayering in the tunnel, i.e. there is no smoke flow in the opposite direction of the ventilation. The possible hazard of fire spread due to ventilation is not considered here [14].

A paper by Wu and Bakar [2] describes a set of experiments on five small-scale tunnels. Only 'tunnel D', which has a rectangular cross-section, is discussed here. Having the lowest height (0.25 m) to width (1 m) aspect ratio in the series of [2], this tunnel is most similar to a closed car park, the configuration studied in Chapter 5. The Wu and Bakar tunnel experiments are an extensive study of the variation of critical velocity with heat release rate in tunnels. The low aspect ratio of tunnel D is especially interesting to validate the numerical simulations for the study of car parks. The formula for critical velocity that was derived by Wu and Bakar from their experiments is still widely used for tunnel ventilation design.

Other numerical studies have already been reported with validation of the simulations by comparing with the Wu and Bakar experiments (e.g. [15]). Below, the application of the N-percent rule is specifically discussed, as well as the possibility of using adiabatic wall conditions in combination with absence of radiation modelling.

4.3.2 Configuration and set-up

The simulations are performed with FDS, version 5.2.5. The tunnel is, as mentioned, 0.25 m (high) by 1 m (wide) by 5 m (long). The computational mesh consists of 640 000 cubic cells of size 1.25 cm.
Two different sets of CFD simulations are performed (73 in total). In the first set, the total (steady) fire heat release rate is imposed and standard FDS radiation modelling and thermal boundary conditions are applied. For radiative heat transfer in FDS, a radiation transport equation for a grey gas is solved. The source term in this transport equation is radiation intensity, described by Planck's law [3,4]. As the radiation intensity defined by Planck's law is highly temperature dependent ($I_b \sim T^4$) (cfr. Eq. (2.10)), small temperature over- or underestimations can lead to large differences in radiation. Therefore, one could consider excluding uncertainties from radiation modelling by only inserting the steady convective heat release rate into the domain. As radiation from the fire mainly heats up the walls, the walls are set to adiabatic in the simulations without radiation. Otherwise, too much of the (convective) heat from the fire would be used in heating up the walls. This approach is followed in the second set of simulations.
Propane is used as fuel in the simulations, as in the experiments [2].
Again, the standard Smagorinsky model with C_S = 0.2 (default in FDS) is used. In [15], it is shown that the influence of the exact value on the results is not large (as long as it does not deviate too strongly from the default value).
A constant velocity is imposed over the entire inlet surface of the tunnel, upstream of the fire.

A quasi steady-state is reached in the simulations after about 120 s for the lowest heat release rate studied. Time-averaged values, determined between 160 s and 180 s, are presented as simulation results for temperature, density and velocity. From previous work [16], a maximum value of turbulent time scale of 5 s was found for RANS simulations of the same set-up. Again, the averaging period is much larger than the turbulent time scales.
In each simulation, a constant velocity (v_{in}) is imposed over the entire inlet area of the tunnel. For each inlet velocity, the corresponding backlayering distance is calculated in the simulations by using the N-percent method (Eq. (4.10)) on the horizontal centre line at ceiling level (with N = 5). Due to the low value of N, a small temperature increase will already result in the detection of the smoke layer at ceiling level, comparable to the use of thermocouples in the original experiments [2].

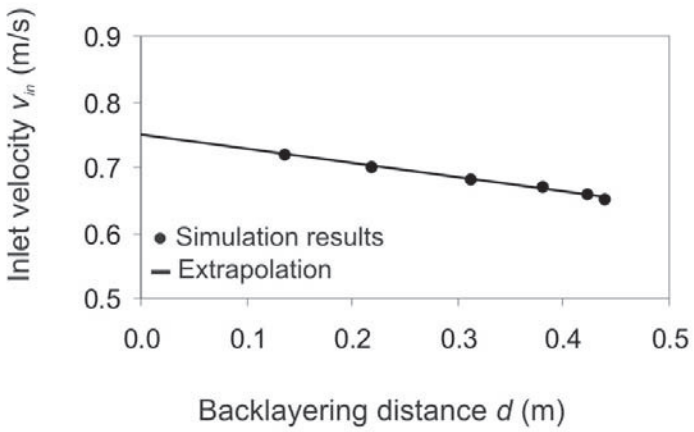

Figure 4.7 Extrapolation to determine critical velocity in tunnel D with heat release rate 22.5 kW (with standard FDS radiation modelling).

Extrapolation of these backlayering distances results in the critical velocity, corresponding to a backlayering distance of 0 m for each heat release rate (Fig. 4.7). This method is identical to what is described in the experiments performed by Wu and Bakar [2].

4.3.3 Simulation results

Table 4.3 lists the experimental data and simulation results for the critical velocity, corresponding to each studied heat release rate with default FDS radiation modelling and thermal boundary conditions.

Table 4.3 Critical velocities with corresponding heat release rates (default settings, χ_r obtained from simulations).

$\dot{Q}$ (kW)	v_{cr} experiments [2] (m/s)	v_{cr} FDS simulations (m/s)	radiative fraction χ_r (%)
1.5	0.34	0.38	37
3.0	0.40	0.47	39
7.5	0.50	0.61	43
10.5	0.54	0.67	44
12.0	0.56	0.68	45
15.0	0.59	0.70	46
22.5	0.65	0.75	48

For every heat release rate, the radiative fraction χ_r as found in the simulations is also listed. This is the fraction of heat loss through radiation to the total heat release rate of the fire:

$$\chi_r = \frac{\dot{Q}_{rad}}{\dot{Q}} \text{ and } \dot{Q} = \dot{Q}_{conv} + \dot{Q}_{cond} + \dot{Q}_{rad}, \tag{4.13}$$

with $\dot{Q}$, $\dot{Q}_{conv}$, $\dot{Q}_{cond}$ and $\dot{Q}_{rad}$ the total heat release rate and convective, conductive and radiation heat losses respectively. The radiation heat loss is calculated by integrating the directional radiation intensity over a default number of angles and over the entire domain boundaries [3,4]. In the simulations, the resulting radiative fraction increases with increasing heat release rate from 37% up to 48%.

Table 4.4 Critical velocities with corresponding heat release rates (adiabatic simulations, χ_r = 0.43 assumed for calculation of $\dot{Q}$).

$\dot{Q}_{conv}$ (kW)	$\dot{Q}$ (kW)	v_{cr} (m/s)
1.0	1.7	0.37
2.0	3.4	0.46
4.9	8.6	0.62
6.8	12.0	0.67
7.8	13.7	0.67
9.8	17.1	0.70
14.6	26.7	0.73

Table 4.4 shows the results for the critical velocity in the simulations without radiation losses and with adiabatic walls. The imposed heat release rate in the numerical simulations now corresponds to the convective heat release rate. Estimating the radiative loss fraction at χ_r = 0.43 (Table 4.3), the corresponding total heat release rate can be calculated.

Fig. 4.8 summarizes the results. The picture reveals two aspects.
Firstly, the simulations with the default settings and the simulations without radiation modelling provide very similar results. This shows that the approach of imposing the convective heat release rate in the numerical simulations, turning off radiation modelling and treating the walls as adiabatic, is valid for the test case under study.

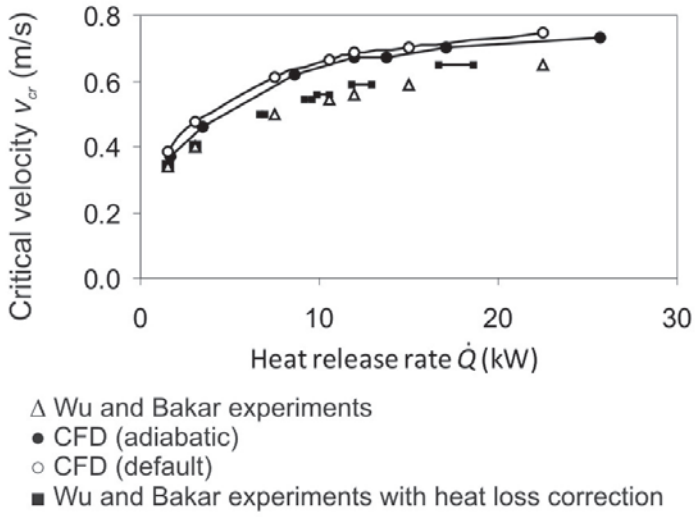

Figure 4.8 Experimental and numerical results for v_{cr} in tunnel D. The squares represent the possible effect of heat loss in the experiments by cooling of the ceiling near the fire.

The second observation is that, whereas the trend for the critical ventilation velocity as function of total heat release rate is very well reproduced, the simulation results overestimate the absolute value of the critical velocity, in line with [16], where tunnel B was examined. A difference, defined as the ratio of the deviation between experimental value and simulation value to the experimental value, of about 25% is found between the experimental and numerical results. This deviation might be due to extra water cooling of the tunnel in the neighbourhood of the fire in the experimental set-up, as mentioned in [2]: when the tunnel walls reached "high" temperatures, they were cooled with water. As this cooling extracts heat from the tunnel, the experimentally measured critical velocity for a "given" fire heat release rate, in fact corresponds to a lower heat release rate value than what is imposed at the burner. The latter value is applied in the numerical simulations. Unfortunately, no details on the water cooling are provided in [2]. Therefore, the temperature from the CFD results is used to estimate from what heat release rate value onwards, cooling was applied. Table 4.5 shows the maximum temperatures $T_{\max}$ near the ceiling in the numerical simulations. In the experiments, it can be suspected that as

the tunnel walls near the fire are made of stainless steel, cooling was almost certainly applied when the heat release rate exceeded 10.5 kW and perhaps already at 7.5 kW.

The heat loss by cooling is estimated as follows. The steel area of the ceiling of the experimental tunnel set-up is A_c = 2.4 m^2. The convection coefficient at the inside of the tunnel is estimated as h = 10 W/m^{2}K to h = 15 W/m^{2}K. Cooling is assumed from the temperatures, obtained in the CFD simulations (i.e. without the water cooling), to 100°C, the boiling temperature for the water at the outside of the tunnel. This implies neglect of thermal resistance caused by conduction in the stainless steel, which indeed has a high conductivity. The heat, removed per unit time from the configuration by the water cooling, can then be calculated as:

$$\dot{Q}_{loss} = h \cdot \int_{A_c} \max\left(T - 373; 0\right) dA \,. \qquad (4.14)$$

A correction of the experimental heat release rate in this sense clearly brings the experimental results closer to the numerical simulation results. A similar argument was provided in a recently published paper by Li [17], where critical velocities in tunnel experiments are also somewhat higher than in the Wu and Bakar tunnel experiments.

The corresponding values for this estimated heat loss are listed in Table 4.5, and indicated with squares in Fig. 4.8.

Table 4.5 Maximum temperatures near the ceiling found in the numerical simulations.

$\dot{Q}$ (kW)	1.5	3.0	7.5	10.5	12.0	15.0	22.5
T_{max} (K)	381	420	615	803	864	923	1136
$\int_{A_c} \left(T - 373\right) dA$ (m^{2}K)			54	93	147	215	387
$\dot{Q}_{loss}$ (kW)			0.5 – 0.8	0.9 – 1.4	1.5 – 2.2	2.2 – 3.2	3.9 – 5.8

The observation that the trend of the dependence of the critical velocity on the fire heat release rate is well reproduced in the numerical simulations and that deviations – after the correction as described – are

less than 10%, allows to conclude that the simulation results are in satisfactory agreement with experimental data for this tunnel configuration.

4.4 Conclusions

Small-scale experiments of fire in an atrium and a tunnel were repeated as numerical CFD simulations. Both cases concern smoke movement and the formation of a quasi steady-state smoke layer.

Several criteria to define the smoke layer interface were studied, of which the N-percent rule (with N = 30) prevails, as it provides results in good agreement with experiments and it is the most unambiguous method.

For the atrium configuration, very good agreement was found between the experimental and numerical results.

In the tunnel simulations, calculations without radiation modelling and using adiabatic walls proved to be a valid alternative for more time-consuming simulations with radiation modelling. Quite good agreement was found between experimental and numerical results, especially when considering the heat loss due to water cooling in the experiments.

An overall conclusion is that the prediction of the quasi steady-state smoke region by CFD is good, especially when the experiments are well documented. Therefore, it is argued that a parameter variation study with numerical simulations within similar configurations is very useful to obtain qualitative results, a good prediction of the trends and insight into the physics of the configurations at hand.

4.5 References

[1] Poreh M, Marshall NR, Regev A, Entrainment by adhered two-dimensional plumes, Fire Safety J. 43: 344-350 (2008)

[2] Wu Y, Bakar MZA, Control of smoke flow in tunnel fires using longitudinal ventilation systems – a study of the critical velocity, Fire Safety J. 35: 363-390 (2000)

[3] McGrattan K, Hostikka S, Floyd J, Baum H, Rehm R, Mell W, McDermott R, Fire Dynamics Simulator (Version 5) Technical Reference Guide, NIST 1018-5, National Institute of Standards and Technology (2008)

[4] McGrattan K, Klein B, Hostikka S, Floyd J, Fire Dynamics Simulator (Version 5) User's Guide, NIST 1019-5, National Institute of Standards and Technology (2008)

[5] Tilley N, Rauwoens P, Merci B, Verification of the accuracy of CFD simulations in small-scale tunnel and atrium fire configurations, Fire Safety J. 46: 186-193 (2011)

[6] Harrison R, Spearpoint M, Physical scale modelling of adhered spill plume entrainment, Fire Safety J. 45: 149-158 (2010)

[7] Kumar S, Cox G, Thomas PH, Air entrainment into balcony spill plumes, Fire Safety J. 45: 159-167 (2010)

[8] Smagorinsky J, General Circulation Experiments with the Primitive Equations. I. The Basic Experiment, Monthly Weather Review 91: 99-164 (1963)

[9] McGrattan KB, Baum HR, Rehm RG,Large Eddy Simulations of Smoke Movement, Fire Safety J. 30: 161-178 (1998)

[10] Thomas PH, Hinkley PL, Theobald CR, Simms DL, Investigations into the flow of hot gases in roof venting. Fire research technical paper no.7, London: The Stationary Office (1963)

[11] He Y, Fernando A, Luo M, Determination of interface height from measured parameter profile in enclosure fire experiment, Fire Safety J. 31: 19-39 (1998)

[12] Cooper LY, Harkleroad M, Quintiere J, Reinkinen W, An Experimental Study of Upper Hot Layer Stratification in Full-Scale Multiroom Fire Scenarios, J. of Heat Transfer 104: 741-749 (1982)
[13] Chow W, Determination of the Smoke Layer Interface Height for Hot Smoke Tests in Big Halls, J. of Fire Science 27: 125-142 (2009)
[14] Beard A, Carvel R, The handbook of tunnel fire safety, Thomas Telford Services Ltd, London (2005)
[15] Hwang CC, Edwards JC, The critical ventilation velocity in tunnel fires – a computer simulation, Fire Safety J. 40: 213-244 (2005)
[16] Van Maele K, Merci B, Application of RANS and LES field simulations to predict the critical ventilation velocity in longitudinally ventilated horizontal tunnels, Fire Safety J. 43: 598-609 (2008)
[17] Li YZ, Lei B, Ingason H, Study of critical velocity and backlayering length in longitudinally ventilated tunnel fires, Fire Safety J. 45: 361-370 (2010)

5 Chapter 5
Smoke extraction in closed car parks

5.1 Introduction

In order to facilitate fire service interventions and to prevent excessive damage in car parks in case of fire, a smoke and heat control (SHC) system is usually installed. A common practice principle concerns the use of mechanical horizontal ventilation. Such a system extracts hot smoke from one or more points of the car park to (partly) keep the car park clear from smoke and to limit smoke temperatures in the car park.
At first sight, there is similarity with longitudinal ventilation in tunnels, for which formulae have been developed for critical velocity, as presented in Chapter 3, Eqs. (3.1) to (3.11). The critical velocity is the minimum velocity required to keep all the smoke in the downstream direction of the fire. In tunnels, the critical velocity is usually defined as an inlet velocity of cold air into the tunnel.

Car parks, however, have a substantially different height to width aspect ratio, compared to tunnels. While in tunnels the width and height are usually of the same order of magnitude, and much smaller than the length ($w \approx h < l$), in car parks the height is usually much smaller than the width and length ($h < w, l$) (Fig. 5.1). Consequently, application of formulae that were developed for tunnels, becomes questionable for car parks.

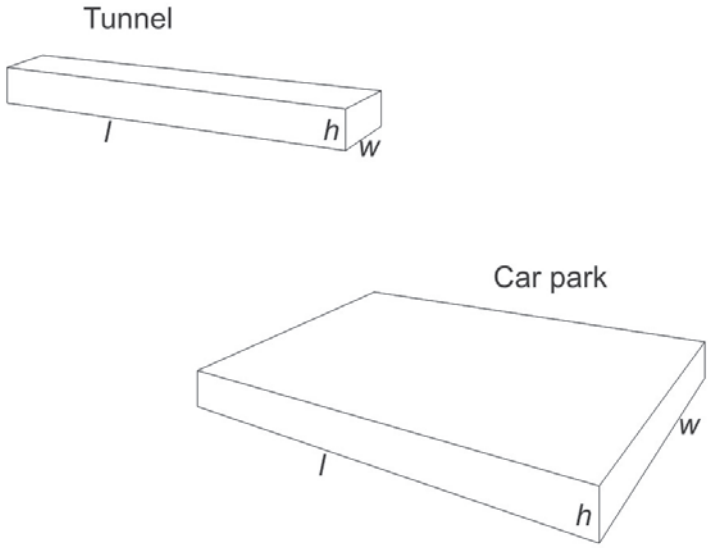

Figure 5.1 Difference in aspect ratios between tunnels ($w \approx h < l$) and car parks ($h < w, l$).

Due to the large width, complex flow patterns can occur in car parks, whereas the flow in tunnels is essentially uni-directional. In [1] it is correctly stated that SHC in car parks cannot be characterized by a single quantity (like ventilation velocity), precisely because of the possibility of complex flow patterns (such as stagnation or recirculation regions). In the present study, though, we only focus on uni-directional flows (Fig. 5.2). In [2,3] flow pattern issues are also discussed.

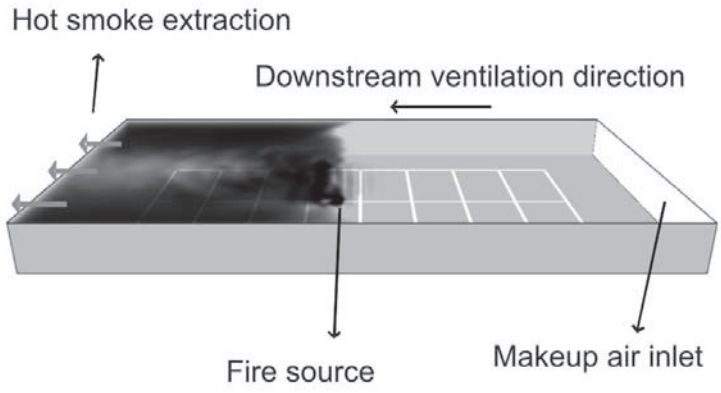

Figure 5.2 Principle of critical horizontal velocity in a car park.

Furthermore, in car parks, usually some backlayering is allowed, e.g. [4-6], meaning that smoke is allowed to travel in the upward direction of the ventilation flow, up to a specified distance. The reason is that the primary design objective for smoke ventilation in car parks is typically not evacuation of people, but to allow for fire services to approach the fire to within a certain distance (typically 10 to 15 m). Consequently, backlayering up to that distance is allowed.
Other than in tunnels, where cold air is often pushed into the tunnel as means of ventilation, in car parks hot smoke is usually extracted by the ventilation system. As the density of this hot extracted smoke is always lower than that of cold entering air, the extraction ventilation velocity will be higher than the incoming cold air velocity, according to conservation of mass. It is important to account for this difference in the design of the ventilation system.

Because of the three above explained differences between car park and tunnel ventilation (aspect ratio – backlayering – extraction ventilation system), an extensive study has been performed with Computational Fluid Dynamics. These CFD simulations are applied as "numerical experiments" and used as input to develop a simple analytical formula for the required ventilation velocity, depending on the circumstances. In Chapter 4, research covering more than 70 CFD simulations, has already confirmed that CFD results, provided they are performed appropriately, are reliable in a small-scale tunnel configuration. In the present chapter, we adopt the same strategy as in Chapter 4. In addition hereto, we illustrate good agreement for a full-scale experimental car park fire set-up, described in [2]. In [3], an extensive study is presented, illustrating good agreement of CFD with a large set of full-scale experiments, particularly for uni-directional flow patterns, as is the case here. The reader is referred to those documents for more detail. Thus, there is sufficient confidence to use the CFD simulations for the development of the analytical formulae for required ventilation velocity in car parks, corresponding to a certain smoke backlayering distance. It is recalled that the formulae will only be valid for uni-directional flows.

The present study concerns more than 350 CFD simulations. Four parameters are varied: the convective fire heat release rate (HRR) per unit area (PUA) ($\dot{q}''_{conv}$), the fire source area (A_F), the car park height (h) and the car park width (w).
Post-processing of all these simulations results in:
- an analytical formula for the critical inlet velocity in the car park ($v_{cr,in}$) in terms of the four parameters mentioned,
- an expression to account for the difference between inlet (v_{in}) and outlet (v_{out}) velocity in the car park, derived from simple fire dynamics theory and confirmed with simulation results, and
- an analytical formula for the required ventilation velocity in the car park when a certain backlayering distance (d) is allowed, expressed as deviation from the critical velocity.

The car park is empty in all configurations. Whereas this might seem strange at first sight, as cars are needed to have a car on fire, the reason for this choice is that this is the basic assumption in current standards for smoke and heat control in standards (e.g. [4,5]). Since the present study intends to serve as input for the further development and improvement of such standards, the assumption of empty car park is adopted. Obvious advantages, compared to the addition of cars as blockages in the car park, are the simplification of the setup, as well as the clarity in setup definition. Indeed, when cars are to be added, the question immediately rises as to where to do so. Beyond any doubt, the addition of cars affects the flow pattern, in the sense that recirculation regions appear behind cars and pressure losses are introduced, definitely when a (large) car is positioned close to a smoke extraction point. Such effects reduce the effectiveness of a smoke extraction system. On the other hand, as the cars are standing on the floor, the ventilation air is forced into a more narrow region in between the ceiling and the top of the car, rather than the area between ceiling and floor. Therefore, for the same volume flow rate, the air velocity, and thus momentum, increases, assisting the pushing of the smoke into a certain direction. To the best of my knowledge, it has not yet been investigated

in a systematic manner whether the assumption of an empty car park is conservative or not, in the context of development of standards. Such an investigation is not within the scope of the present study. The goal here is to develop a relationship for the required ventilation velocity, with the assumption of an empty car park, to support the development of smoke and heat control standards for large car parks.

5.2 Setup of the simulations

In the simulations, a basic configuration of the car park is chosen. In this configuration, the car park is 16 m wide, 2.4 m high and 32 m long. The ceiling is flat and the fire is located centrally in the car park. It has dimensions 5 m x 5.2 m. The convective heat release rate of the fire is $\dot{q}''_{conv}$ = 152.5 kW/m^2. Thus, the total fire has a source area of A_F = 26 m^2 and convective heat release rate of 4 MW, a value of the order of magnitude as used in standards regarding car park fire safety [4-6].

The entire rear wall of the car park is modelled as smoke extraction. In doing so, the simulated car park is regarded as a representative part of a longer car park, assuming that effects on the flow field near the fire, of the ventilation system further downstream, are negligible. In the full-scale experiments of [2] e.g., it has been confirmed that the exact position of the extraction fans in the car park, positioned even less than 15 m downstream of the fire source, does not affect the smoke backlayering pattern.

The front wall of the car park is entirely open in all simulations, so makeup air can freely enter the car park (Fig. 5.2) and the ventilation air flow pattern is essentially uni-directional.

In the simulations, only one of the four parameters of the basic configuration is varied at a time. The ranges of values for the parameters are listed in Table 5.1.

Table 5.1 Variation limits of the four parameters.

parameter	$\dot{q}''_{conv}$ (kW/m^2)	A_F (m^2)	h (m)	w (m)
minimum value	46	1	1.2	8
maximum value	1419	26	3	43.2
basic configuration	152.5	26	2.4	16

The simulations have been performed with FDS (Fire Dynamics Simulator, version 5.2.5 [7,8]). Good agreement between small-scale experiments and simulations for a tunnel configuration has been shown in Chapter 4. Similar settings for the simulations are used in the present chapter. The size of the mesh cells is particularly important.
Cells are of size 20 cm x 20 cm x 10 cm in all simulations here, resulting in a grid of 307,200 cells in the basic configuration that was mentioned above. The characteristic length scale of the fire, calculated as

$$D^* = \left(\frac{\dot{Q}}{\rho_o T_o c_p \sqrt{g}} \right)^{2/5}, \qquad (5.1)$$

results in a value D^* = 2 m for a total fire heat release rate of 6 MW. The criterion of [9] of having at least 10 cells within the characteristic diameter is thus satisfied. In Chapter 4, meshes with 10 cells within D^* were also used, leading to good agreement between simulations and experiments.

With respect to the quality of the computational grid, the discussion held in section 4.2.2 again holds. The D^* criterion may not be sufficient, since other
characteristic length scales are also present in the car park configuration: the ceiling jet and the smoke layer thickness. The ceiling jet is now an important feature of the smoke dynamics, but missing the details need not imply a substantial loss in accuracy regarding the smoke backlayering distance (particularly when a smoke backlayering

distance of 15 m is allowed, i.e. one is not directly interested in the near-field region of the fire).

The quality of the computational grid is again illustrated by means of a comparative study of the simulation results to experimental data (as done in Chapter 4) and a grid refinement study, as presented below.

Another grid has been studied with cell size 16 cm x 16 cm x 5 cm. Temperature profiles, averaged over 20 s within the quasi-steady-state regime of a simulation of the basic configuration with extraction velocity v_{out} = 2.0 m/s are shown in Fig. 5.3 (top view) and Fig. 5.4 (symmetry plane). The pictures show temperatures in a plane underneath the ceiling (at z = 2.3 m) and in the symmetry plane of the car park (x = 8 m), respectively.

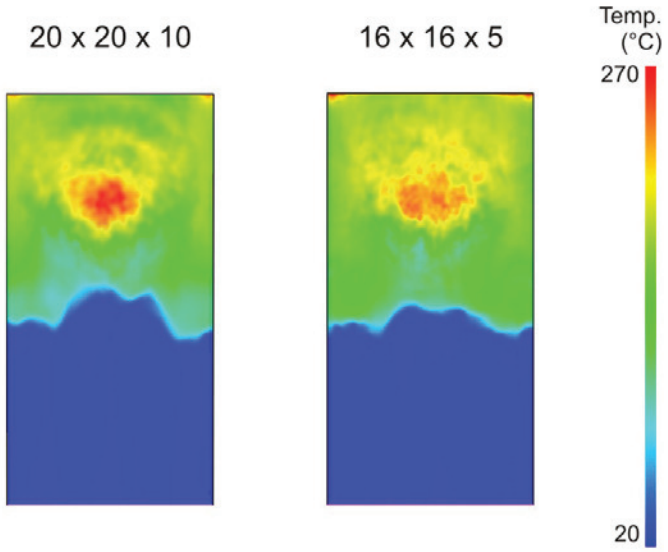

Figure 5.3 Grid refinement in car park: temperatures at z = 2.3 m. Cell sizes in [cm x cm x cm].

The figures show practically identical backlayering distances in the two simulations. In the simulation on the finer mesh, finer structures are seen within or near the fire and at the lower edge of the smoke layer. While differences are very clearly observed, especially near the fire, the influence on the smoke backlayering distance is small. As this distance is the key output from the simulations in the present study, the 20 cm x 20

cm x 10 cm grid in here considered as sufficiently fine and this grid is used in the remaining simulations.

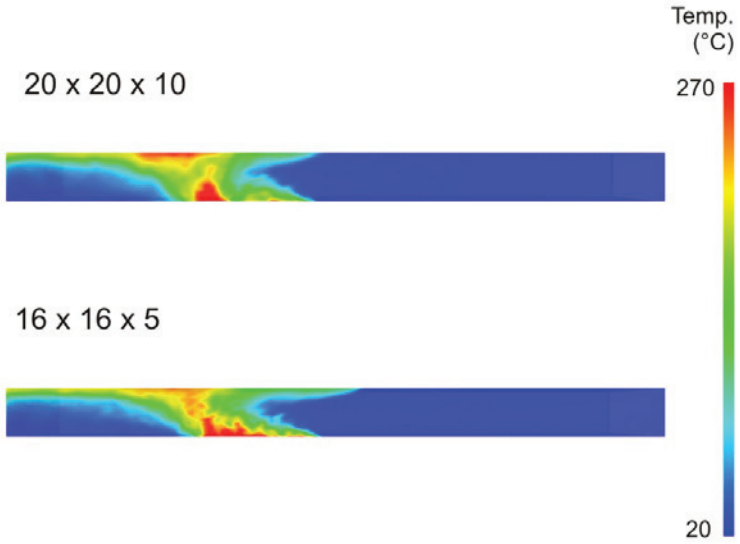

Figure 5.4 Grid refinement in car park: temperatures at x = 8 m. Cell sizes in [cm x cm x cm].

As in Chapter 4, the standard Smagorinsky LES turbulence model [10] with Smagorinsky constant C_s = 0.2 is used. The Prandtl number has the constant default value 0.7.

Radiation is turned off in the simulations. The total heat release rate is specified in the simulations, together with a radiative fraction (χ_r): the convective heat release rate is imposed, with $\dot{q}''_{conv} = (1-\chi_r)\dot{q}''$, and uncertainties due to radiation modeling are avoided. In the simulations presented here, the radiative fraction is equal to χ_r = 0.34, in agreement with e.g. [4,5].

All walls are modelled as adiabatic, so that there is no additional heat loss through the structure. In the context of tunnels, Chapter 4 has shown that the approach of imposing the convective heat release rate in the numerical simulations, turning off radiation modelling and treating the walls as adiabatic, is valid.

It is also important to appreciate that LES are unsteady in nature. Therefore, it is important to discuss the simulation results in terms of 'averages'. All simulations have been executed until a quasi-steady-state situation is reached. The results have been time averaged over a period

of 20 s in the quasi-steady state regime. These averages are presented below as the 'simulation results'.

5.3 Results

Within this section, the post-processing procedure is first explained. In a second part, an analytical formula is constructed for the critical inlet velocity in terms of the four parameters. The third section concerns the difference between inlet velocity (of cold air) and outlet velocity (of hot smoke). Finally, smoke backlayering up to a certain distance from the fire source is discussed and a relation for the corresponding ventilation velocity is derived.

5.3.1 Post-processing procedure

In the simulations, an outlet velocity is imposed at the rear end of the car park, over the entire cross-section. However, it is more interesting to define a critical inlet velocity – in terms of the four varied parameters – in order to compare the derived equation to the formulae that have already been developed for critical inlet velocity in tunnels. The inlet velocity in the simulations is determined as the average inlet velocity over the entire cross-section of the inlet opening.

As mentioned, quasi-steady state values are averaged over time, more specifically between 160 s and 180 s after the start of the simulations. The initial conditions correspond to still air at ambient temperature (T_0 = 20°C). At time t = 0 s, the fire convective heat release rate value is immediately imposed as steady value.

In order to determine the backlayering distance, the N-percent rule [11] is used. At ceiling height, on the longitudinal centreline of the car park, the interface temperature is defined as

$$T_{\mathrm{int}} = T_0 + \left(T_{\max} - T_0\right)\mathrm{N}/100\,. \tag{5.2}$$

T_{max} is the maximum temperature found on the centreline in the averaged results. The relatively low value N = 10 is used, since a small

temperature increase on the centreline indeed indicates smoke backlayering and the backlayering distance does not change much in the range N = 5 – 20 (Fig. 5.5). This corresponds to the method, often used in experiments, where thermocouple data indicate presence of smoke.

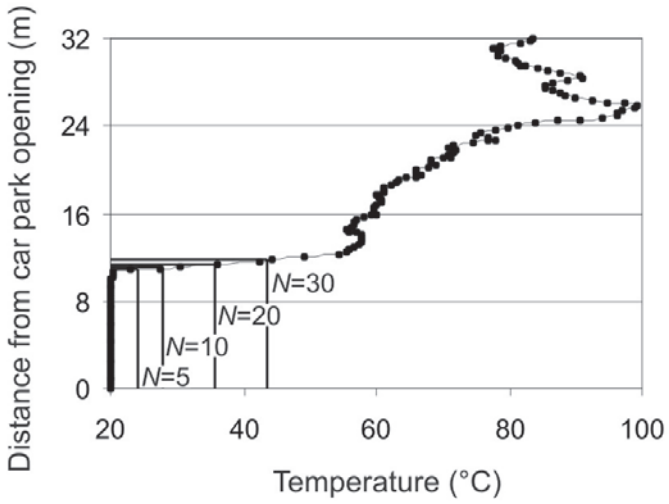

Figure 5.5 Backlayering distance variation with the value of N in the N-percent rule on centerline temperature data.

The critical inlet velocity ($v_{cr,in}$) is then defined as the velocity for which the backlayering distance is d = 0 m. It is computed by linear extrapolation of backlayering distance values as function of inlet velocity (Fig. 5.6). In e.g. [12], the same method has been applied to tunnel experiments.

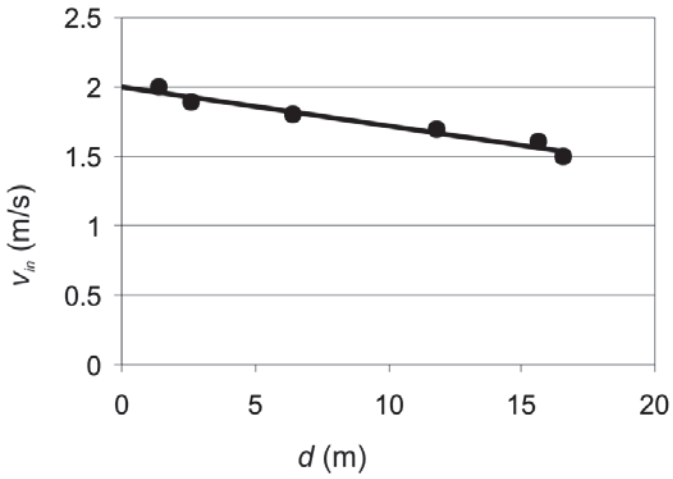

Figure 5.6 Linear extrapolation of backlayering distance to calculate the critical inlet velocity.

5.3.2 Critical inlet velocity

In this paragraph, an analytical formula for the critical inlet velocity ($v_{cr,in}$) in car parks is constructed in terms of the four varied parameters. In the figures below, the simulation results for critical inlet velocity are presented as black dots (unless mentioned otherwise). The resulting global expression for critical inlet velocity, as presented at the end of this paragraph, is already displayed on the figures as a black line. These black lines are thus not necessarily a 'best fit' curve in individual figures. Rather, it is a conservative curve, constructed in such a manner that most simulation results are below (and close to) the curve. It is recalled that all simulations correspond to essentially uni-directional flows (i.e. no stagnation or recirculation regions), so that the formula only applies to such circumstances.

Variation of convective heat release rate per unit area

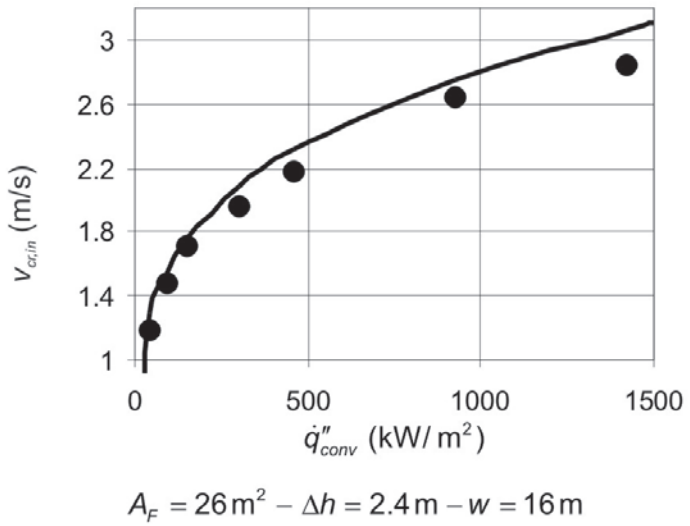

Figure 5.7 Critical inlet velocity with variable convective heat release rate per unit area.

Fig. 5.7 displays the variation of critical inlet velocity when the convective heat release rate of the fire varies between 46 and 1491 kW/m^2. The critical velocity increases with $\dot{q}''_{conv}$ by a $1/4^{th}$ power law:

$$v_{cr,in} \sim \dot{q}''^{1/4}_{conv} \tag{5.3}$$

The analytical formula (black line) provides a conservative overestimation of the critical velocity, due to the (slightly conservative) factor (0.26) in Eq. (5.6). The exponent 0.25, however, is quite accurate, not a conservative estimate.

Variation of fire source area

In Fig. 5.8, the variation of the critical inlet velocity with fire source area (between 1 and 26 m^2) is presented. The critical velocity increases with A_F with a $1/5^{th}$ power law:

$$v_{cr,in} \sim A_F^{1/5} \tag{5.4}$$

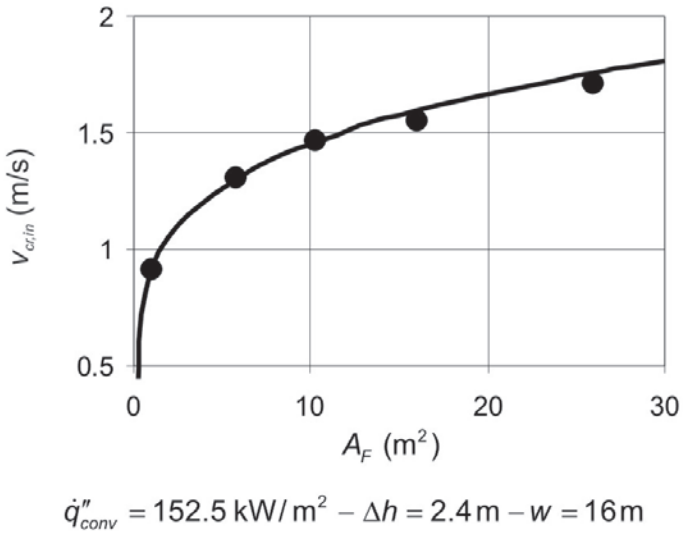

Figure 5.8 Critical inlet velocity with variable fire source area.

Variation of car park width

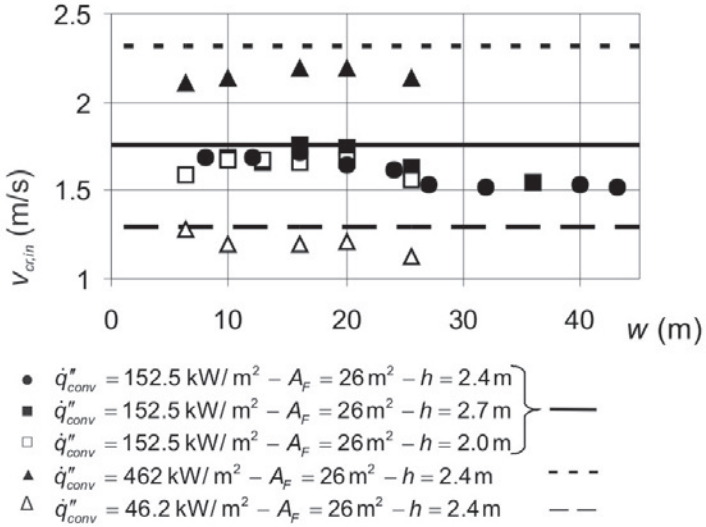

Figure 5.9 Critical inlet velocity with variable car park width.

Depending on the setup, the car park width is varied between 6.4 m and 43.2 m (Fig. 5.9). Five setups have been studied:

- the basic configuration with $\dot{q}''_{conv}$ = 152.5 kW/m² and height h = 2.4 m (black dots);
- two configurations with another car park height (h = 2.7 m, black squares and h = 2.0 m, white squares);

- two configurations with different HRRPUA ($\dot{q}''_{conv}$ = 46.2 kW/m^2, white triangles and long-dashed line; and $\dot{q}''_{conv}$ = 462 kW/m^2, black triangles and short-dashed line).

Globally, the required inlet velocity hardly varies with the car park width. Therefore, Eq. (5.6) does not contain a dependence on w. As a result, Eq. (5.6) corresponds in the figure to the dashed or solid horizontal lines, the position of which is determined by the HRRPUA. The figure shows that the formula is a little conservative sometimes, particularly for larger car park widths. Note that, for larger car park widths, it is more difficult to guarantee uni-directional flow, so a somewhat conservative approach is desirable.

The results for the basic configuration (black dots), indeed reveal that for small widths, the critical inlet velocity ($v_{cr,in}$) is higher than for larger widths. When the width exceeds 16 m (for the case studied), the critical inlet velocity starts decreasing, because the channelling effect by the side walls diminishes. For large enough widths (w > 27 m for the case studied), the critical velocity becomes independent of the car park width. As soon as the side walls are so far away that there is no channelling effect anymore, it does not matter exactly how far away they are.

Fire source elevation height

Before examination of the impact of the variation of car park height, it is important to note that not only can the ceiling be lower, but also the fire source can be positioned higher in the car park, resulting in the same "height difference" (Δh) between ceiling and fire source. In most simulations here, the fire source has been positioned on the floor of the car park. In real situations, though, this is not always true. Therefore, simulations have also been performed with an elevated fire source in the basic configuration car park as mentioned before. In the simulations, elevated fire sources of 0.2, 0.6, 0.9 and 1.2 m have been studied, resulting in height differences of respectively Δh = 2.2, 1.8, 1.5 and 1.2 m in the basic configuration. Simulations have also been performed with

the fire source on floor level, but with lower car park height, also resulting in values $\Delta h = h$ = 1.2, 1.5, 1.8 and 2.2 m.

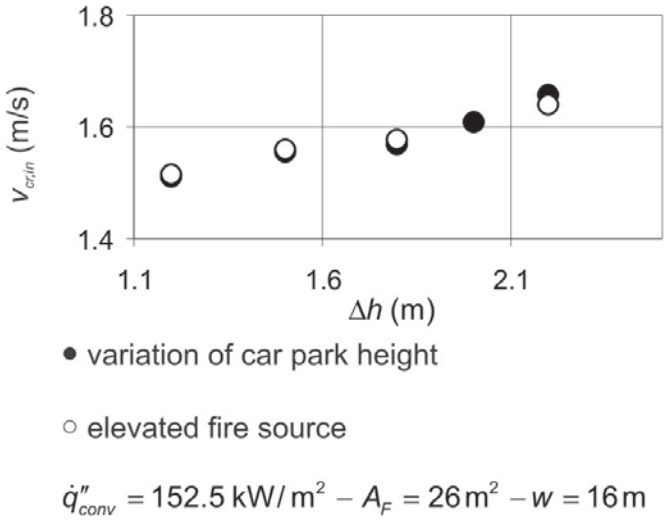

Figure 5.10 Critical inlet velocity with variable height difference between fire source area and ceiling.

Fig. 5.10, displaying the critical inlet velocity ($v_{cr,in}$) with variable height difference, for simulations with and without elevated fire source, clearly shows that agreement between results with the same Δh is very good. Therefore, the height difference Δh should be the parameter in the equation for critical velocity, not the car park height h itself.

Variation of car park height

Fig. 5.11 shows the results of two setups for the variation of the car park height. As the fire source is on floor level in these simulations, $h = \Delta h$ here.

In the basic configuration, the car park height is varied between 1.2 m and 3 m (black dots). At first, the critical velocity increases with increasing height. From a certain height value on, however, a maximum value for $v_{cr,in}$ seems to be reached. This is confirmed by the simulation results for variable height in a w = 32 m wide car park, where the height is varied between 2.4 m and 10 m (white dots). A maximum value for $v_{cr,in}$ is clearly found in the simulations.

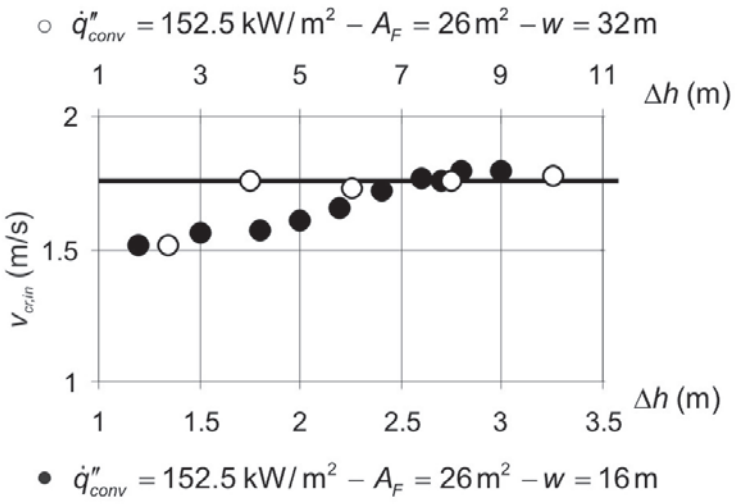

Figure 5.11 Critical inlet velocity with variable car park height.

It is interesting to note that the flame height of the fire, calculated with the Heskestad expression, is

$$l_F = 0.235\dot{Q}^{2/5} - 1.02D_F = 2.53\,\text{m}\,. \qquad (5.5)$$

Thus, for a large number of the simulations, the flame impinges on the car park ceiling, some of the combustion occurs under the ceiling and does not add to the upward momentum of the fire-induced flow. An increase in ceiling height then increases this momentum, leading to an increase in required ventilation velocity. Once the ceiling is sufficiently higher than the flame height, the required ventilation becomes essentially independent of the exact car park height. Typically, the car park height will not exceed 3 m. Eq. (5.6), corresponding to the horizontal line, is conservative for lower heights.

Resulting equation

All the above is combined into one relation for critical inlet velocity:

$$v_{cr,in} = 0.26\dot{q}''^{1/4}_{conv} A_F^{1/5}\,, \qquad (5.6)$$

with a factor 0.26 $\text{m}^{11/10}/(\text{s kW}^{1/4})$ and the convective heat release rate per unit area in kW/m^2. As mentioned above, the critical velocity

resulting from this equation has already been shown as a black line in Figs. 5.7, 5.8, 5.10 and 5.11.

Fig. 5.12 displays the agreement between the values for critical inlet velocity as retrieved from the simulations and those calculated from Eq. (5.6).
The figure shows good agreement between the simulations and the derived formula. When the agreement is not perfect, the equation is conservative: Eq. (5.6) imposes a higher value for critical inlet velocity than what is obtained from the simulations. It has been explained that this choice has been made on purpose. It is to be considered as some safety margin.

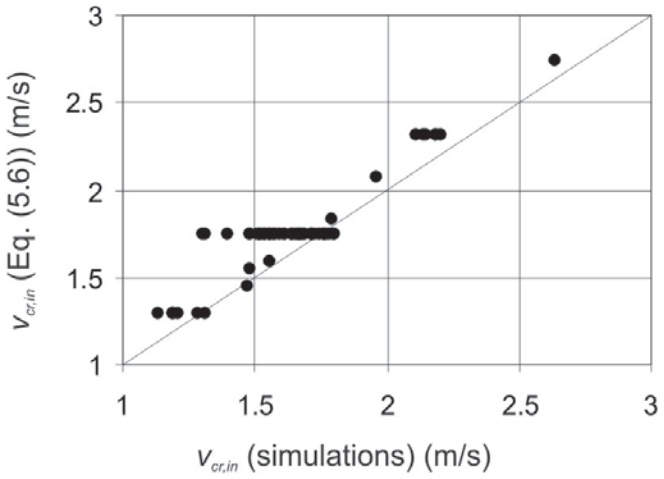

Figure 5.12 Critical inlet velocity from simulations and from Eq. (5.6).

In [13], preparatory work has already been presented for the determination of the critical extraction velocity for uni-directional flows in car parks. As the formula proposed in [13] concerned critical extraction velocity (unlike the inlet velocity presented in this paper), some differences can be expected. The trends that the required velocity increases with increasing HRRPUA, fire source area and (up to a certain value) car park height, as well as the small dependence of critical velocity on the car park width, have been confirmed. In the present study, the CFD results have been examined, including the use of a more

recent version of FDS and taking advantage of insights from the extensive validation study in Chapter 4; and the expression has been made independent of car park height or width, as argued above.

5.3.3 Relation between outlet (extraction) and inlet velocity

As cold air is coming in and hot smoke is extracted out of the car park, the inlet and outlet velocity are not equal to each other, as mass is conserved. In the car park simulations, the outlet velocity is imposed and the inlet velocity is calculated as post-processing step. In the previous section, a formula has been provided for the critical inlet velocity. However, in practical design of car parks, smoke is usually extracted from the space. Therefore, a relation between outlet and inlet velocity is necessary.

This relation is firstly derived from simple fire dynamics theory. Afterwards, it is compared to the simulation results.

For the simplified calculation it is assumed that smoke properties (c_p and M_w) are equal to those of air. Furthermore, a constant temperature (T_{out}) over the entire outlet cross-section ($A_{cs} = wh$) is assumed, although in reality, this temperature may vary over the height of the car park.

By combining the equations for conservation of mass

$$\rho_{in} v_{in} A_{cs} = \rho_{out} v_{out} A_{cs}\,, \tag{5.7}$$

the ideal gas law

$$T_{out} \rho_{out} = T_{in} \rho_{in}\,, \tag{5.8}$$

and the energy balance from the fire

$$\dot{Q}_{conv} = \dot{q}''_{conv} A_F = \dot{m} c_p \Delta T = c_p \left(T_{out} - T_{in}\right) \rho_{in} v_{in} wh\,, \tag{5.9}$$

the difference between outlet and inlet velocity can be described as function of the four parameters already mentioned above, and the properties of the cold incoming air:

$$v_{out} - v_{in} = \frac{\dot{q}''_{conv} A_F}{whp_{in} c_p T_{in}}. \tag{5.10}$$

In each simulation, this difference has also been calculated as the difference between the imposed outlet velocity and the calculated average inlet velocity. Fig. 5.13 displays the outlet and inlet velocity difference calculated with Eq. (5.10) and the difference obtained directly from the simulations.

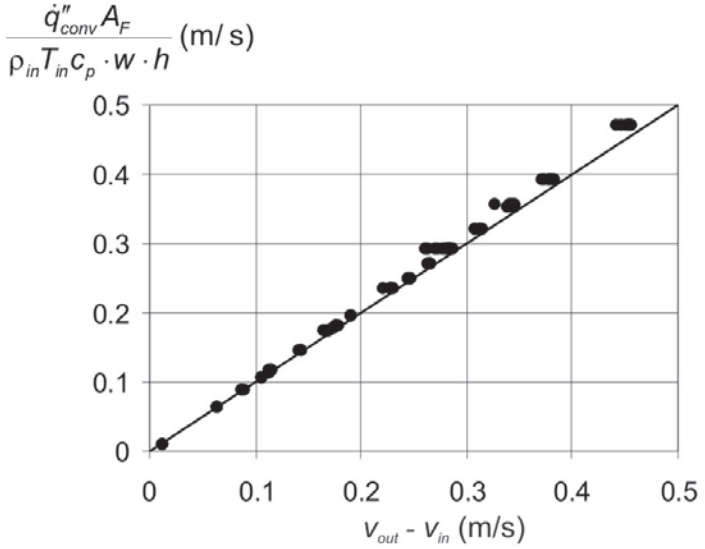

Figure 5.13 Difference between outlet and inlet velocity from Eq. (5.10) and as obtained from the simulations.

The theoretically derived relation is almost exactly confirmed by the simulation results. Thus, the assumptions made can be regarded as correct, and Eq. (5.10) can be used as the formula to account for the difference between outlet (extraction) and inlet velocity in the car park.

5.3.4 Backlayering distance as function of inlet ventilation velocity

It was mentioned above that the critical velocity has been calculated by linear extrapolation of the data of backlayering distance (d) as function of inlet velocity (v_{in}) (Fig. 5.6). The implicit assumption that the relation between backlayering distance and inlet velocity is linear, is indeed confirmed in the simulations. The correlation can be written as

$$d = a\left(v_{cr} - v\right). \tag{5.11}$$

The reason that this correlation is written with v_{cr} and v, instead of $v_{cr,in}$ or v_{in} is because it can be applied to both inlet and outlet velocities. Indeed, Eq. (5.10) shows that for a given scenario of a car fire in a car park, the difference between outlet and inlet velocity is a constant value. Therefore the difference between critical inlet velocity and actual inlet velocity can, by including Eq. (5.10), also be written as

$$v_{cr,in} - v_{in} = \left(v_{cr,out} - \frac{\dot{q}''_{conv} A_F}{wh\rho_{in} c_p T_{in}} \right) - \left(v_{out} - \frac{\dot{q}''_{conv} A_F}{wh\rho_{in} c_p T_{in}} \right) = v_{cr,out} - v_{out}, \tag{5.12}$$

being the difference between critical outlet velocity and actual outlet velocity.

The factor a has been defined for every configuration studied. Fig. 5.14 displays all calculated values. The factor a ranges between 30 and 50, with an average value of a = 40 s. As the expression for v_{cr} is conservative, it can be argued that the use of the average value 40 in Eq. (5.11) is sufficiently safe for most cases.

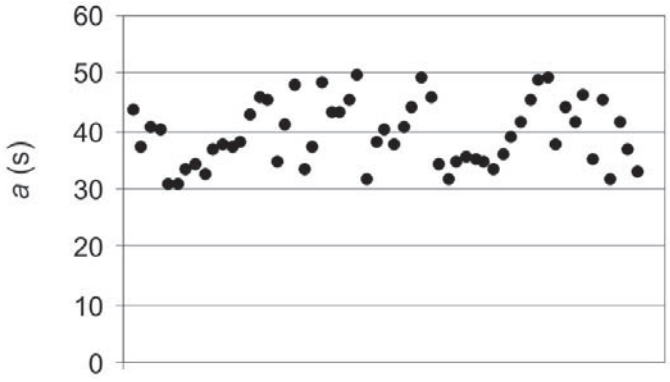

Figure 5.14 Relation between backlayering distance and ventilation velocity: factor *a*.

5.3.5 Conclusion on formulae

In this section, three formulae have been presented to calculate the critical inlet velocity in a large closed car park with flat ceiling and uni-directional flow patterns, the difference between outlet and inlet velocity and the smoke backlayering distance corresponding to a certain ventilation velocity:

$$v_{cr,in} = 0.26 \dot{q}''^{1/4}_{conv} A_F^{1/5} \tag{5.6}$$

$$v_{out} - v_{in} = \frac{\dot{q}''_{conv} A_F}{w h \rho_{in} c_p T_{in}} \tag{5.10}$$

$$d = 40\left(v_{cr} - v\right) \tag{5.11}$$

The reader is reminded of the fact that the ranges of the values tested have been summarized in Table 5.1. Use of the expressions (Eq. (5.9) to (5.11)) beyond these ranges may result in loss of accuracy.

5.3.6 Discussion

Eq. (5.6) has been obtained by fitting the numerical simulation results. While the physics are obviously included in these simulations, one could wonder whether the scaling parameters involved in this relationship could be derived from a simple theory, taking into account the apparent simplicity of the configuration at hand. Unfortunately, despite this seemingly simple configuration in terms of geometry and boundary conditions, it is, to the best of our understanding, prohibitively complex to allow scaling by means of a simple theory, due to the fact that the problem is governed by momentum issues, and the flow field is by no means simple. This is explained next.

The upward momentum above the fire source obviously depends on the (convective) fire HRR, as well as on entrainment of air (and thus on fire source dimensions) and rise height. In the case of a free axisymmetric (smoke) plume, treating the fire as a point source, the scaling laws are well-known in the smoke plume region. The momentum (product of upward velocity and mass flow rate) increases with height as $z^{4/3}$ and

$HRR^{2/3}$. In the configuration at hand, however, there is no smoke plume region. Indeed, the flames reach the (low) ceiling, as mentioned in section 5.3.2. This makes the point source assumption unrealistic. Also, since part of the combustion can take place under the ceiling, the (expansion) effect on the flow field is different from the situation where the HRR is converted into upward momentum first (while air is entrained), and then redirected into a horizontal motion after impingement onto the ceiling. Moreover, entrainment of air from an oncoming air flow with velocities in the order of 1m/s and more, is entirely different from entrainment of air in still conditions.

Last but not least, although the dominant flow is essentially unidirectional from inlet to outlet, the smoke spreading itself is not. Indeed, unlike tunnel configurations, where practically all the momentum of the smoke is directed into the same direction as the ventilation air flow (partly in the same sense, partly in the opposite sense), this is not the case in car park configurations. Sideward smoke motion is not prevented by the oncoming ventilation air flow and a V-shaped smoke pattern is observed in a top view of the car park near critical ventilation conditions (Fig. 5.15). The degree of 'channeling effect' depends on the car park width (as mentioned in section 5.3.2).

Figure 5.15 V-shaped smoke pattern in a top view of the car park near critical ventilation conditions.

All these issues make, to the best of our understanding, scaling from a simple theory extremely difficult, which motivates the use of CFD simulations to establish relationship Eq. (5.6).

5.4 Range of validity

As mentioned a few times before, the analytical expressions are only valid as long as the flow is essentially uni-directional. Complex flow patterns, such as recirculation or stagnation region flows, are not covered. Indeed, the numerical simulations from which the formulae were derived, have been performed for car parks with the front side entirely open.

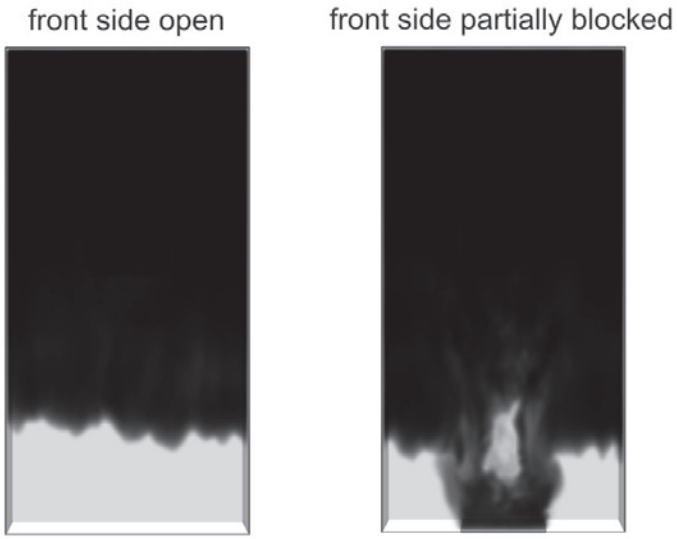

Figure 5.16 Effect of difference in inlet opening configuration on the smoke pattern in a car park.

In order to illustrate the possible difference in smoke backlayering pattern, some simulations have also been performed with the front side of the car park partly blocked (Fig. 5.16). The partial blocking of the front opening creates a recirculation region. When the smoke enters that region, the smoke backlayering is fundamentally different from the situation with the front entirely open and the backlayering distance substantially increases for the same extraction flow rate. A more

complete study of the effect of the inlet opening on the flow pattern is provided in [2,3]. Fig. 5.16 is only included here to illustrate the important limitation of the validity range of the formulae to uni-directional flow patterns.

5.5 Comparison with large scale experiments

In the facilities of WarringtonFireGent, a large series of full-scale car park fire tests have been performed [2]. One series of tests is similar to the car park configuration discussed in the present chapter. The car park is w = 28.6 m wide, 30 m long and h = 2.7 m high, with front side entirely open and exhaust ventilators to extract smoke at the rear end. The fire source is a hexane pool burner, placed in the middle of the car park. The fuel floats on water (at height 45 cm above the ground) in a 3 m x 1.4 m tray.

Fig. 5.17 shows one result from [3], where numerical simulations are presented for the large-scale fire tests as described in [2]. For more details and a sensitivity study on the parameters as defined here, the reader is referred to [2] and [3]. The basic simulation settings in [3] are:

- Car park dimensions: 28.6 m (width) x 30 m (length) x 2.7 m.
- Mesh cells size: 20 cm x 20 cm x 15 cm.
- Turbulence model: Standard Smagorinsky LES, $C_S = 0.20$.
- Combustion model: default mixture fraction combustion model.
- Fixed radiative heat loss by imposing a constant value of the radiative fraction χ_r to eliminate uncertainty from radiation modeling.
- Boundary conditions:
    - The ceiling, floor and side walls are adiabatic.
    - 4 equidistant supporting beams under the ceiling have depth 25 cm and width 20 cm.
    - The smoke extraction rate is imposed through 4 openings in the ceiling of 1m x 1m each, positioned 1 m from the back wall.

- The fire is modeled as a fuel source of fixed area at height equal to 0.45 m, corresponding to the situation in the experiments of [2], in the middle of the car park.
- All simulations concern (quasi-)steady state conditions with fixed heat release rate. As in the experiments [2], hexane (C_6H_{14}) is used as fuel.

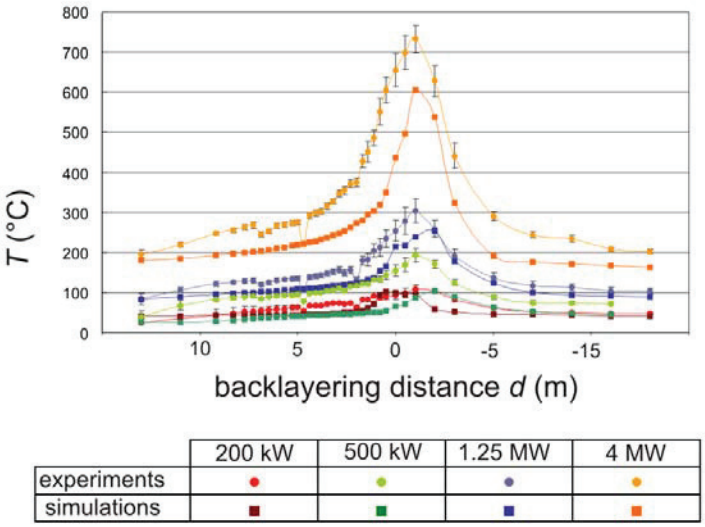

Figure 5.17 Effect of difference in inlet opening configuration on the smoke pattern in a car park.

Fig. 5.17 reveals that the trends with increasing fire HRR are well captured in the simulations in the configuration as presented above. The maximum temperatures are under-predicted, but the global profile shapes (and thus the smoke backlayering distances) are well predicted. Note that no effort has been made to try and improve the temperature predictions (e.g. no radiation correction has been applied to thermocouple measurements): the only issue of interest is the presence or not of smoke. As such, the profile shape is much more important than the absolute values and Fig. 5.17 shows that the quality of the CFD simulation results is sufficient to rely upon them to establish correlations.

As explained above, different heat release rates and smoke extraction flow rates have been studied. To compare the experimental results to

the above derived Eq. (5.6), a series of four experiments characterized in Table 5.2 is discussed here.

Table 5.2 Experimental input data.

Exp. #	1	2	5 + 6
$\dot{V}_{out}$ (m³/s)	55.6	55.6	27.8
$\dot{q}''_{conv}$ (kW/m²)	143	238	95

In Table 5.3, the backlayering distance is reported, as predicted by the formulae above:

$$d = 40\left(v_{cr,out} - v_{out}\right) = 40\left(v_{cr,in} + \frac{\dot{q}''_{conv} A_F}{wh\rho_{in} c_p T_{in}} - \frac{\dot{V}_{out}}{wh}\right)$$
$$= 40\left(0.26\dot{q}''^{1/4}_{conv} A_F^{1/5} + \frac{\dot{q}''_{conv} A_F}{wh\rho_{in} c_p T_{in}} - \frac{\dot{V}_{out}}{wh}\right) \quad (5.13)$$

The values for the car park configuration are: A_F = 4.2 m², h = 2.7 m, Δh = 2.25 m, w = 28.6 m. $\dot{V}_{out}$ and $\dot{q}''_{conv}$ are retrieved from Table 5.2.

Table 5.3 Backlayering distances from experiments and simulations.

Exp. #	1	2	5	6
prediction d (m)	14	21	24	24
experimental d (m)	13	16	24	26

In the experiments, the smoke backlayering distances have been determined by the same method as in the simulations, i.e. the N-percent rule has been applied on the centreline average temperature profiles under the ceiling of the car park (Table 5.3). Backlayering further than the car park front side in the experiments corresponds to extrapolation of the temperature profile inside the car park, to where it would reach the interface temperature T_{int} as defined by the N-percent rule (Eq. (5.2)). Fig. 5.18 shows an example of this, where the interface temperature (dashed line) is below the temperatures measured in the

car park and a backlayering distance is found by extrapolation. The thin vertical line shows the position of the car park opening.

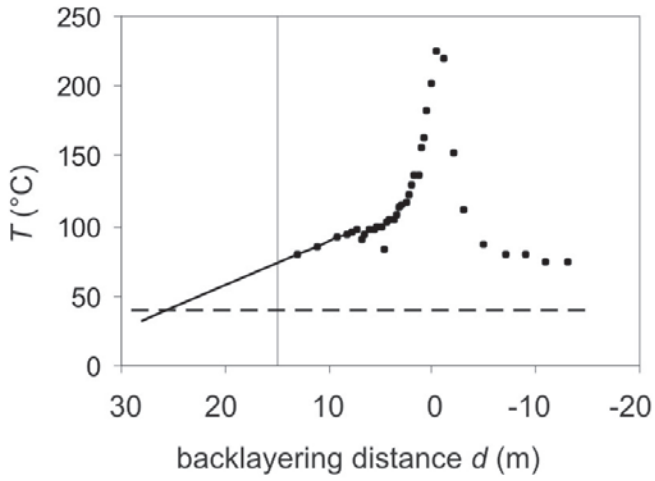

Figure 5.18 Extrapolation (—) of measured temperatures (•) to the interface temperature (--) for estimation of the backlayering distance.

It is obvious that such extrapolation is not a scientifically correct method for calculating a 'possible' backlayering distance if the car park should have been longer. It only gives an indication of the order of backlayering distance.

Table 5.3 reveals that agreement is not perfect, but the trends are well predicted. Thus, the combination of the proposed formulae for uni-directional flow patterns in car parks seems to provide a reasonable estimate for the smoke backlayering distance for given extraction flow rate and fire source.

5.6 Conclusion

In this chapter, a large set of (more than 350) CFD simulations have been used as 'numerical experiments'. From parameter variation in the simulations, formulae for horizontal smoke extraction system design in large car parks have been derived.

Four parameters have been varied (convective HRRPUA, fire source area, car park height and car park width). From the parameter variation, three formulae have been proposed:
- an analytical formula for the critical inlet velocity in the car park ($v_{cr,in}$):

$$v_{cr,in} = 0.26\dot{q}''^{1/4}_{conv} A_F^{1/5} \tag{5.6}$$

- an expression to account for the difference between inlet (v_{in}) and outlet (v_{out}) velocity in the car park, derived from simple fire dynamics theory and confirmed with simulation results:

$$v_{out} - v_{in} = \frac{\dot{q}''_{conv} A_F}{wh\rho_{in} c_p T_{in}} \tag{5.10}$$

- and an analytical formula for the required ventilation velocity in the car park when a certain backlayering distance (d) is allowed, expressed as deviation from the critical velocity:

$$d = 40\left(v_{cr} - v\right) \tag{5.11}$$

These formulae are only valid for car parks with uni-directional smoke and air flow pattern, centrally placed fire source and with flat ceiling.

Agreement with full-scale car park experiments has been discussed, confirming the derived equations for the configuration studied.

The results presented in Chapter 5 have also been submitted to be published as a journal paper [14].

5.7 References

[1] Chow WK, Use of a time constant for designing a smoke control system in car parks, J. of Fire Sciences 13: 357-377 (1995)

[2] Deckers X, Haga S, Tilley N, Sette B, Merci B, Smoke control in case of fire in a large car park: Full-Scale Experiments, Fire Safety J. (Special Issue) (2012), submitted

[3] Deckers X, Haga S, Tilley N, Merci B, Smoke control in case of fire in a large car park: CFD Simulations of Full-Scale Experiments, Fire Safety J. (Special Issue) (2012), submitted

[4] NBN S21-208-2, Fire protection inside buildings – Design of smoke and heat exhaust ventilation systems (SHEVS) for indoor car parks (2007)

[5] EN 12101-11, Smoke and heat control system - Part 11: Design, installation & commissioning requirements for enclosed car parks, Draft Version (2011)

[6] BS 7346-7, Code of practice on functional recommendations and calculation methods for smoke and heat control systems for covered car parks (2006)

[7] McGrattan K, Hostikka S, Floyd J, Baum H, Rehm R, Mell W, McDermott R, Fire Dynamics Simulator (Version 5) Technical Reference Guide, NIST 1018-5, National Institute of Standards and Technology (2008)

[8] McGrattan K, Klein B, Hostikka S, Floyd J, Fire Dynamics Simulator (Version 5) User's Guide, NIST 1019-5, National Institute of Standards and Technology (2008)

[9] McGrattan KB, Baum HR, Rehm RG, Large Eddy Simulations of Smoke Movement, Fire Safety J. 30: 161-178 (1998)

[10] Smagorinsky J, General Circulation Experiments with the Primitive Equations. I. The Basic Experiment, Monthly Weather Review 91: 99-164 (1963)

[11] Cooper LY, Harkleroad M, Quintiere J, Reinkinen W, An Experimental Study of Upper Hot Layer Stratification in Full-Scale Multiroom Fire Scenarios, J. of Heat Transfer 104: 741-749 (1982)

[12] Wu Y, Bakar MZA, Control of smoke flow in tunnel fires using longitudinal ventilation systems – a study of the critical velocity, Fire Safety J. 35: 363-390 (2000)
[13] Tilley N, Merci B, Relation between horizontal ventilation velocity and backlayering distance in large closed car parks, Proceedings of the Ninth International Symposium on Fire Safety Science 777-787 (2008)
[14] Tilley N, Deckers X, Merci B, CFD study of relation between ventilation velocity and smoke backlayering distance in large closed car parks, Fire Safety J, submitted

6 Chapter 6 Extrapolation of data from reduced-scale set-ups to full-scale atria

6.1 Introduction

The atrium configuration of the 2D adhered spill plume – as introduced in Chapter 3 – is presented again in Fig. 6.1. For the design of the smoke and heat exhaust system, several one-line formulae have been developed to calculate the required smoke mass flow rate ($\dot{m}$) to be extracted at the ceiling of the atrium, in order to ensure a certain smoke free height above the spill edge (z_s). These formulae have been presented in Chapter 3, Eqs. (3.13) to (3.25).

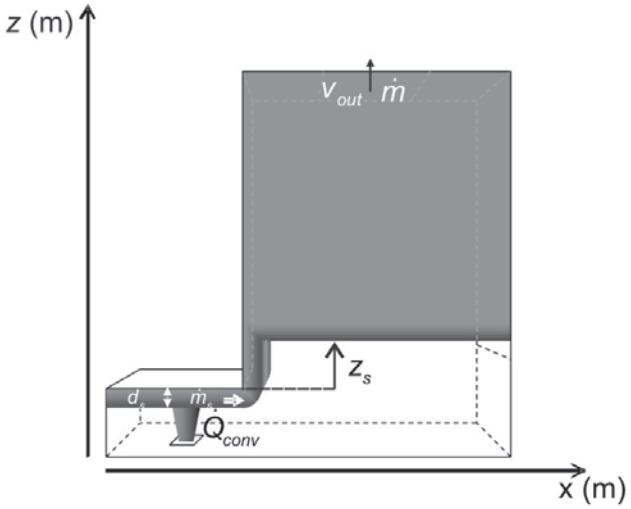

Figure 6.1 Schematic representation of smoke filling in an atrium configuration (fire in adjacent room).

All these expressions rely on (a large set of) reduced-scale experiments. Being less expensive, safer to control and easier to handle for a parameter variation study, and requiring less space, reduced-scale experiments are indeed usually preferred over full-scale experiments.
However, for reduced-scale data formulae to be used in full-scale configurations, proper scaling must be applied. It is commonly assumed that – as long as the flow is sufficiently turbulent – scaling based on Froude number is sufficient in fire problems. This assumption is also relied upon in the above mentioned formulae, based on reduced-scale experiments. Indeed, to keep the Froude number constant, together with other dimensionless numbers like Reynolds, would be practically impossible in experiments. The reduced-scale experimental setup should then be in non-atmospherical conditions (different gravity, and/or different "air" viscosity), which is very difficult and expensive to obtain. Therefore only the Froude number is used for scaling, if the flow is sufficiently turbulent.

With CFD (Computational Fluid Dynamics) calculations, a parameter variation in full-scale configurations is easier to study. One could perform numerical simulations for a set of reduced-scale experiments and then scale the configuration up to check whether the developed formula is still valid in the full-scale setup. However, also with CFD simulations, scaling must be done in a proper way. This is the topic of the present chapter.
In the present chapter, FDS (Fire Dynamics Simulator, version 5.5.3 [1,2]) is used as CFD code. Therefore the governing equations are written below as in the FDS manual. However, conclusions on dimensionless numbers are valid for the equations to be solved in any CFD program. The three basic governing flow equations (conservation of mass and total momentum, and transport of sensible enthalpy), in their instantaneous form, serve as starting point. The important dimensionless numbers and scaling of terms are derived. Such theoretical studies have already been reported in text books (e.g. [3]). The novelty in the chapter at hand is that this scaling theory is carefully

and extensively analyzed by means of a set of CFD simulations, using a Large Eddy Simulation (LES) approach with the standard Smagorinsky subgrid scale model [4] to model turbulence.

6.2 Governing equations – scaling laws

The most important scaling features are briefly mentioned here, as they are relevant in the discussion of the results. For a more extensive theoretical discussion, the reader is referred to e.g. [3].

6.2.1 Instantaneous equations and dimensionless numbers

Conservation of mass

For a single phase flow, this reads:

$$\frac{\partial \rho}{\partial t} + \nabla \cdot \rho \mathbf{v} = 0 \tag{6.1}$$

Stating that $\frac{\rho}{t} \sim \frac{\rho v}{L}$ implies

$$t \sim L/v \,. \tag{6.2}$$

In time-dependent scaled simulations, it is important to use this scaling factor to compare instantaneous flow fields at corresponding times. In other words, results at time t_r in reduced-scale, must be compared to results at time $t_f = (L_f\ v_r)/(L_r\ v_f)\ t_r$ in the full-scale setup. Obviously, instantaneous LES results are of limited value. Below, results are shown as time-averages within the quasi steady-state range for comparison purposes. The relation $t_f = (L_f\ v_r)/(L_r\ v_f)\ t_r$ implies that it takes longer to reach quasi steady-state conditions in larger configurations.

Conservation of momentum

$$\frac{\partial}{\partial t}\left(\rho\mathbf{v}\right)+\nabla\cdot\rho\mathbf{vv}=-\nabla\left(p+\rho_0 g\mathbf{z}\right)+\left(\rho_0-\rho\right)\mathbf{g}+\nabla\cdot\boldsymbol{\tau} \tag{6.3}$$

$$\text{with } \boldsymbol{\tau}=\mu\left(2\mathbf{S}-\frac{2}{3}\boldsymbol{\delta}\left(\nabla\cdot\mathbf{v}\right)\right) \tag{6.4}$$

$$S_{ij}=\frac{1}{2}\left(\frac{\partial v_i}{\partial x_j}+\frac{\partial v_j}{\partial x_i}\right) \tag{6.5}$$

Equation (6.3) reveals that $\frac{\rho v}{t}\sim\frac{\rho v^2}{L}\sim\frac{p}{L}\sim\Delta\rho g\sim\mu\frac{v}{L^2}$, resulting in two important dimensionless numbers:

- The Froude number, comparing inertia and buoyancy forces, which is important in flows driven by natural convection: $\mathrm{Fr}=v\sqrt{\rho}\,/\sqrt{gL\Delta\rho}$. As natural convection is predominant in the test case at hand, keeping Fr constant is the logical first choice, which is also followed in the derivation of the one-line formulae from reduced-scale experiments as presented in Chapter 3.

Maintaining temperatures equal in original and scaled setups, the Froude number is typically simplified to:

$$\mathrm{Fr}=\frac{v}{\sqrt{gL}}. \tag{6.6}$$

This definition for Fr is used below.

- The Reynolds number, comparing inertia and viscous forces, which is used primarily in flows with forced convection:

$$\mathrm{Re}=\frac{\rho vL}{\mu}=\frac{vL}{\nu}. \tag{6.7}$$

In both Reynolds and Froude number, L is a representative distance length scale.

Transport of sensible enthalpy

$$\frac{\partial}{\partial t}\left(\rho h_s\right)+\nabla\cdot\rho h_s\mathbf{v}=\frac{\partial p}{\partial t}+\dot{q}'''-\nabla\cdot\dot{\mathbf{q}}''+\tau_{ij}\nabla\mathbf{v} \tag{6.8}$$

With $\dot{\mathbf{q}}''=-k\nabla T-\sum_a h_{s,a}\rho D_a\nabla Y_a+\dot{\mathbf{q}}_r''$ (6.9)

$$h_s=\sum_a Y_a h_{s,a}=\sum_a\left(Y_a\int_{T_0}^{T}c_{p,a}T'dT'\right) \tag{6.10}$$

As the equation for transport of sensible enthalpy is written in the form as used in FDS simulations, the reader is referred to the FDS manuals [1, 2] for more information on the different terms in this equation.

$$\frac{\rho c_p T}{t}\sim\frac{\rho c_p T v}{L}\sim\frac{p}{t}\sim\frac{\dot{Q}}{L^3}\sim\frac{kT}{L^2}\sim\frac{\rho c_p T D}{L^2}\sim\mu\frac{v^2}{L^2}$$

- From transport of sensible enthalpy, the velocity scales as

$$v\sim\frac{\dot{Q}}{L^2\rho c_p\Delta T}. \tag{6.11}$$

- The ratio of kinematic viscosity (or 'momentum' diffusivity) and thermal diffusivity is the Prandtl number:

$$\mathrm{Pr}=\frac{\nu}{\alpha}=\frac{\mu c_p}{k}. \tag{6.12}$$

- Similarly, the Schmidt number expresses the ratio of momentum diffusivity and mass diffusivity:

$$\mathrm{Sc}=\frac{\nu}{D}. \tag{6.13}$$

- A final important dimensionless number is the Rayleigh number, a combination of Re, Pr and Fr. The Rayleigh number, primarily used for natural convection, is:

$$\mathrm{Ra}=\frac{\mathrm{Re}^2\,\mathrm{Pr}}{\mathrm{Fr}^2}=g\frac{L^3}{\nu\alpha}\frac{\Delta\rho}{\rho}. \tag{6.14}$$

6.2.2 Influence of numerics and modelling

The above presented dimensionless numbers are based on molecular thermophysical properties. In CFD, Direct Numerical Simulation of the flow, in which all turbulent scales down to the Kolmogorov scale, i.e. the smallest turbulent scale, are fully resolved, is prohibitively expensive due to the fine grid requirements. Therefore, the flow field is typically resolved on a much coarser mesh, making use of models to describe the influence of small unresolved turbulent scales on the large resolved scales. In LES, the equation for conservation of momentum is filtered, using a density weighting or Favre averaging, yielding

$$\frac{\partial\left(\bar{\rho}\tilde{\mathbf{v}}\right)}{\partial t}+\nabla\cdot\left(\bar{\rho}\tilde{\mathbf{v}}\tilde{\mathbf{v}}\right)=-\nabla\left(\bar{p}+\rho_0 g\mathbf{z}\right)+\left(\rho_0-\bar{\rho}\right)\mathbf{g}+\nabla\cdot\left(\bar{\boldsymbol{\tau}}-\boldsymbol{\tau}^*\right). \tag{2.19}$$

$\boldsymbol{\tau}^*$ denotes the residual stress tensor and represents the effect of the unresolved scales on the resolved ones. The energy equation is treated analogously. The residual stress tensor is typically modeled by means of an eddy viscosity model. As such, turbulent viscosity and diffusivities are introduced, contributing in e.g. the Reynolds-number. In FDS, for instance, by default the standard Smagorinsky turbulence model is used. In this model, the turbulent dynamic viscosity is defined as (cfr. Eq. (2.22)):

$$\mu_T=\bar{\rho}\left(C_s\Delta\right)^2\left|\tilde{\mathbf{S}}\right|, \tag{6.15}$$

with Δ the grid cell size. Although FDS uses an adjusted modelling approach, the here below derived conclusions remain and it is thus not necessary to go into more detail on the FDS approach. It is interesting to note that the turbulent viscosity globally scales as:

$$\nu_T\sim\left(\frac{\Delta}{L}\right)^2 vL\,. \tag{6.16}$$

When the ratio Δ/L goes to 0, the turbulent viscosity decreases and the simulation evolves towards a DNS simulation.

If the same number of mesh cells is used in the reduced-scale and full-scale setup, the cell size scales proportional to the configuration

dimensions, and the ratio Δ/L is constant. The turbulent viscosity then scales as

$$\nu_T \sim vL\,. \tag{6.17}$$

This reveals that the modelled turbulence scales properly in the sense that the Reynolds number based on turbulent viscosity,

$$\mathrm{Re}_T = \frac{vL}{\nu_T}, \tag{6.18}$$

is automatically preserved.

When looking more closely to the filtered equation for conservation of momentum (Eq. (2.19)), it reveals that $\frac{\rho v}{t} \sim \frac{\rho v^2}{L} \sim \frac{p}{L} \sim \Delta\rho g \sim \mu\frac{v}{L^2} \sim \mu_T\frac{v}{L^2}$. Thus, the turbulent Reynolds number that results from this is shown here to be automatically preserved when using the Smagorinsky LES model and when the grid cell size is scaled proportional to the configuration dimensions.

In a similar way, the filtered equation for conservation of energy can be derived to show that a turbulent Pr number is automatically preserved when maintaining the Fr number constant.

6.2.3 Scaling of experiments

When scaling up experimental configurations, obviously no modelling effects are taken into account. In experimental test cases, the results are what they are, by definition according to reality (which is measured up to a certain accuracy level).

However, it is important to recall the physics of scaling when dealing with experiments. Especially the difference between laminar and turbulent flow is important. The distinction laminar/turbulent relies on the Reynolds number (Eq. (6.7)) or the Rayleigh number (Eq. (6.14)). If the same fluid is used in reduced-scale and full-scale setup, temperatures are kept equal and Fr is constant, the Reynolds number scales as $\mathrm{Re} \sim vL \sim L^{3/2}$, while Ra scales as $Ra \sim L^3$. As a consequence,

there is a potential danger that a laminar, or weakly turbulent, reduced-scale experiment is scaled up, via the Froude-number, to a strongly turbulent full-scale configuration. In this case, the two configurations need not give similar results.
Only when both reduced-scale and full-scale setups have a turbulent flow behaviour (Reynolds and Rayleigh numbers are high, say Re > 10^4 and Ra > 10^9), self-similar behaviour can be expected.

6.3 Results

6.3.1 Setup of simulations

A number of CFD simulations have been performed to investigate the effects of scaling. The geometric configuration is always kept the same, similar to the atrium configuration used in Chapter 4. In the 'basic' simulation, the atrium height equals H_a = 3.24 m and the width W_s = 0.81 m. These dimensions have been multiplied by a factor 9 (H_a = 29.16 m, W_s = 7.29 m). The grid consists of 43200 cubic cells in the adjacent room and 518400 cells of the same size (2.25 cm x 2.25 cm x 2.25 cm in the basic simulation) in the atrium.
As the turbulence in the rising spill plume is determined by the inlet (i.e. the smoke layer emerging from the adjacent room into the atrium), the atrium width at the spill edge (W_s) is taken as characteristic length scale in the calculation of the Re and Ra numbers.
In scaling the configurations, the Froude number is always preserved. The temperature field has also been kept identical to that in the original simulation. As the height of the smoke layer is defined by application of the N-percent rule to the temperature profile [5], the ratio of this height to the atrium height will also be preserved then. Also, c_p values and densities remain practically unchanged. Gravity and ambient molecular dynamic viscosity can be changed. The Reynolds number (Eq. (6.7)) indeed provides the scaling for dynamic viscosity:

$$\nu \sim v_{out} W_s , \tag{6.19}$$

with v_{out} a velocity defined below.
The turbulent Schmidt and Prandtl numbers are kept constant.
Keeping the Froude number (Eq. (6.6)) constant, the outlet velocity is scaled as

$$v_{out} \sim \sqrt{gW_s} \tag{6.20}$$

As boundary conditions, a constant velocity v_{out} is imposed over the entire surface of the opening in the atrium ceiling. The walls of the atrium are modelled as adiabatic.
To represent the fire, a flow of hot air is inserted as heat source in the adjacent room of the atrium. As such, issues in combustion modelling, which are not relevant for the sake of the present study, are avoided.
The heat release rate of this flow is calculated as

$$\dot{Q}_{conv} = A_F \cdot u \cdot \rho_{in} \cdot (T_{in} - T_0) \cdot c_p \tag{6.21}$$

In the 'basic' simulation, the heat release rate is 4.34 kW, with A_F = 0.0506 m^2, T_{in} = 510°C, u = 0.39 m/s and ρ_{in} = 0.45 kg/m^3.
The equivalence of velocity (Eq. 12) leads to the proper scaling law for the heat release rate of the fire:

$$\dot{Q} \sim v_{out} W_s^2 \tag{6.22}$$

6.3.2 Simulations

Eight simulations are analyzed in this paper. Table 6.1 summarizes the dimensionless numbers. Re, Ra and Fr numbers have been determined using v_{out} and W_s. The numbers show that the flow is turbulent (Re > 10^4 and Ra > 10^9) in simulations 1 through 6. Simulations 7 and 8, however, have low Re and Ra numbers, so the flow is much less turbulent (or not even turbulent at all).

Table 6.1 Important dimensionless numbers in the eight simulations. Scaling factor a = 9.

Sim. nº	Re	$10^{-4} \cdot$ Re	Ra	$10^{-9} \cdot$ Ra	Fr	Fr
1	Re_1	1.6	Ra_1	2.2	Fr_1	0.106
2	$a^{3/2}\,Re_1$	44.0	$a^3\,Ra_1$	1592	Fr_1	0.106
3	$a^{3/2}\,Re_1$	44.0	$a^3\,Ra_1$	1692	Fr_1	0.106
4	Re_1	1.6	Ra_1	2.2	Fr_1	0.106
5	Re_1	1.6	Ra_1	2.4	Fr_1	0.106
6	Re_1	1.6	Ra_1	2.3	Fr_1	0.106
7	$a^{-3/2}\,Re_1$	0.06	$a^{-3}\,Ra_1$	0.003	Fr_1	0.106
8	$a^{-1}\,Re_1$	0.18	$a^{-2}\,Ra_1$	0.03	Fr_1	0.106

Table 6.2 summarizes the parameter variations. The actually imposed values are presented in Table 6.3. While simulations 1, 3 and 5 concern a reduced-scale atrium (W_s = 0.81 m), simulations 2, 4 and 6 represent a more realistic atrium (W_s = 7.29 m). Simulations 1 and 2 are both in regular atmospheric conditions (gravity and viscosity), and thus represent scaling from reduced-scale experiment to full-scale configuration. Note that in simulation 2, the Re and Ra numbers are not preserved with respect to simulation 1.

In simulations 3 and 4, only the ambient molecular viscosity is modified. As Reynolds and Rayleigh numbers are high, the flow is sufficiently turbulent and a variation in the molecular viscosity is not expected to affect the result.

In simulations 5 and 6, the gravity is artificially reduced in the simulations. With Eq. (6.20), (6.21) and (6.22), the other initial parameters (Table 6.3) can be calculated to ensure that Re, Ra and Fr are preserved with respect to simulation 1. This kind of scaling is hardly ever possible in experiments, as changing gravity is very difficult to accomplish. Yet, it is an interesting numerical test case to perform with CFD.

Simulation 7 and 8 again concern the reduced-scale atrium, with only a change in molecular viscosity. Again, it is scaled by Froude scaling, so the Fr number is preserved, but Re and Ra are not. In fact, Re and Ra are

lower than the turbulence limit in these simulations. Table 6.4 lists the numbers of the simulations and the differences between them.

Table 6.2 Scaling of the imposed parameters in the eight simulations. Scaling factor a = 9.

Sim. nº	Q	μ	u_{out}	g	W_s
1 'basic'	Q_1	μ_1	u_1	g_1	$W_{s,1}$
2	$a^{5/2}\, Q_1$	μ_1	$a^{1/2}\, u_1$	g_1	$a\, W_{s,1}$
3	Q_1	$a^{-3/2}\, \mu_1$	u_1	g_1	$W_{s,1}$
4	$a^{5/2}\, Q_1$	$a^{3/2}\, \mu_1$	$a^{1/2}\, u_1$	g_1	$a\, W_{s,1}$
5	$a^{-1/2} Q_1$	$a^{-1/2}\, \mu_1$	$a^{-1/2}\, u_1$	$a^{-1}\, g_1$	$W_{s,1}$
6	$a^2 Q_1$	$a\, \mu_1$	u_1	$a^{-1}\, g_1$	$a\, W_{s,1}$
7	Q_1	$a^{3/2}\, \mu_1$	u_1	g_1	$W_{s,1}$
8	Q_1	$a\, \mu_1$	u_1	g_1	$W_{s,1}$

Table 6.3 Initial values of the imposed parameters in 'basic' simulation 1.

Q_1	μ_1	$u_{out,1}$	g_1	$W_{s,1}$	H_1
kW	kg/sm	m/s	m/s²	m	m
4.34	$18 \cdot 10^{-6}$	0.3	9.81	0.81	3.24

Table 6.4 Numbering and specific features of all eight performed simulations.

	reduced-scale	full-scale
atmospheric conditions	1	2
changed viscosity (turbulent flow)	3	4
changed viscosity (laminar flow)	7, 8	
changed gravity	5	6

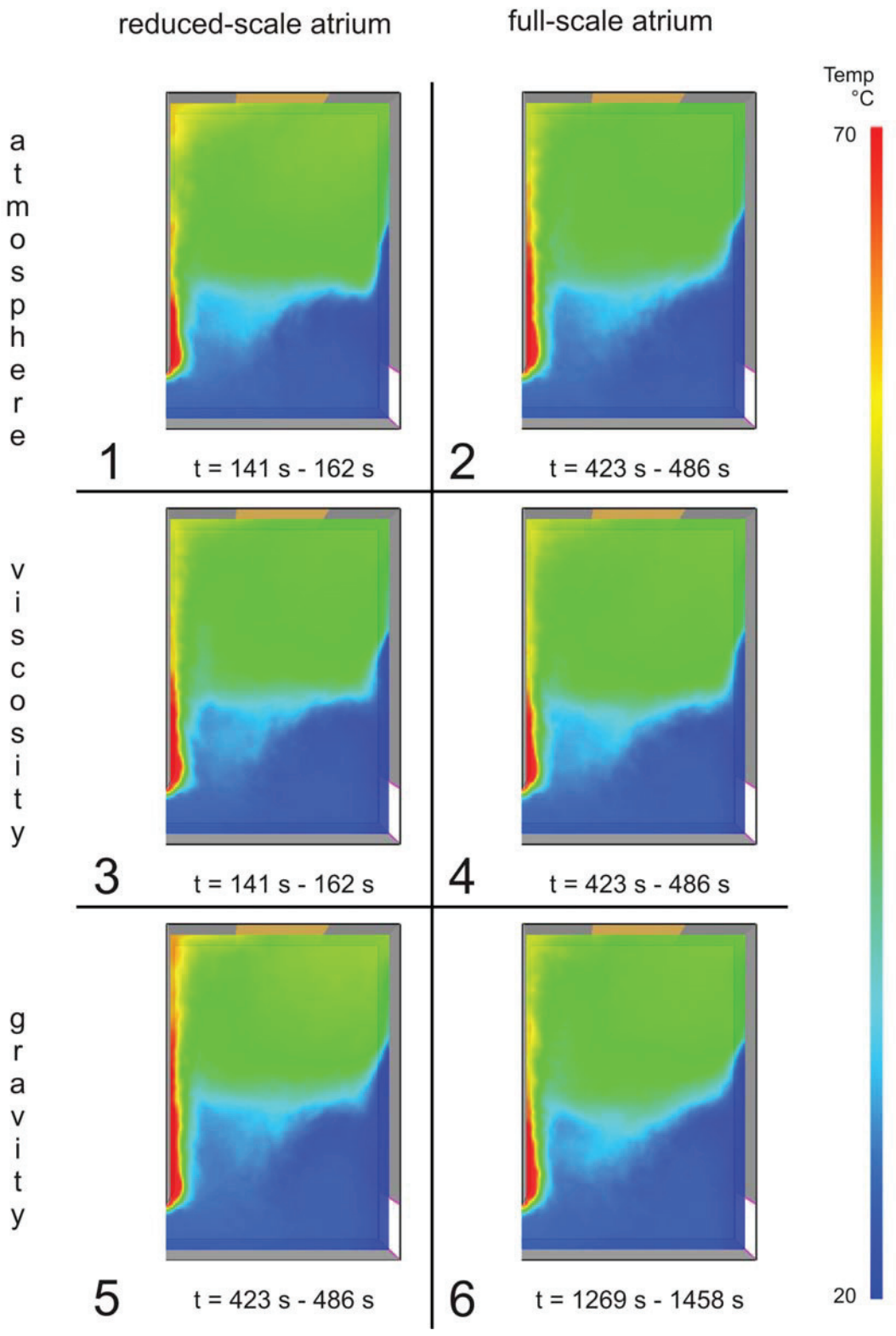

Figure 6.2 Averaged temperature fields in the vertical symmetry plane at corresponding times of simulations 1-6.

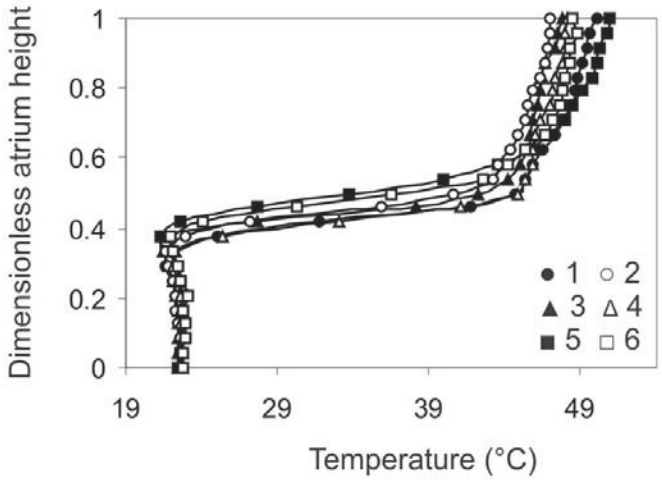

Figure 6.3 Temperature simulation data on a vertical line in the atrium.

Figs. 6.2 and 6.3 show the results for temperature in simulations 1 through 6. While Fig. 6.2 shows an averaged quasi-steady state temperature field in the vertical symmetry plane for each simulation, Fig. 6.3 displays the temperature profile on a vertical line in the atrium in all six simulations together. Both figures show that the temperature fields all agree well with each other. This reveals that, for the test case under study, scaling based on the Froude number alone is allowed. This also indicates that the correlations, derived for reduced-scale setups, can be applied to full-scale configurations. It is recalled here that this is usually assumed to only be true when all configurations are 'sufficiently' turbulent.

In simulations 7 and 8, on the other hand, the Re and Ra number are below the turbulence limit. In simulation 8, they are in the transition zone towards turbulent flows. The comparison of simulations 1, 3, 7 and 8 (all in the reduced-scale configuration, the only difference is the molecular viscosity) is displayed in Figs. 6.4 and 6.5.

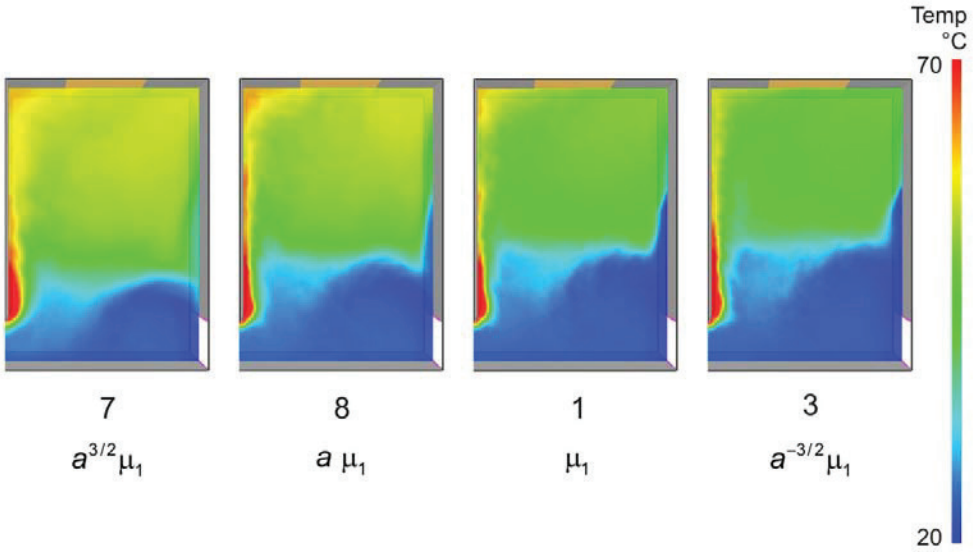

Figure 6.4 Averaged temperature fields between t = 141 s – 162 s of simulations 7, 8, 1 and 3. Ordering from left to right: laminar → turbulent.

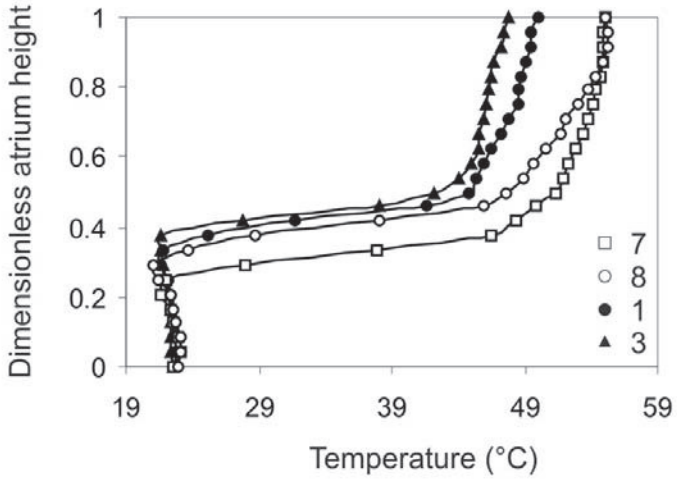

Figure 6.5 Temperature simulation data on a vertical line in the atrium.

The figures clearly show that the (laminar) simulation 7 is not in agreement with the other ones. Also the result of simulation 8, still deviates a little from the 'fully' turbulent results of simulations 1 and 3. As the Re and Ra numbers are too low for the flow to be sufficiently turbulent, data from these simulations are thus not representative, despite preservation of the Fr number. Note that simulation 4 has the same molecular viscosity as simulation 7. Between these two

simulations, only the dimensions of the setup have changed, the same difference as between simulations 1 and 2. However, both in simulations 1 and 2, the flow is turbulent, and thus the temperature results are in agreement. As from simulation 7 to simulation 4, the flow goes from laminar to turbulent, this agreement is no longer found.
Thus, this analysis confirms that Froude scaling is only allowed as long as flow in the reduced-scale setup is still sufficiently turbulent, and that this is automatically captured in the simulations.

6.4 Conclusion

Scaling of experimental and numerical setups has been discussed, based on dimensionless numbers. In particular, CFD simulation results on an atrium configuration have been analyzed. Scaling based on only the Froude number is allowed as long as all configurations are sufficiently turbulent.
When using a Smagorinsky turbulence model in LES simulations, the turbulent Reynolds number is automatically preserved in Froude scaling, if the mesh cell dimensions are scaled proportionally to the geometry dimensions. Thus, as long as the flow is sufficiently turbulent, Froude scaling applies also in CFD simulations.
If the flow is not sufficiently turbulent, the CFD simulations clearly and automatically reveal that Froude scaling is no longer reliable. Therefore, care must be taken not to operate in too low Reynolds or Rayleigh number ranges when performing model scale studies, be it in ‘real’ or ‘numerical’ experiments.

6.5 References

[1] McGrattan K, Klein B, Hostikka S, Floyd J, Fire Dynamics Simulator (Version 5) User's Guide, NIST 1019-5, National Institute of Standards and Technology (2008)

[2] McGrattan K, Hostikka S, Floyd J, Baum H, Rehm R, Mell W, McDermott R, Fire Dynamics Simulator (Version 5) Technical Reference Guide, NIST 1018-5, National Institute of Standards and Technology (2008)

[3] Quintiere J, Fundamentals of Fire Phenomena, John Wiley and Sons, Chichester (2006)

[4] Smagorinsky J, General Circulation Experiments with the Primitive Equations. I. The Basic Experiment, Monthly Weather Review 91: 99-164 (1963)

[5] Cooper LY, Harkleroad M, Quintiere J, Reinkinen W, An Experimental Study of Upper Hot Layer Stratification in Full-Scale Multiroom Fire Scenarios, J. of Heat Transfer 104: 741-749 (1982)

Chapter 7
Smoke extraction in atria, the 2D adhered spill plume

7.1 Introduction and setup

Similar to work presented in Chapters 4 and 6, the reduced-scale experimental atrium setup from Poreh et. al [1] is used as a starting point for a numerical study. In the experimental setup, a set of reduced-scale atrium experiments was carried out. In these experiments, the fire is located in the room adjacent to the atrium (Fig. 7.1) and four different convective heat release rates have been studied ($\dot{Q}_{conv}$). For every heat release rate, the extraction mass flow rate at the top of the atrium ($\dot{m}$) is varied, resulting in different smoke free heights above the spill edge (z_s) in the atrium. The mass flow rate at the spill edge ($\dot{m}_s$) and depth of the emerging smoke layer (d_s) are measured.

From the set of experiments, Poreh et. al proposed a single formula [1] to calculate the required extraction mass flow rate to ensure a certain smoke free height in the atrium:

$$\frac{\dot{m}(z_s)}{\dot{Q}_{conv}^{1/3}} = C\left(z_s + z_0\right) \tag{7.1}$$

with $C = 0.3 C_m \rho_0 W_s^{2/3}$ (7.2)

$$z_0 = d_s + \frac{\dot{m}_s}{C\dot{Q}_{conv}^{1/3}} \tag{7.3}$$

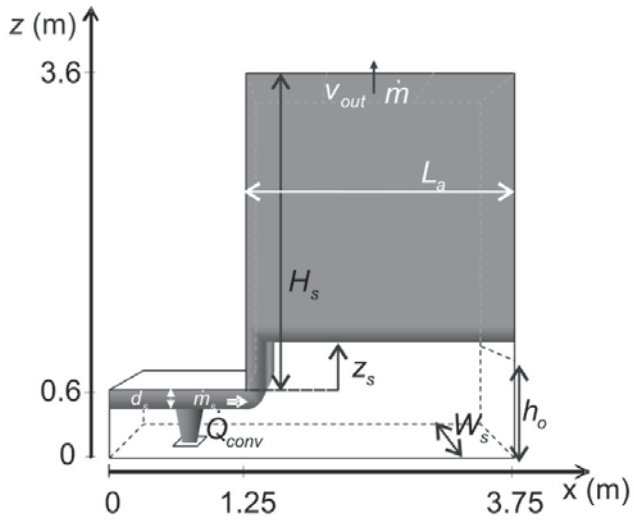

Figure 7.1 Atrium and adhered spill plume, basic configuration.

In these equations, z_0 is the virtual origin of the adhered spill plume, W is the width of the atrium and C_m = 0.21 for adhered spill plumes.
Substituting for C_m = 0.21 and ρ_0 = 1.2 kg/m^3, Eq. (7.1) becomes

$$\dot{m}(z_s) = 0.076 W_s^{2/3} \dot{Q}_{conv}^{1/3} (z_s + d_s) + \dot{m}_s . \qquad (7.4)$$

In recent work, an experimental study of the 2D adhered spill plume by Harrison and Spearpoint [2] includes a variation of the atrium width W_s. The results of Poreh et. al [1] were confirmed and a slightly better agreeing relation was suggested:

$$\dot{m}(z_s) = 0.08 W_s^{2/3} \dot{Q}_{conv}^{1/3} (z_s + d_s) + \dot{m}_s . \qquad (7.5)$$

The experimental setup of Poreh et. al [1] is here again reproduced in CFD simulations, carried out with FDS (Fire Dynamics Simulator, version 5.2.5 [3-4]). In Chapter 4, good agreement has already been shown between the numerical simulations and the experiments for a grid with cubic cells with edge size 2.5 cm.
Now, a grid with fewer cubic cells of edge size 5 cm is applied. As the grid contains fewer cells, the calculation cost of the simulations is significantly reduced.

As in Chapter 4, radiation is turned off in the simulations, only convective heat release rate of the fire is inserted and the walls of the atrium and adjacent room are modelled as adiabatic. The Smagorinsky LES turbulence model with C_s = 0.2 is used. As the Reynolds numbers (Chapter 6, $\mathrm{Re} = vW_s/\nu$) of all simulations reported in the present chapter are between 15000 and 80000, all flows are clearly turbulent.
The smoke layer interface temperature is calculated with the N-percent rule with N = 30 (Chapter 4):

$$T_{\mathrm{int}} = T_0 + \left(T_{\max} - T_0\right)\mathrm{N}/100\,. \qquad (7.6)$$

From the interface temperature, the smoke layer interface height above the spill edge (z_s) is calculated. The values for d_s, $\dot{m}(z_s)$, $\dot{m}_s$ and z_0 are calculated from the simulation output data as explained in Chapter 4.
At the outlet opening in the ceiling of the atrium, a constant velocity v_{out} is imposed for the extraction of smoke from the atrium.

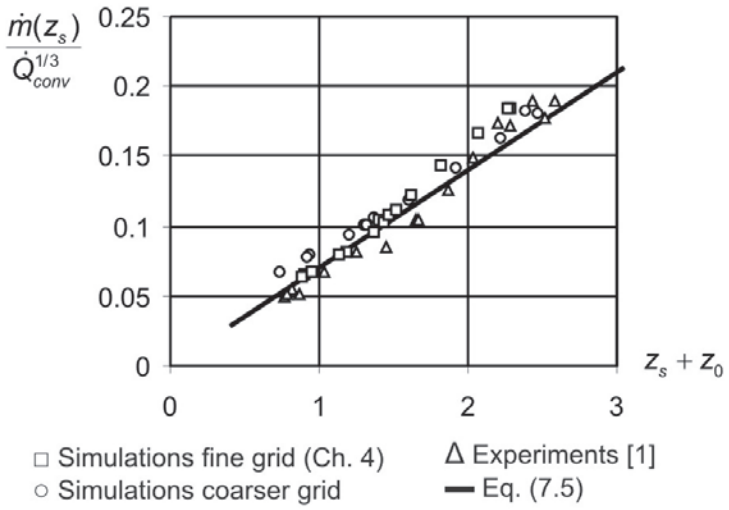

Figure 7.2 Confirmation of the validity of the coarser-grid simulations.

Fig. 7.2 shows the results of experiments as reported in [1], simulations with the finer grid as reported in Chapter 4 and the coarser grid simulations of the present chapter, as mentioned above. The picture shows only little deviation between experiments, finer-grid and coarser-grid simulation results. Thus, the conclusion here is that the relatively

coarse grid is sufficient for a parameter variation study with CFD simulations.

In the remainder of the present chapter, a basic configuration is first presented, on which the extraction mass flow rate is varied beyond the range studied in both [1] and [2]. First, the mass flow rate is varied by changing the extraction velocity. Afterwards, it is also changed by varying the extraction outlet area and with natural ventilation.
Starting from this basic configuration, variations of fire heat release rate, atrium width, atrium height above the spill edge and atrium length are performed and presented in paragraph 7.3. A new relation for the entire smoke extraction rate range is also presented there. In paragraph 7.4, variation of some of the ventilation parameters is discussed: position of the smoke extraction opening and size and position of the makeup air inlet opening.

In the present chapter, the results are presented as graphs picturing the change in smoke layer interface height z_s for varying mass flow rate $\dot{m}(z_s)$. Eq. (7.5) can be rewritten as:

$$\dot{m}\left(z_s\right)=\left(0.08W_s^{2/3}\dot{Q}_{conv}^{1/3}\right)z_s+\left(0.08W_s^{2/3}\dot{Q}_{conv}^{1/3}d_s+\dot{m}_s\right). \qquad (7.7)$$

For every combination of input variables (fire heat release rate and atrium width) studied, the input values and the values for $\dot{m}_s$ and d_s as obtained from the simulations, are inserted.

For example, the basic configuration as presented in paragraph 7.2 concerns the combination of heat release rate $\dot{Q}_{conv}=11.9\,\mathrm{kW}$ and atrium width W_s = 0.9 m (as in the results reported in [1] and Chapter 4). Values for smoke layer depth and mass flow rate emerging from the adjacent room were found to be d_s = 0.17 m and $\dot{m}_s$ =0.09 kg/s. This way, Eq. (7.7) becomes:

$$\dot{m}(z_s)=0.17z_s+0.119. \qquad (7.8)$$

As the atrium height is 3.6 m and the spill edge is at height 0.6 m, the maximum value to be obtained for the smoke free height above the spill edge is z_s = 3 m, corresponding to an extraction mass flow rate of 0.63 kg/s with Eq. (7.8).

7.2 Basic configuration and multi-dimensional smoke layer

The basic configuration, as mentioned, has a fire heat release rate $\dot{Q}_{conv} = 11.9\,\text{kW}$ and atrium width W_s = 0.9 m. Within this configuration, the extraction mass flow rate is varied. Although this was of course also the variation in Chapter 4 and in the experiments of Poreh et. al [1] and Harrison and Spearpoint [2], the extraction mass flow rate is now increased beyond the range studied in [1], [2] and Chapter 4.

In the simulations, it appears that as the extraction mass flow rate increases beyond a certain value, the smoke layer becomes multi-dimensional, meaning that interface height changes with *x*-position in the atrium (Fig. 7.3).
This effect is due to the limited atrium size, and the central position of the extraction outlet. As the smoke jet underneath the ceiling of the atrium has a momentum in the *x*-direction, not all the smoke is extracted by the mechanical smoke extraction outlet in the *z*-direction. The non-extracted smoke creates a large-scale vortex in the atrium and thus causes the multi-dimensional effect.

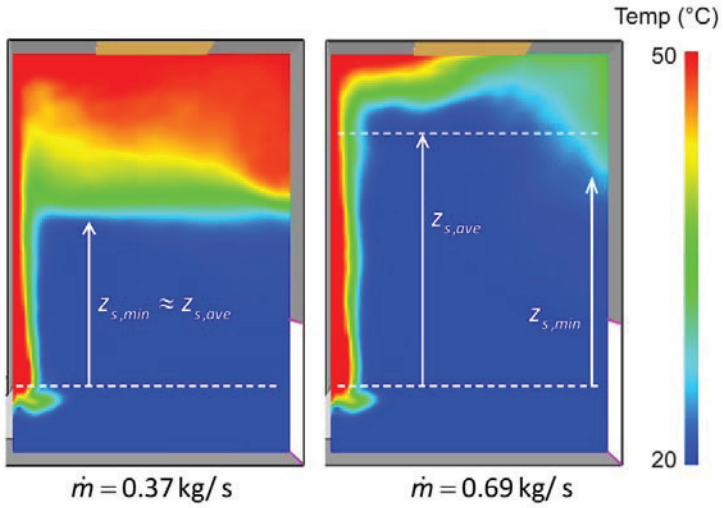

Figure 7.3. One-dimensional (left) versus multi-dimensional (right) smoke layer pattern in atrium. Temperature fields at y = 0.45 m, time-averaged quasi steady-state data for 20s.

In this smoke layer pattern, it is not straightforward to define an unambiguous value for smoke free height. In the remainder of this chapter, both the minimum and average values of the smoke free height in the atrium are shown in the presentation of the results. As long as these minimum and average smoke free heights have the same value, the smoke layer is one-dimensional. When the minimum value becomes lower than the average one, the smoke layer shows the multi-dimensional pattern.

Fig. 7.4 shows the variation of the extraction mass flow rate within and beyond the range mentioned above, by changing the outlet velocity v_{out} at the extraction outlet between 0.2 m/s and 0.9 m/s while maintaining the outlet opening area constant at 1 m x 0.9 m. The experiments from [1] and lower-range finer-grid simulations of Chapter 4 are also shown in the picture, as well as Eq. (7.7) (black line).

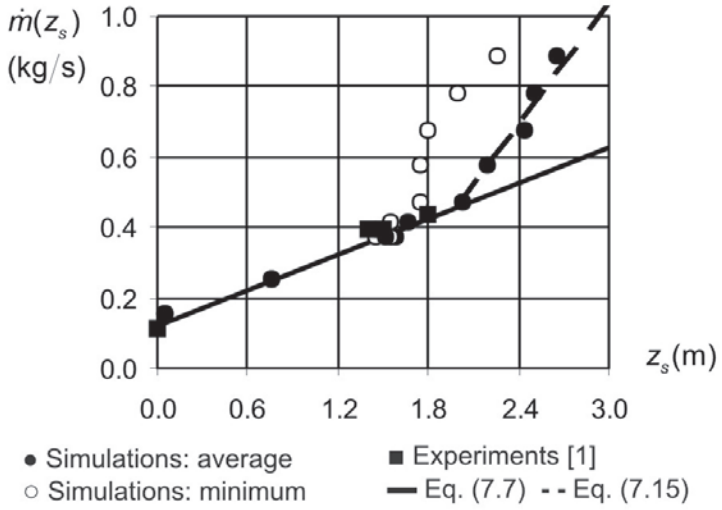

Figure 7.4 Basic configuration simulation results.

The graph clearly shows that the results of both experiments and simulations are in very good agreement with Eq. (7.7) for extraction mass flow rates below 0.4 kg/s. Within this range, the smoke layer pattern is still one-dimensional.

When the extraction mass flow rate exceeds 0.4 kg/s, however, the smoke layer becomes multi-dimensional and the results start to differ from the proposed Eq. (7.7).

It appears that the average smoke layer interface height follows a new slope in the graph, starting from a certain threshold value. From that point onward, the smoke layer height still increases with increasing mass flow rate, but slower than for lower extraction mass flow rates. Because of the multi-dimensional smoke layer effect, the vortex at the right-hand side of the atrium (Fig. 7.3) will cause a lower smoke-free height than what would be expected from extrapolation of the one-dimensional smoke layer results. The dashed line already indicates the resulting relation presented later on in the present chapter, Eq. (7.15).

For now, this relation can be presented as

$$\dot{m}(z_s) = a\, z_s + b\,. \tag{7.9}$$

The smoke layer shows the multi-dimensional effect here starting from a value of $z_s \approx 2$ m on, which is at $z_s = 2/3\ H_s$.

7.3 Variation of fire and atrium configuration

7.3.1 Variation of fire heat release rate

The question is now first raised if for other heat release rate values, the same effect can be noted. Thus, for other heat release rate values (as also studied in [1] and Chapter 4), the extraction mass flow rate is varied beyond the range that has already been studied.

Figs. 7.5 and 7.6 show the results. The black line in the figures (Eq. (7.7)) is calculated with the corresponding heat release rate and atrium width (W_s = 0.9 m). Again both the experiments of [1] and simulations of Chapter 4 are also presented in the graphs, together with resulting relation Eq. (7.15) presented further in the present chapter and represented as a dashed line.

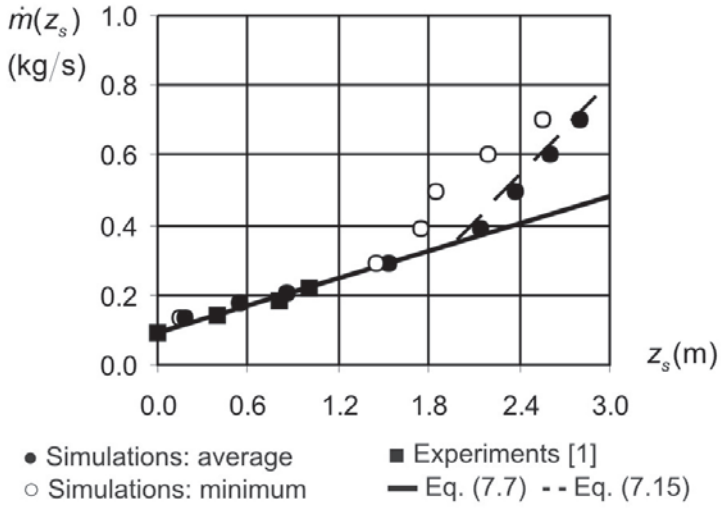

Figure 7.5 Simulation results for heat release rate variation: $\dot{Q}_{conv}$ = 5.4 kW .

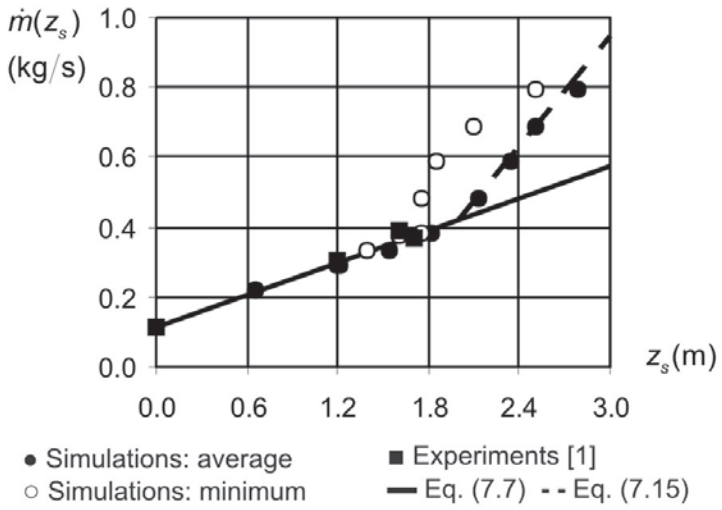

Figure 7.6 Simulation results for heat release rate variation: $\dot{Q}_{conv}$ = 8.8 kW .

The graphs indeed show the same effect: the slope of the increase in smoke layer height with increasing extraction mass flow rate starts to differ from Eq. (7.7) from a certain threshold value on. Again, this threshold value is at z_s = 2/3 H_s, confirming the limit already found above.
The slope of the dashed lines (Eq. (7.9)) is found to vary as

$$a \sim \dot{Q}_{conv}^{1/3} . \tag{7.10}$$

This is in line with Eq. (7.5).

7.3.2 Variation of the outlet opening area and natural ventilation

With mechanical ventilation, the extraction mass flow rate at the ceiling of the atrium can be altered by means of the extraction velocity v_{out}, with fixed outlet opening area (see before), but also by variation of the outlet area while maintaining a constant outlet velocity.

Fig. 7.7 shows the results of the simulation where the outlet area is varied, maintaining the outlet velocity at v_{out} = 0.6 m/s. The average smoke layer height in the atrium clearly shows the same trend as in the

previous section. The slope of the increase of the smoke layer height z_s is thus really dependent on the increase of extraction mass flow rate $\dot{m}(z_s)$ and not on the way in which $\dot{m}(z_s)$ is increased.

Note that the deviation from the solid line is not a plugholing effect: even in the simulation with the highest extraction mass flow rate in Fig. 7.7, the entire outlet opening area is extracting smoke.

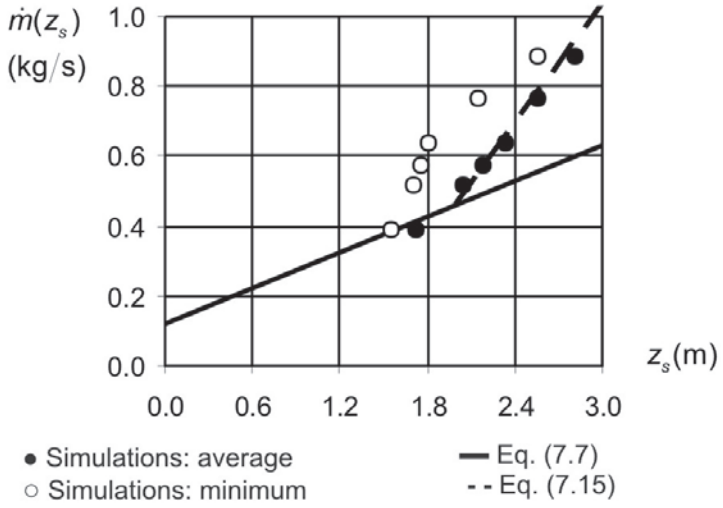

Figure 7.7 Variation of outlet extraction area: simulation results.

The smoke can also be removed from the atrium by means of natural ventilation. In this situation, the extraction opening area is varied, but no velocity is imposed, allowing smoke to freely exit the atrium through the opening. The increase of ventilation opening is performed until the situation is reached where the opening is so large that makeup air starts to flow through this opening into the atrium. This situation is beyond the scope of the present study. The extraction opening area is increased from 0.49 m^2 to 1.35 m^2. The results are displayed in Fig. 7.8.

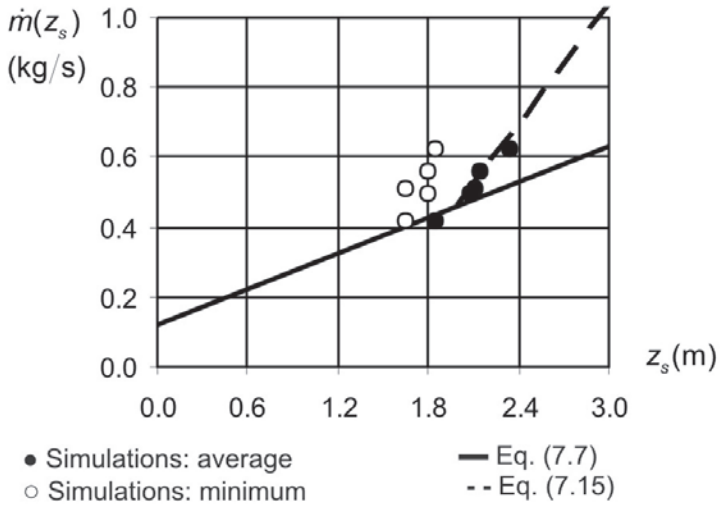

Figure 7.8 Natural ventilation in atrium: simulation results.

Again, deviation from the proposed Eq. (7.7) is noted for higher outlet mass flow rates. Above the threshold value, the multi-dimensional smoke layer is present in the simulations, following the same slope as for forced extraction.

Fig. 7.9 shows the variation of outlet mass flow rate $\dot{m}$ and outlet velocity v_{out} for increasing outlet area in the natural ventilation simulations. Although the outlet velocity decreases with increasing outlet area, the resulting mass flow rate increases with increasing outlet area. For an outlet area of 0.9 m^2 (as in paragraph 7.2), the outlet velocity in the case of natural ventilation is $v_{out} \approx 0.6$ m/s, the velocity that was used in studying the effect of variation of the outlet opening area, above in the present paragraph.

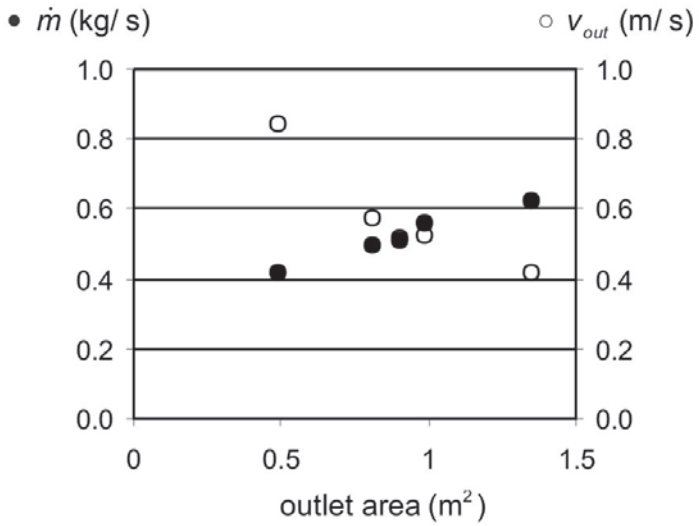

Figure 7.9 Mass flow rate and outlet velocity for natural ventilation in atrium.

7.3.3 Variation of the atrium width

While maintaining a constant fire heat release rate value $\dot{Q}_{conv} = 11.9\text{kW}$, the width of the atrium is now varied. Starting from the basic configuration with width W_s = 0.9 m, the width is increased (W_s = 1.2 m) and decreased (W_s = 0.75 m and 0.6 m). The results of these simulations (and resulting Eq. (7.15) presented as dashed line) are shown in Figs 7.10, 7.11 and 7.12.

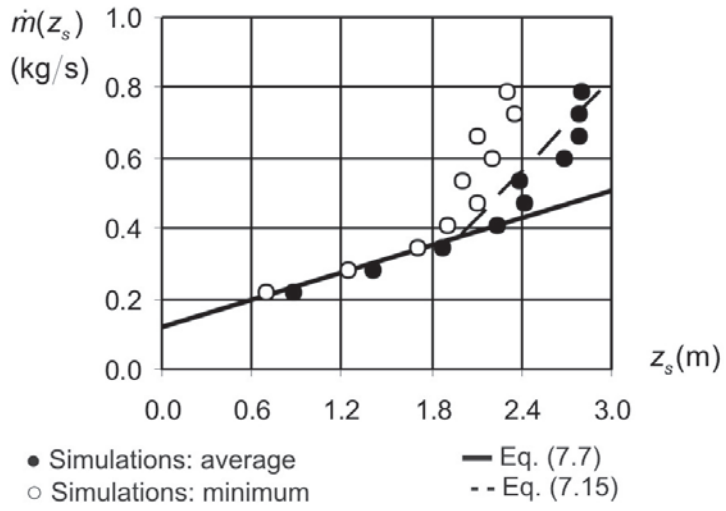

Figure 7.10 Simulation results for the variation of width: W_s = 0.6 m.

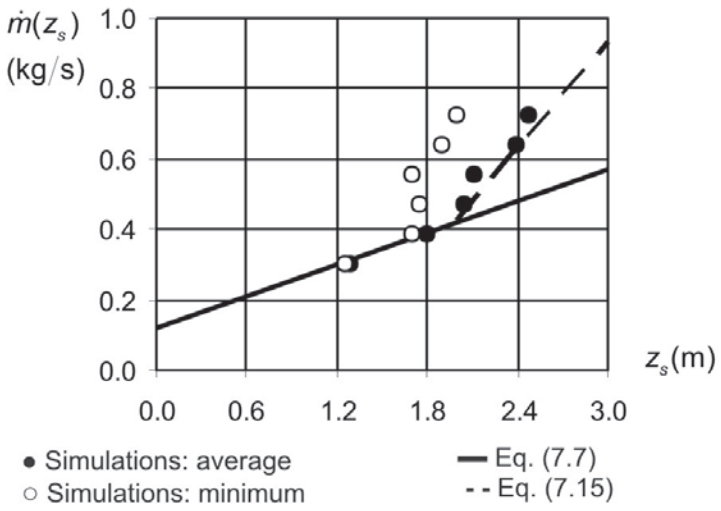

Figure 7.11 Simulation results for the variation of width: W_s = 0.75 m.

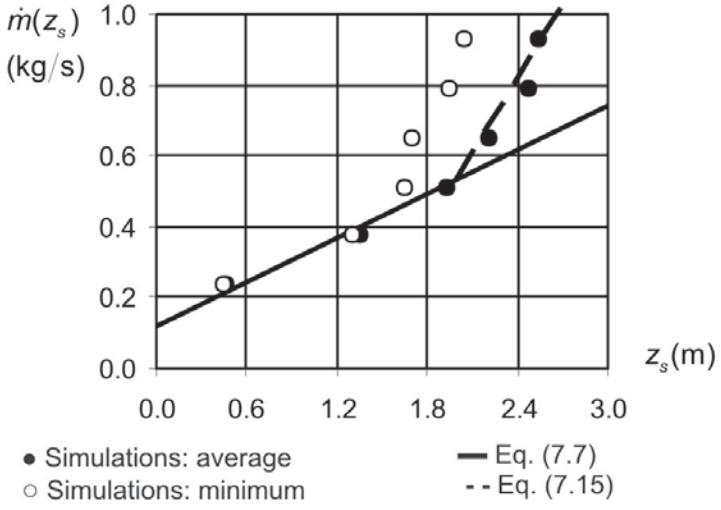

Figure 7.12 Simulation results for the variation of width: W_s = 1.2 m.

Again, the threshold value for the formation of the multi-dimensional smoke layer is at $z_s = 2/3\ H_s$. The slope of the dashed lines varies with

$$a \sim W_s^{2/3}. \tag{7.11}$$

This is again in line with Eq. (7.5).

To confirm the effects of changing fire heat release rate and atrium width together, a set of simulations is performed with W_s = 0.6 m and $\dot{Q}_{conv} = 5.4$ kW. Fig. 7.13 shows that the proposed trends (variation of the slope with $W_s^{2/3}$ and $\dot{Q}_{conv}^{1/3}$) are confirmed.

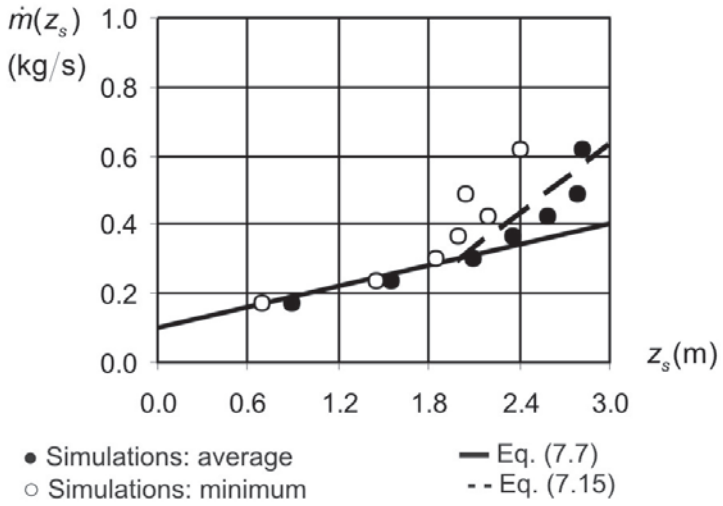

Figure 7.13 Simulation results for $\dot{Q}_{conv}$ = 5.377 kW and W_s = 0.6 m.

7.3.4 Variation of the atrium height and length

In the above results, the threshold value for the start of the multi-dimensional smoke layer effect in the atrium is found at z_s = 2/3 H_s. A variation of H_s has been performed in order to verify if this value is general.

Figs. 7.14, 7.15 and 7.16 show the results for the variation of atrium height above the spill edge, H_s = 2.4 m, 4.2 m and 5.4 m.

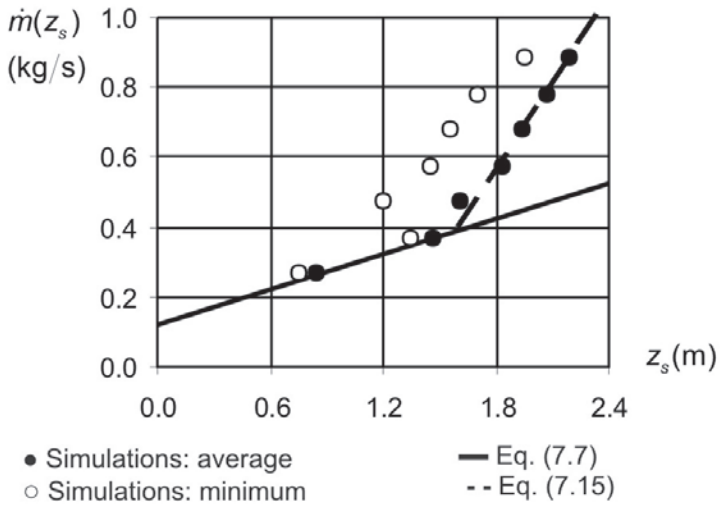

Figure 7.14 Simulation results for the variation of height: H_s = 2.4 m.

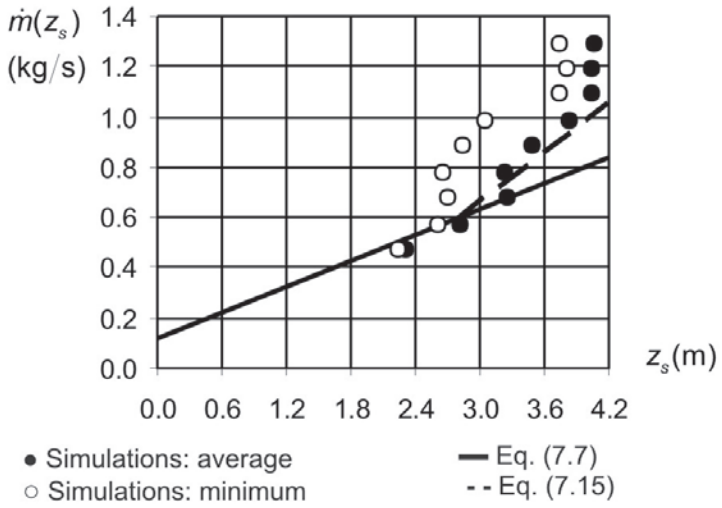

Figure 7.15 Simulation results for the variation of height: H_s = 4.2 m.

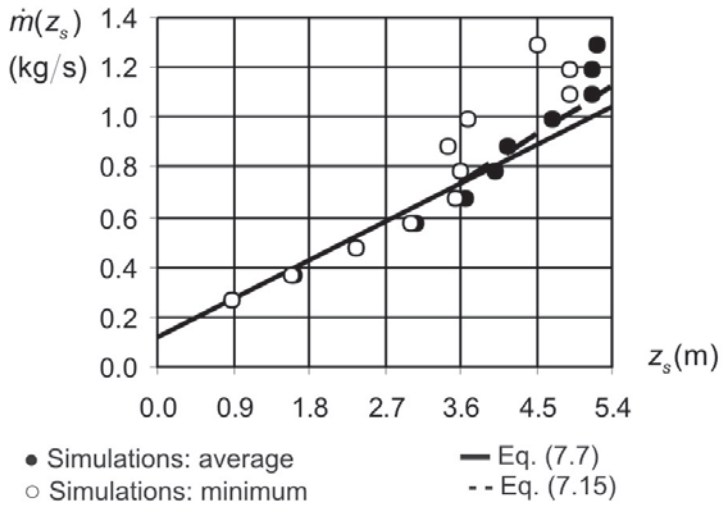

Figure 7.16 Simulation results for the variation of height: H_s = 5.4 m.

It is confirmed that the threshold value for the smoke layer transformation from one-dimensional into multi-dimensional is at z_s = $2/3\ H_s$.

Not only can the height of the atrium vary in size, the length L_a can also be altered (Fig. 7.1). One can foresee that a smaller atrium has a similar effect to a higher one, so the inverse effect of the variation of atrium height H_s is expected. The length of the atrium is in the present study varied from the basic configuration (L_a = 2.5 m) to lower (L_a = 1.25 m and 2 m) and higher (L_a = 3 m and 3.75 m) values. Figs. 7.17, 7.18, 7.19 and 7.20 show the results of these variations.

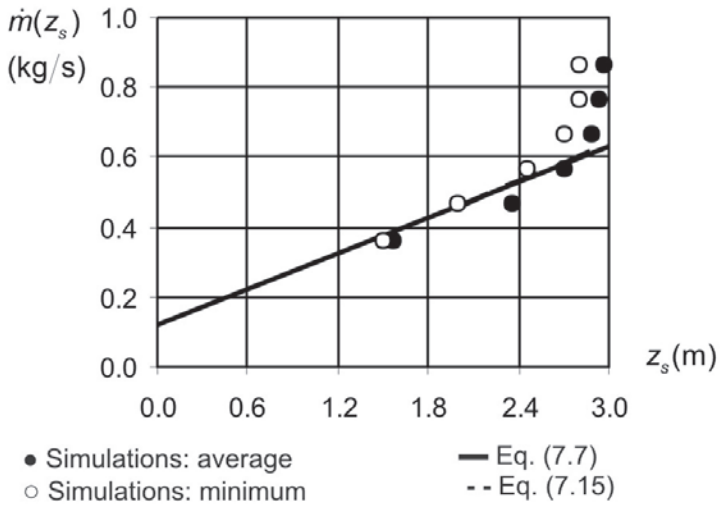

Figure 7.17 Simulation results for the variation of length: L_a = 1.25 m.

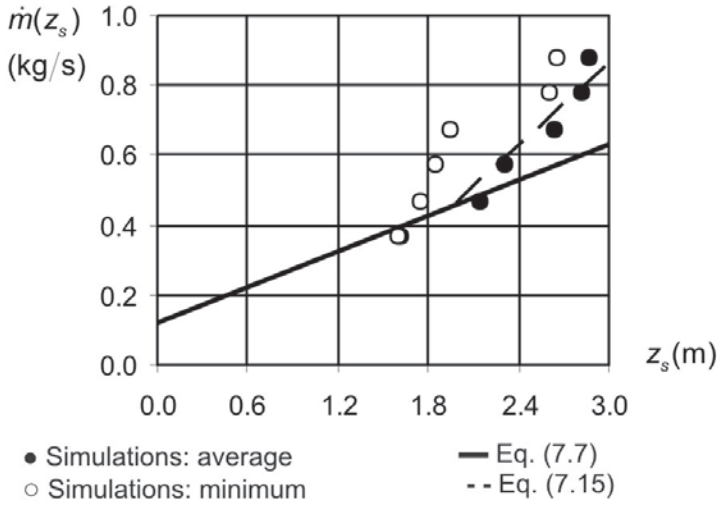

Figure 7.18 Simulation results for the variation of length: L_a = 2 m.

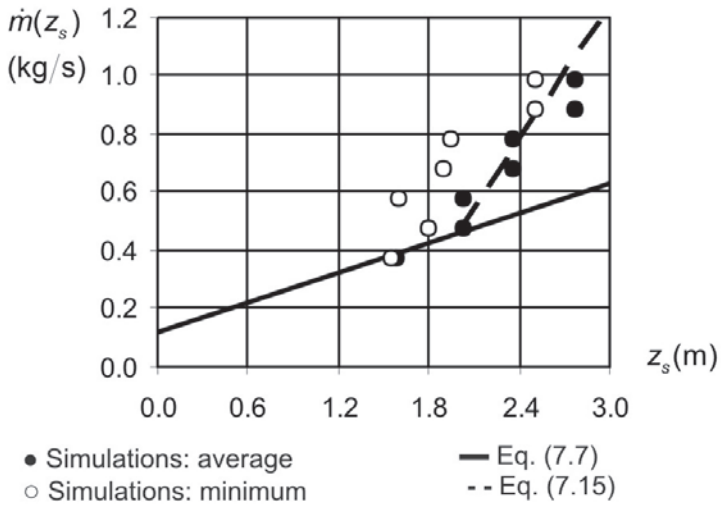

Figure 7.19 Simulation results for the variation of length: L_a = 3 m.

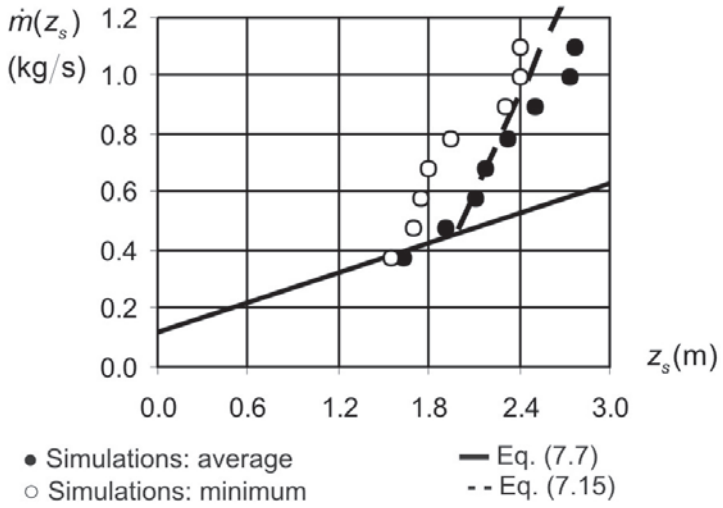

Figure 7.20 Simulation results for the variation of length: L_a = 3.75 m.

As expected, the results indeed show that an atrium with smaller length (Figs. 7.17 and 7.18) behaves similar as a higher atrium (Figs. 7.15 and 7.16), i.e. a smaller slope in Eq. (7.9). The atria with larger length (Fig. 7.19 and 7.20) have a higher slope, similar to a lower atrium (Fig. 7.14). The slope of the dashed lines shows a variation:

$$a \sim \left(\frac{L_a}{H_s} \right)^{5/3} \quad \text{for } H_s/L_a < 2.5 \tag{7.12}$$

More research on the impact of the variation of atrium length and height is desirable. At first sight, the exponent 5/3 is found from the simulations. However, more research would be useful to either confirm or adjust this value.

7.3.5 Discussion

In the present paragraph, the threshold value for the start of the multi-dimensional effect in the atrium is proposed to be at $z_s = 2/3H_s$. With Eq. (5), this corresponds to a threshold value for $\dot{m}(z_s)$ at

$$\dot{m}\left(z_s\right) = 0.08 W_s^{2/3} \dot{Q}_{conv}^{1/3} \left(\frac{2}{3} H_s + d_s\right) + \dot{m}_s \tag{7.13}$$

From the variation of parameters in the above presented numerical simulations, it can be suggested that the slope of the multi-dimensional smoke layer equation in the presentation of $\dot{m}(z_s)$ versus z_s (Eq. (7.9)) follows a slope

$$a = 2.5^{5/3} \cdot 0.08 \left(\frac{L_a}{H_s}\right)^{5/3} W_s^{2/3} \dot{Q}_{conv}^{1/3} . \tag{7.14}$$

In the configuration with L_a = 2.5 m and H_s = 3 m, this becomes $a = 3.4 \cdot 0.08 \cdot W_s^{2/3} \dot{Q}_{conv}^{1/3}$. It is important to consider that when further research would suggest an adjustment of the exponent 5/3 in Eq. (7.12), that the factor 2.5 in Eq. (7.14) (together with its exponent) needs to be adjusted accordingly to agree with this relation.

As the new relation (Eq. (7.9)) has to cross the relation for one-dimensional smoke layer (Eq. (7.5)) at the threshold value, the resulting equation for the multi-dimensional smoke layer becomes:

$$\dot{m}\left(z_s\right) - \dot{m}_s = 0.08 W_s^{2/3} \dot{Q}_{conv}^{1/3} \left(2.5^{5/3} \left(\frac{L_a}{H_s}\right)^{5/3} \left(z_s - \frac{2}{3} H_s\right) + \frac{2}{3} H_s + d_s\right) \text{for} \frac{H_s}{L_a} < 2.5 . \tag{7.15}$$

Indeed, at z_s = 2/3 H_s, the threshold value for $\dot{m}(z_s)$ becomes Eq. (7.13). For H_s/L_a = 2.5, Eq. (7.15) equals Eq. (7.5) for one-dimensional smoke layers. Furthermore, both Eq. (7.13) and Eq. (7.15) correspond to Froude scaling, i.e. when Froude scaling is applied to scale up the reduced-scale configuration to a full-scale atrium: $L_f = a\ L_r$, both the left hand side and right hand side of Eq. (7.15) will scale as $a^{5/2}$, so the equation is preserved and thus can be used both for reduced- and full-scale configurations.

In total, the resulting relations for extraction mass flow rate for adhered plumes in limited atria can be written as

$$\begin{cases} \dot{m}(z_s) - \dot{m}_s = 0.08 W_s^{2/3} \dot{Q}_{conv}^{1/3} (z_s + d_s) \\ \qquad\qquad \text{for } z_s < \dfrac{2}{3} H_s \ \text{ or } \ \dfrac{H_s}{L_a} > 2.5 \\ \dot{m}(z_s) - \dot{m}_s = 0.08 W_s^{2/3} \dot{Q}_{conv}^{1/3} \left(2.5^{5/3} \left(\dfrac{L_a}{H_s} \right)^{5/3} \left(z_s - \dfrac{2}{3} H_s \right) + \dfrac{2}{3} H_s + d_s \right) \\ \qquad\qquad \text{for } z_s > \dfrac{2}{3} H_s \text{ and } \dfrac{H_s}{L_a} < 2.5 \end{cases} \tag{7.16}$$

Fig. 7.21 shows the results of simulated values of average smoke free height above the spill edge versus calculated values with Eq. (7.16). Good agreement is noticed between the simulation data and the proposed relation.

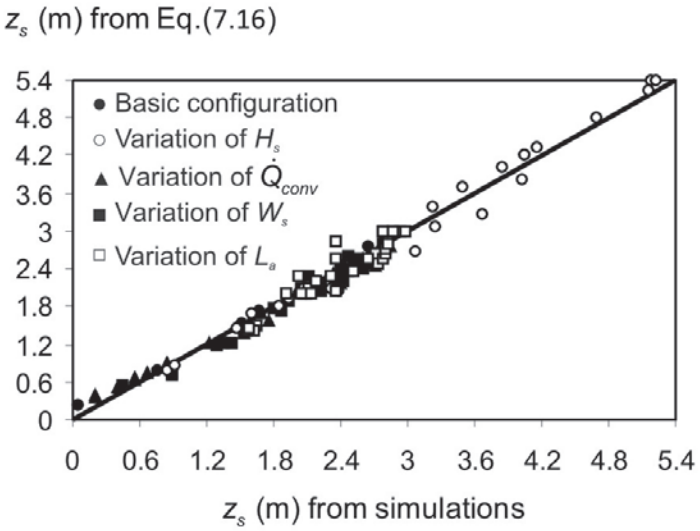

Figure 7.21 Smoke free height above spill edge from Eq. (7.16) and as obtained from the simulations.

7.4 Variation of ventilation parameters

The above result of paragraph 7.3 is valid for an atrium configuration with the smoke extraction outlet in the centre of the atrium ceiling, and the makeup air inlet opening in the atrium wall opposed to the adjacent room where the fire occurs (Fig. 7.1).

However, other configurations of outlet and inlet opening can occur in real atria. Therefore, the effects of those parameters are studied by using the same approach as above: using simulations as 'numerical experiments' to study a parameter variation in the atrium. The varied parameters in the present paragraph are:
- position of the smoke extraction opening
- position of the makeup air inlet opening
- size of the makeup air inlet opening.

In the present paragraph, the effect of the different parameters is studied for a single heat release rate $\dot{Q}_{conv} = 11.9\,\mathrm{kW}$ and a single atrium width, length and height above the spill edge W_s = 0.9 m, L_a = 2.5 m, H_s = 3 m. By inserting these values into Eq. (7.16), and substituting for

emerging mass flow rate and smoke layer thickness $\dot{m}_s$ = 0.09 kg/s and d_s = 0.17 m (as in paragraph 7.1), the relation between extraction mass flow rate $\dot{m}(z_s)$ and smoke free height above the spill edge z_s becomes:

$$\begin{cases} \dot{m}(z_s) = 0.178\, z_s + 0.119 & \text{for } z_s < 2\,\text{m} \\ \dot{m}(z_s) = 0.681\, z_s - 0.903 & \text{for } z_s > 2\,\text{m} \end{cases} \tag{7.17}$$

7.4.1 Smoke extraction opening position

The position of the smoke extraction outlet is the first ventilation parameter variation studied. Fig. 7.22 shows the position of the extraction outlet in the three different configurations studied. The middle outlet configuration corresponds to the basic configuration (Fig. 7.1).

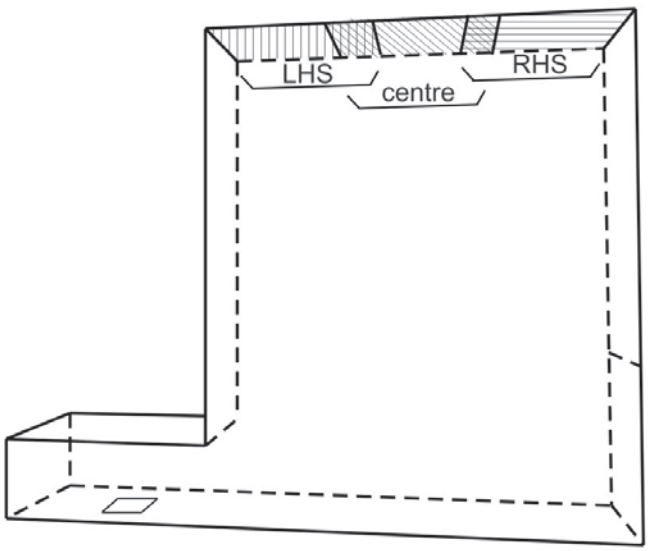

Figure 7.22 Extraction outlet position.

The results from the simulations of left- and right-hand-side positioned outlet are displayed in Figs. 7.23 and 7.24, respectively.

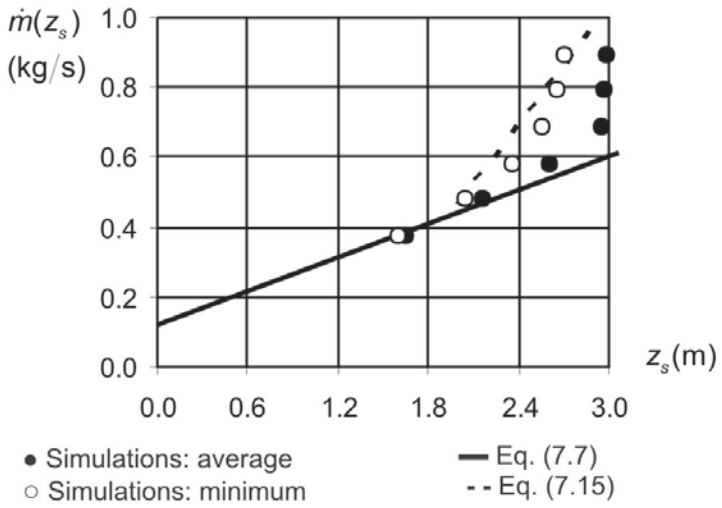

Figure 7.23 Simulation results of left-hand-side positioned outlet.

In the configuration when the outlet is placed at the left hand side (Fig. 7.23), the increase of average smoke layer height with increasing extraction mass flow rate follows the proposed relation by Harrison and Spearpoint (Eq. (7.5)) almost perfectly. From the threshold value on, however, the smoke layer also starts to become multi-dimensional in the atrium. But as the extraction outlet is now placed exactly above the rising adhered smoke plume, there is no horizontal momentum of the smoke layer near the outlet, in contrast to the configuration with the extraction outlet placed in the centre of the ceiling. Therefore, the multi-dimensional effect is much less pronounced in the atrium if the extraction outlet is above the rising plume.

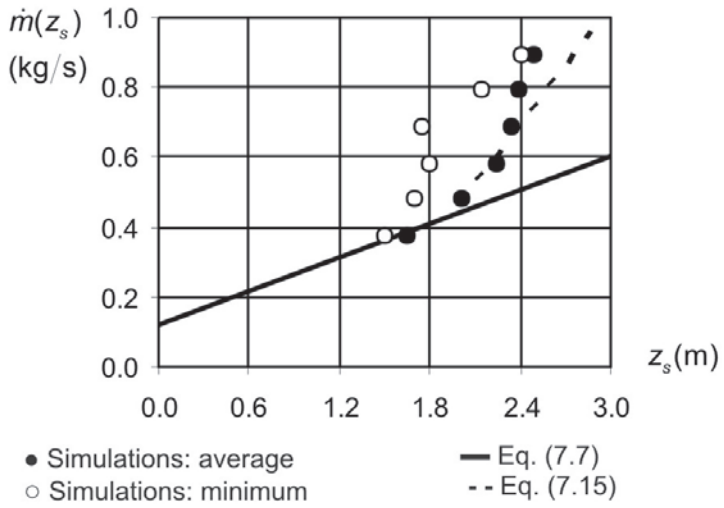

Figure 7.24 Simulation results of right-hand-side positioned outlet.

When the extraction outlet is at the right hand side of the atrium ceiling (Fig. 7.24), on the contrary, the slope of the increase of smoke layer height with increasing extraction mass flow rate beyond the threshold value deviates a little from the proposed Eq. (7.17) such that the situation for the right-hand-side outlet is a little "worse": for the same extraction mass flow rate, the smoke layer interface height is lower in the atrium. In this case, the suggested slope is not conservative. However, the difference is quite small.

As in many realistic situations the location of the fire is not predefined, a smoke extraction outlet in the centre of the atrium is a reasonable compromise. Possibly, it is not the best position for the smoke extraction, but at the same time, it is not the worst either. Also in design calculations, one cannot rely on the assumption that the extraction opening is in the 'ideal' position.

7.4.2 Makeup air inlet position

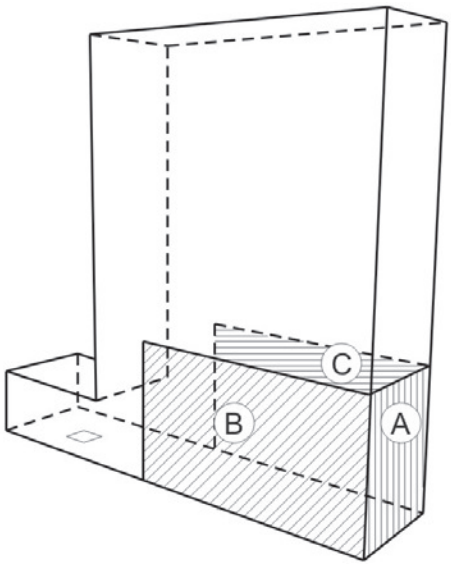

Figure 7.25 Position of the makeup air inlet openings.

A second parameter is the variation of the makeup air inlet position. Fig. 7.25 shows the atrium configuration with the location of the different studied inlet positions.
In the basic configuration of Fig. 7.1, the inlet is in the wall of the atrium opposite to the adjacent room where the fire occurs (position A). The inlet positions B and C are designed such that the smoke layer emerging from the adjacent room can turn around the spill edge, without smoke leaving the atrium through the inlet air openings. That is why makeup air inlet positions B and C are only 2 m wide, and thus do not cover the entire side of the atrium. Any situation where smoke is able to leave the atrium through a makeup air inlet opening is beyond the scope of the present study.

A first variation from the basic situation is when the front and back side of the atrium are partly open (inlet positions B + C) and the opening of the basic configuration (A) is closed. Fig. 7.26 shows the result of the simulations with inlet opening B+C.

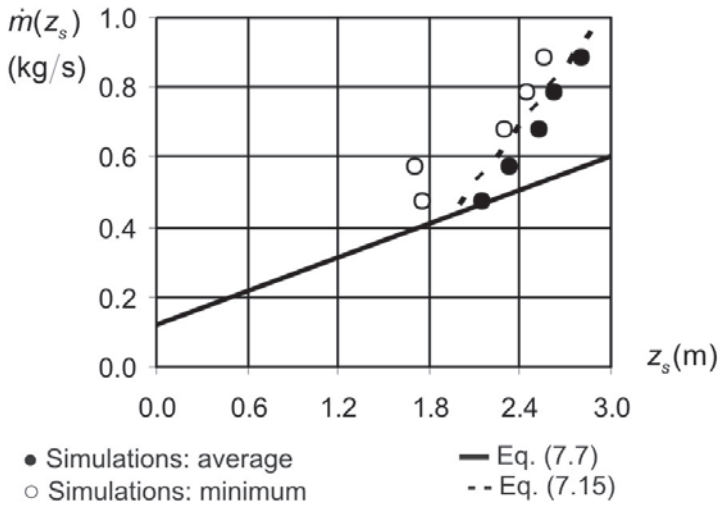

Figure 7.26 Simulation results for inlet opening B+C.

Compared to the basic configuration results in Fig. 7.27, the results in Fig. 7.26 show less of the multi-dimensional smoke layer pattern, as the difference between $z_{s,ave}$ and $z_{s,min}$ is smaller.

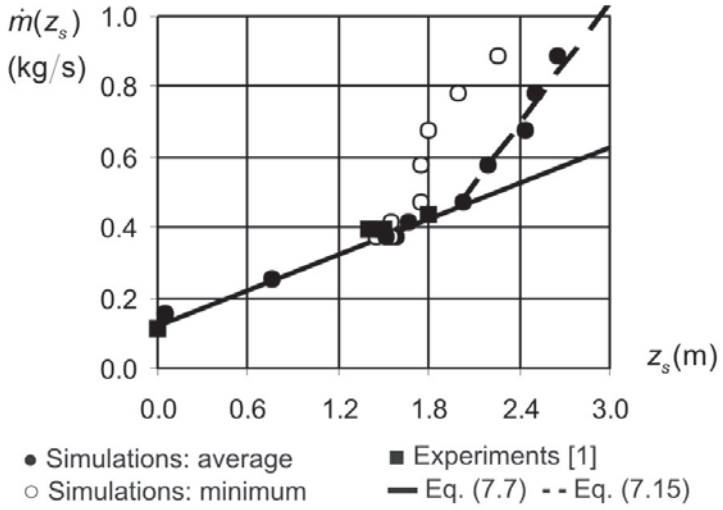

Figure 7.27 Repetition of Fig. 7.4: Basic configuration simulation results.

However, the results for $z_{s,ave}$ with opening B+C are very similar to those with opening A, and Eq. (7.17) agrees well with the increase of $z_{s,ave}$ with $\dot{m}(z_s)$ for inlet opening position B + C.

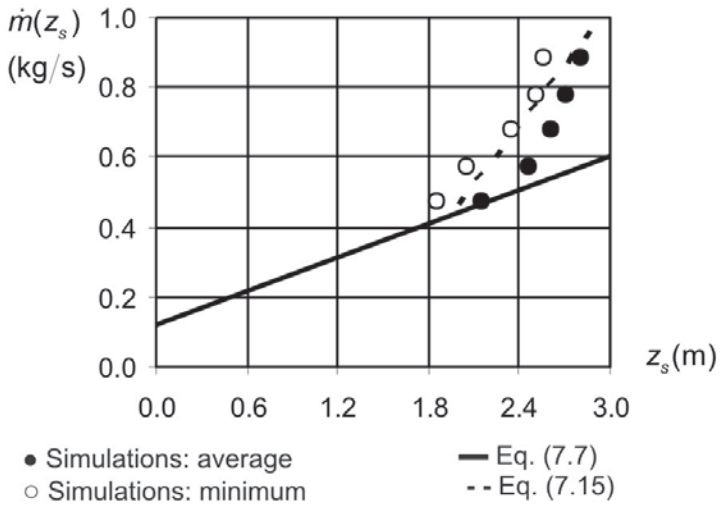

Figure 7.28 Simulation results for inlet opening B.

Fig. 7.28 shows the result of the configuration with only inlet opening B present. The graph shows that the result is slightly better (higher smoke free height for the same extraction mass flow rate) than the previous two configurations (opening A and B+C), but not significantly.

In this configuration (inlet B) it is interesting to study the smoke layer pattern from a different view, as the makeup air inlet opening is now no longer placed symmetrically along the y = 0.45 plane in the atrium. A view of the temperature field in the plane x = 2.5, however, reveals no asymmetric effects in the atrium (Fig. 7.29). Apparently, the inlet opening is large enough not to create a significant disturbance in the smoke layer (see below in paragraph 7.5.3).

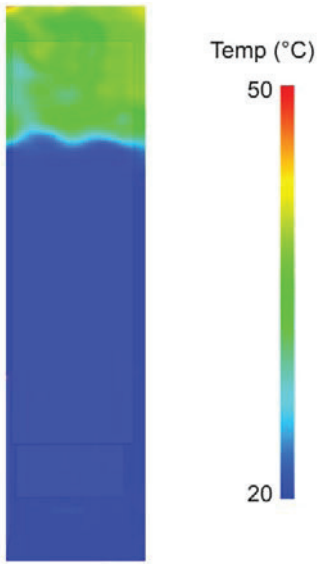

Figure 7.29 Average temperature field between t = 80 s and t = 100 s in plane x = 2.5 m for only inlet opening B present.

Fig. 7.30 shows the last studied inlet position configuration, where all inlet positions (A+B+C) are open in the atrium. The results of these simulations are again in quite good agreement with Eq. (7.18) and also with Fig. 7.26 (openings B+C). This leads to conclude that the exact position of the inlet opening does not strongly affect the smoke layer pattern in the atrium, even when an asymmetric makeup air opening is present.

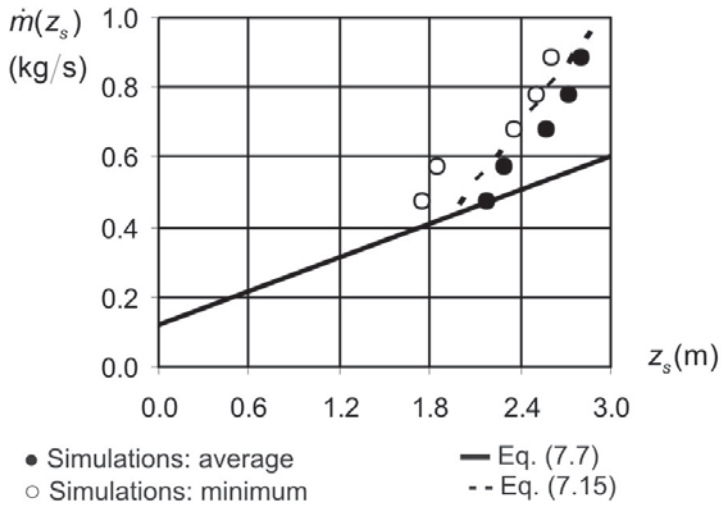

Figure 7.30 Simulation results for inlet opening A+B+C.

7.4.3 Makeup air inlet opening size

The last studied parameter in the present chapter is the size of the makeup air inlet opening. Opening configuration A is considered, with variation of the height h_o of the opening (Fig. 7.1). In the basis configuration of paragraph 7.2, the opening height is h_o = 1.2 m. Larger (h_o = 1.5 m) and smaller (h_o = 1.0 m, 0.6 m, 0.3 m) are discussed in the present paragraph.

With an opening height of h_o = 1.5 m, the average smoke layer height in the atrium follows the same pattern as in the basic configuration of Fig. 7.27 (where the opening height is h_o = 1.2 m) with increasing extraction mass flow rate (Fig. 7.31).

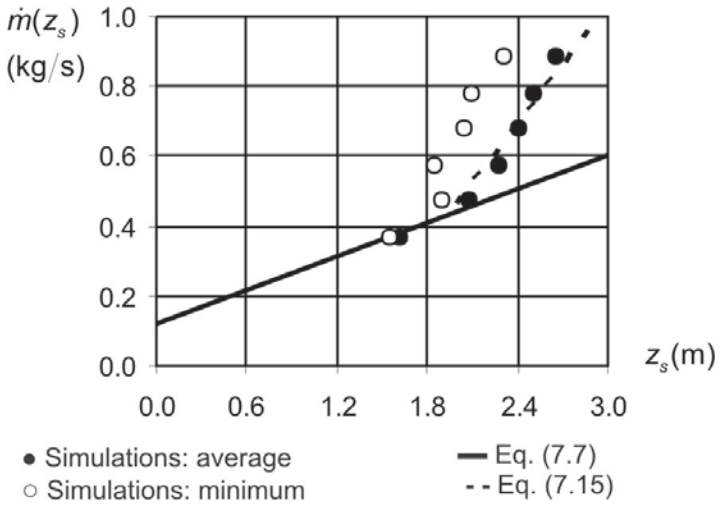

Figure 7.31 Simulation results for inlet opening height h_o = 1.5 m.

Also in the configuration with opening height h_o = 1.0 m, the same slope (Eq. (7.17)) is found in the results (Fig. 7.32).

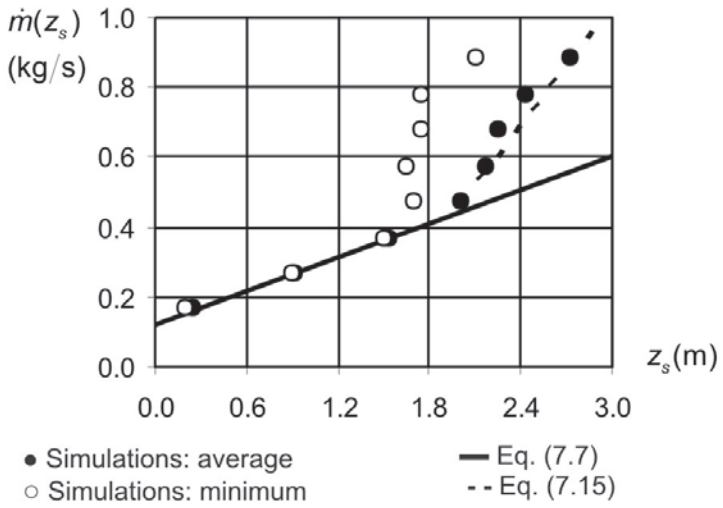

Figure 7.32 Simulation results for inlet opening height h_o = 1.0 m.

When the opening height is decreased to h_o = 0.6 m high, however, the suggested formula (Eq. (7.18)) agrees with the results only up to an extraction mass flow rate of about 0.4 kg/s (inlet velocity of 0.73 m/s) (Fig. 7.33). For higher mass flow rates, the smoke layer clearly becomes multi-dimensional, and a large difference is found between values for average and minimum smoke layer height. From an extraction rate of 0.8 kg/s onwards, however, the smoke layer height is again similar to the proposed Eq. (7.17).

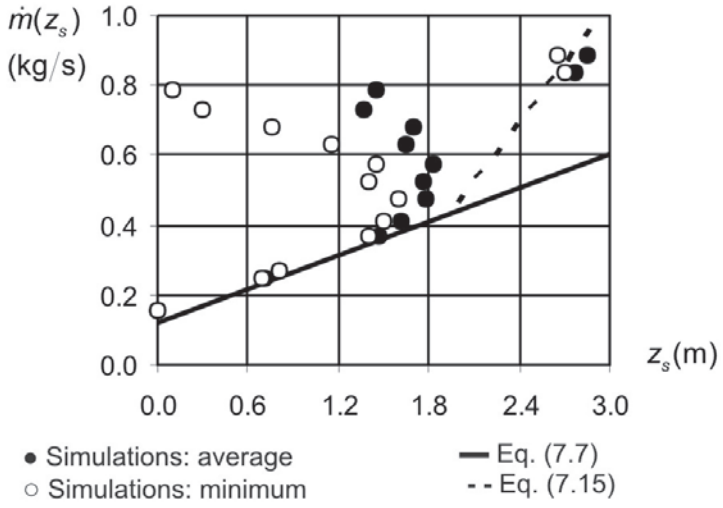

Figure 7.33 Simulation results for inlet opening height h_o = 0.6 m.

With an opening height of only h_o = 0.3 m, Fig. 7.34 shows that already for low extraction mass flow rates, the smoke layer height in the atrium deviates from the suggested formula (Eq. (7.17)). The smoke layer height in the atrium is even lower than the spill edge of the adjacent room. The atrium is almost completely filled with smoke, no matter how much is extracted. This is because the incoming makeup air through the opening is at quite high velocity, and causes significant disturbance in the formation of the smoke layer in the atrium (Fig. 7.35). The smoke layer becomes multi-dimensional from an inlet velocity of 0.84 m/s onward.

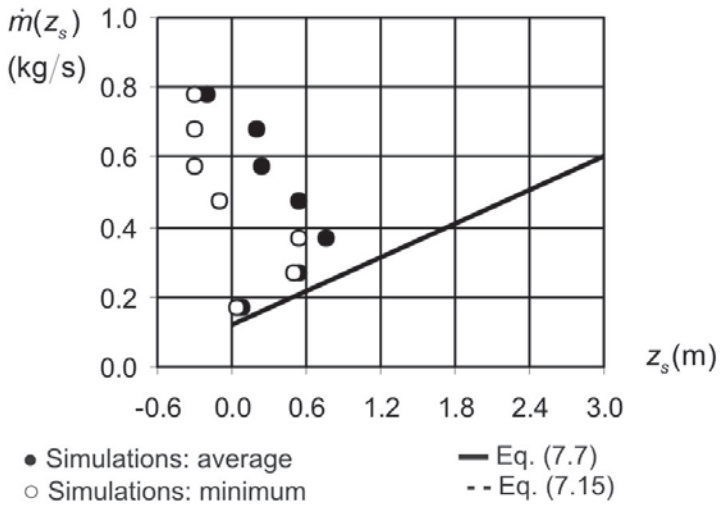

Figure 7.34 Simulation results for inlet opening height h_o = 0.3 m.

The previous results demonstrate that the size of the inlet opening does not have influence on the smoke layer pattern as long as the opening is large enough. When the opening is not large enough, though, a major effect on the smoke layer pattern in the atrium is seen. Fig. 7.35 shows the velocity profiles inside the atrium for opening heights 0.3 m, 1 m and 1.5 m.

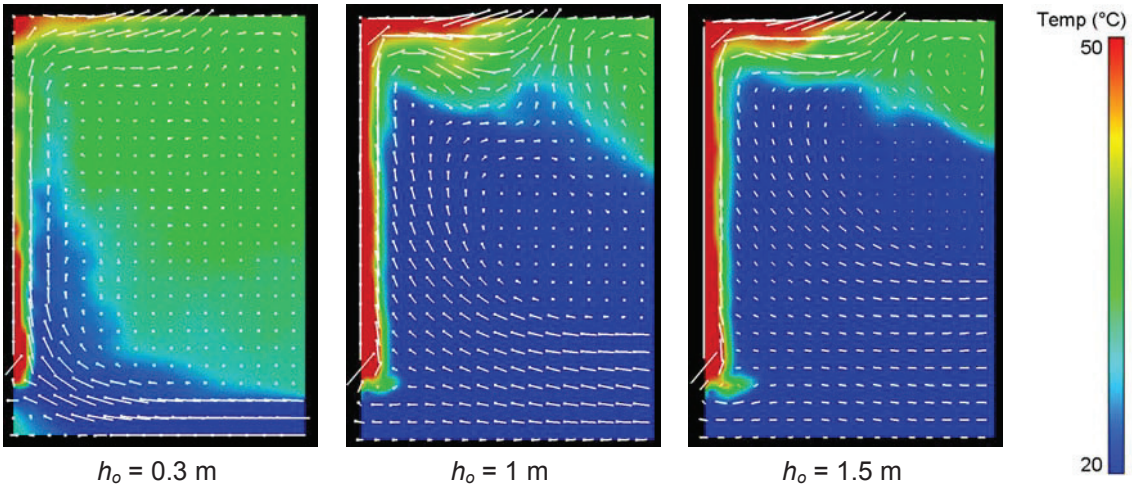

Figure 7.35 Temperature fields and flow patterns at y = 0.45 m in atrium. Time-averaged quasi steady-state data for 20 s.

Note that if the reduced-scale atrium were to represent a full-scale atrium at size 1/10, the opening of 1 m high corresponds to a full-scale opening of 10 m high, so about three floors. This is quite a substantial makeup air inlet opening. As there is a major effect on the smoke layer pattern in the atrium if the opening is not large enough, it is important to consider this influence in the design of an atrium building.

7.5 Conclusion

In this chapter, parameter variation by means of CFD calculations was presented for 2D adhered spill plumes in atria. It was shown that when the extraction mass flow rate is increased beyond the range that had been studied before in experimental research, the smoke layer in the atrium shows a multi-dimensional effect with a smoke recirculation zone. This multi-dimensional effect causes the mass flow extraction rate corresponding to a certain smoke free height above the spill edge to deviate from the experimentally suggested formulae for one-dimensional smoke layers.

By performing a variation of four parameters of the fire and atrium configuration (fire heat release rate, atrium width at the spill edge, atrium height above the spill edge and atrium length) an adjusted

formula was proposed to include the multi-dimensional smoke layer effect:

$$\begin{cases} \dot{m}(z_s) - \dot{m}_s = 0.08 W_s^{2/3} \dot{Q}_{conv}^{1/3} (z_s + d_s) \\ \qquad\qquad \text{for } z_s < \frac{2}{3} H_s \text{ or } \frac{H_s}{L_a} > 2.5 \\ \dot{m}(z_s) - \dot{m}_s = 0.08 W_s^{2/3} \dot{Q}_{conv}^{1/3} \left(2.5^{5/3} \left(\frac{L_a}{H_s} \right)^{5/3} \left(z_s - \frac{2}{3} H_s \right) + \frac{2}{3} H_s + d_s \right) \\ \qquad\qquad \text{for } z_s > \frac{2}{3} H_s \text{ and } \frac{H_s}{L_a} < 2.5 \end{cases} . \tag{7.18}$$

It was noted that the proposed exponent 5/3 for the variation of the slope with atrium length and width should be studied further in order to be able to confirm or adjust this value.

A variation of three ventilation parameters was also performed (position of smoke extraction, position and size of makeup air inlet). The smoke extraction was shown to perform best when placed above the rising plume. However, as in most cases it is impossible to predict the exact location of the fire, the option where the smoke extraction is positioned in the middle of the atrium ceiling is suggested. The position of the makeup air inlet was shown not to have large impact on the smoke flow behaviour in the atrium.

The size of the makeup air inlet opening, however, is of large importance. It was shown that for large openings, the exact size does not matter. In case of smaller openings, however, the high velocity of the incoming air will disturb the smoke flow field in the atrium, and the entire atrium can be filled up with smoke, no matter how large the extraction rate is. Further research will be needed to quantify the occurrence of this effect.

7.6 References

[1] Poreh M, Marshall NR, Regev A, Entrainment by adhered two-dimensional plumes, Fire Safety J. 43: 344-350 (2008)

[2] Harrison R, Spearpoint M, Physical scale modelling of adhered spill plume entrainment, Fire Safety J. 45: 149-158 (2010)

[3] McGrattan K, Hostikka S, Floyd J, Baum H, Rehm R, Mell W, McDermott R, Fire Dynamics Simulator (Version 5) Technical Reference Guide, NIST 1018-5, National Institute of Standards and Technology (2008)

[4] McGrattan K, Klein B, Hostikka S, Floyd J, Fire Dynamics Simulator (Version 5) User's Guide, NIST 1019-5, National Institute of Standards and Technology (2008)

8 Chapter 8 Conclusions

The present study had a focus on fire smoke extraction in large closed car parks and atria. In both configurations, so-called 'numerical experiments' were used to study the effect of several parameter variations.

As a first step, the validity of the simulations was confirmed by performing numerical simulations of experimentally studied configurations from literature. The small-scale experiments of fire in an atrium and a tunnel were repeated as numerical CFD configurations. Both cases concern smoke movement and the formation of a quasi steady-state smoke layer.
Several criteria to define the smoke layer interface were studied, of which the N-percent rule (with N = 30) prevails, as it provides results in good agreement with experiments and it is the most unambiguous method.

For the atrium configuration, very good agreement was found between the experimental and numerical results.

In the tunnel simulations, calculations without radiation modelling and using adiabatic walls proved to be a valid alternative for more time-consuming simulations with radiation modelling. Quite good agreement was found between experimental and numerical results, especially when considering the heat loss due to water cooling in the experiments.

An overall conclusion is that the prediction of the quasi steady-state smoke region by CFD is good, especially when the experiments are well documented. Therefore, it is argued that a parameter variation study with numerical simulations within similar configurations is very useful to obtain qualitative results, a good prediction of the trends and insight into the physics of the configurations at hand.

In large closed car parks, the ventilation system is designed to extract hot smoke from the fire, thus cooling the fire environment and allowing fire services to approach the fire up to a certain distance. In the present study, a large set of (more than 350) CFD simulations has been used as 'numerical experiments'. Four parameters have been varied (convective HRRPUA, fire source area, car park height and car park width). From the parameter variation, three formulae have been proposed:
- an analytical formula for the critical inlet velocity in the car park ($v_{cr,in}$):

$$v_{cr,in} = 0.26 \dot{q}''^{1/4}_{conv} A_F^{1/5}$$

- an expression to account for the difference between inlet (v_{in}) and outlet (v_{out}) velocity in the car park, derived from simple fire dynamics theory and confirmed by simulation results:

$$v_{out} - v_{in} = \frac{\dot{q}''_{conv} A_F}{w h \rho_{in} c_p T_{in}}$$

- and an analytical formula for the required ventilation velocity in the car park when a certain backlayering distance (d) is allowed, expressed as deviation from the critical velocity:

$$d = 40\left(v_{cr} - v\right)$$

These formulae are only valid for car parks with uni-directional air flow pattern, centrally placed fire source and with flat ceiling. Agreement with full-scale car park experiments has been discussed, confirming the derived equations for the configuration studied.

In the study concerning smoke extraction in atria, a small-scale setup is used for parameter variation in the simulations. Therefore, scaling of setups was first discussed, based on dimensionless numbers. In particular, CFD simulation results were discussed with LES to model turbulence. Scaling based on the Froude number only, is allowed as long as all configurations are sufficiently turbulent. When using a Smagorinsky turbulence model, the turbulent Reynolds number is indeed automatically preserved in scaling configurations by preserving the Froude number, if the mesh cell dimensions are scaled proportionally to the geometry dimensions. Thus, as long as the flow is sufficiently turbulent, Froude scaling is allowed. However, if the flow is not sufficiently turbulent, Froude scaling can be questioned. A number of CFD simulation results on an atrium configuration have confirmed this theoretical result and illustrated that these features are automatically captured in the CFD simulations.

After this study on scaling, parameter variation for smoke extraction of 2D adhered spill plumes in atria by using numerical simulations was studied. It was shown that when the extraction mass flow rate is increased beyond the range that had been studied before in experimental research, the smoke layer in the atrium shows a multi-dimensional effect with a smoke recirculation zone. This multi-dimensional effect causes the mass flow extraction rate corresponding to a certain smoke free height above the spill edge to deviate from the experimentally suggested formulae for one-dimensional smoke layers.
By performing a variation of four parameters of the fire and atrium configuration (fire heat release rate, atrium width at the spill edge, atrium height above the spill edge and atrium length) an adjusted formula was proposed to include the multi-dimensional smoke layer effect:

$$\begin{cases} \dot{m}(z_s) - \dot{m}_s = 0.08 W_s^{2/3} \dot{Q}_{conv}^{1/3} (z_s + d_s) \\ \qquad\qquad \text{for } z_s < \frac{2}{3} H_s \text{ or } \frac{H_s}{L_a} > 2.5 \\ \dot{m}(z_s) - \dot{m}_s = 0.08 W_s^{2/3} \dot{Q}_{conv}^{1/3} \left(2.5^{5/3} \left(\frac{L_a}{H_s} \right)^{5/3} \left(z_s - \frac{2}{3} H_s \right) + \frac{2}{3} H_s + d_s \right) \\ \qquad\qquad \text{for } z_s > \frac{2}{3} H_s \text{ and } \frac{H_s}{L_a} < 2.5 \end{cases}$$

It was noted that the proposed exponent 5/3 for the variation of the slope with atrium length and width should be studied further in order to be able to confirm or adjust this value.

A variation of three ventilation parameters was also performed (position of smoke extraction, position and size of makeup air inlet). The smoke extraction was shown to perform best when placed above the rising plume. However, as in most cases it is impossible to predict the exact location of the fire, the option where the smoke extraction is positioned in the middle of the atrium ceiling is suggested. The position of the makeup air inlet was shown not to have large impact on the smoke flow behaviour in the atrium.

The size of the makeup air inlet opening, however, is of large importance. It was shown that for large openings, the exact size does not matter. In case of smaller openings, however, the high velocity of the incoming air will disturb the smoke flow field in the atrium, and the entire atrium can be filled with smoke, no matter how large the extraction rate is.

9 Chapter 9 Recommendations for future work

The work presented in the present study concerns the smoke extraction in car parks and atria. Although new formulae have been developed here to calculate the necessary extraction rate in both configurations, issues remain to be addressed in the future.

For the car park configuration, the suggested formulae of Chapter 5 are confirmed only for uni-directional flow patterns. Complex flow patterns including recirculation or stagnation region flows remain to be studied. Furthermore, the configurations studied in the present work concern car parks with flat ceiling and the fire placed in the middle. Other ceiling configurations or fire positions can also be studied. Recent work including these two effects is reported in [1]. The trends from the present study are confirmed there for another fire position. The effect of beams on the ceiling, however, can show a substantial difference. More research to quantify these influences would be interesting.

In the atrium configuration study, only the 2D adhered spill plume has been studied in the present research. A similar approach with using CFD simulations as numerical experiments could be followed for research on the 3D adhered spill plume, or the 2D or 3D free spill plume in atria.
Within the 2D adhered spill plume configuration as studied in Chapter 7, the parameter variation can still be extended. The proposed trends can be further confirmed for broader ranges of values and new parameters can be studied. For example, the configuration of the fire origin room

(position of the fire, presence of openings in the room) and the effect of the presence of a downstand and/or balconies on the mass flow rate of the spill plume can be studied.

As the present work is a numerical study, recommendations for future work also include experimental study of the car park and atrium configurations. As shown in Chapter 5, a full-scale experimental car park setup has already confirmed the proposed relation for the smoke extraction velocity. Also for the atrium configuration, experimental study of the proposed trends and formula would be of great value for the confirmation of the presented results.

References

[1] Baert L, Evaluatie en ontwikkeling van methoden voor een brandveilig ontwerp van RWA installaties in ondergrondse parkeergarages, Master's thesis, Ghent University (2011)

References

Baert L, Evaluatie en ontwikkeling van methoden voor een brandveilig ontwerp van RWA installaties in ondergrondse parkeergarages, Master's thesis, Ghent University (2011)

Beard A, Carvel R, The handbook of tunnel fire safety, Thomas Telford Services Ltd, London (2005)

BS 7346-7, Code of practice on functional recommendations and calculation methods for smoke and heat control systems for covered car parks (2006)

Chow WK, Use of a time constant for designing a smoke control system in car parks, J. of Fire Sciences 13: 357-377 (1995)

Chow WK, Cui E, CFD simulations on Balcony Spill Plume, J. of Fire Sciences 16: 468-485 (1998)

Chow WK, Li J, Simulation on Natural Smoke Filling in Atrium with a Balcony Spill Plume, J. of Fire Sciences 19: 258-283 (2001)

Chow W, Determination of the Smoke Layer Interface Height for Hot Smoke Tests in Big Halls, J. of Fire Science 27: 125-142 (2009)

Chung TJ, Computational Fluid Dynamics, Cambridge University Press, Cambridge (2002)

Cooper LY, Harkleroad M, Quintiere J, Reinkinen W, An Experimental Study of Upper Hot Layer Stratification in Full-Scale Multiroom Fire Scenarios, J. of Heat Transfer 104: 741-749 (1982)

Danziger NH, Kennedy WD, Longitudinal ventilation analysis for the Glenwood Canyon tunnels, 4th International Symposium on Aerodynamics and Ventilation of Vehicle Tunnels, BHr Group, 169-186 (1982)

Deckers X, Haga S, Tilley N, Merci B, Smoke control in case of fire in a large car park: CFD Simulations of Full-Scale Experiments, Fire Safety J. (Special Issue) (2012) in preparation

Deckers X, Haga S, Tilley N, Sette B, Merci B, Smoke control in case of fire in a large car park: Full-Scale Experiments, Fire Safety J. (Special Issue) (2012) in preparation

Drysdale D, An Introduction to Fire Dynamics, John Wiley and Sons, Chichester (1998)

EN 12101-11, Smoke and heat control system - Part 11: Design, installation & commissioning requirements for enclosed car parks, Draft Version (2011)

Erlebacher G, Hussaini MY, Speziale CG, Zang TA, Toward the Large-Eddy Simulation of Compressible Turbulent Flows, J. of Fluid Mechanics 238: 155-185 (1992)

Hansell GO, Morgan HP, Marshall NR, Smoke flow experiments in a model atrium, Building Research Establishment Occasional Paper, OP 55 (1993)

Harrison R, Spearpoint M, Entrainment of air into a balcony spill plume, J. of Fire Protection Engineering 16: 211-245 (2006)

Harrison R, Spearpoint M, The Balcony Spill Plume: Entrainment of Air into a Flow from a Compartment Opening to a Higher Projecting Balcony, Fire Technology 43: 301-317 (2007)

Harrison R, Entrainment of Air into Thermal Spill Plumes, Fire Engineering Research Thesis, Christchurch, New Zealand (2009)

Harrison R, Spearpoint M, Physical scale modelling of adhered spill plume entrainment, Fire Safety J. 45: 149-158 (2010)

He Y, Fernando A, Luo M, Determination of interface height from measured parameter profile in enclosure fire experiment, Fire Safety J. 31: 19-39 (1998)

Huggett C, Estimation of Rate of Heat Release by Means of Oxygen Consumption Measurements, Fire and Materials 4: 61-65 (1980)

Hwang CC, Edwards JC, The critical ventilation velocity in tunnel fires – a computer simulation, Fire Safety J. 40: 213-244 (2005)

Karlsson B, Quintiere JG, Enclosure Fire Dynamics, CRC Press, Boca Raton, FL (2000)

Kumar S, Cox G, Thomas PH, Air entrainment into balcony spill plumes, Fire Safety J. 45: 159-167 (2010)

Kunsch JP, Simple model for control of fire gases in a ventilated tunnel, Fire Safety J. 37: 67-81 (2002)

Law M, A Note on Smoke Plumes from Fires in Multi-level Shopping Malls, Fire Safety J. 10: 197-202 (1986)

Law M, Measurements of Balcony Smoke Flow, Fire Safety J. 24: 189-195 (1995)

Lee CK, Chaiken RF, Singer JM, Interaction between duct fires and ventilation flow: An experimental study, Combustion Science and Technology 20: 59-72 (1979)

Lee L, Emmons HW, A study of natural convection above line fires, J. Fluid Mechanics 11: 353-368 (1961)

Li YZ, Lei B, Ingason H, Study of critical velocity and backlayering length in longitudinally ventilated tunnel fires, Fire Safety J. 45: 361-370 (2010)

Lougheed GD, McCartney CJ, Gibbs E, Balcony spill plumes, Final Research Project Report 1247. National Research Council, Canada (2006)

Marshall NR, Harrison R, Experimental Studies of thermal spill plumes. Building Research Establishment Occasional Paper OP1 (1996)

McCaffrey BJ, Purely Buoyant Diffusion Flames: Some Experimental Results, NBSIR 79-1910, National Bureau of Standards (1979)

McGrattan KB, Baum HR, Rehm RG, Large Eddy Simulations of Smoke Movement, Fire Safety J. 30: 161-178 (1998)

McGrattan K, Hostikka S, Floyd J, Baum H, Rehm R, Mell W, McDermott R, Fire Dynamics Simulator (Version 5) Technical Reference Guide, NIST 1018-5, National Institute of Standards and Technology (2008)

McGrattan K, Klein B, Hostikka S, Floyd J, Fire Dynamics Simulator (Version 5) User's Guide, NIST 1019-5, National Institute of Standards and Technology (2008)

Miles S, Kumar S, Cox G, The balcony spill plume – some CFD simulations, Proceedings of the Fifth International Symposium on Fire Safety Science: 237-247 (1997)

Morgan HP, Marshall NR, Smoke Hazards in Covered, Multi-level Shopping Malls: and Experimentally Based Theory for Smoke Production, BRE CP48/75, Borehamwood (1975)

Morgan HP, Marshall NR, Goldstone BM, Smoke Hazards in Covered, Multi-level shopping Malls: some Studies using a Model 2-storey Mall, BRE CP45/76, Borehamwood (1976)

Morgan HP, Marshall NR, Smoke Control Measures in a Covered Two-storey Shopping Mall having Balconies as Padestrian Walkways, BRE CP11/79, Borehamwood (1979)

Morgan HP, Gosh BK, Garrad G, Pamlitschka R, De Smedt J-C, Schoonbaert LR, Design Methodologies for Smoke and Heat Exhaust Ventilation, BRE Report 368, Building Research Establischment, Watford UK (1999)

NBN S21-208-2, Fire protection inside buildings – Design of smoke and heat exhaust ventilation systems (SHEVS) for indoor car parks (2007)

NFPA 92B, Smoke Management Systems in Malls, Atria and Large Areas, National Fire Protection Association (2005).

Oka Y, Atkinson GT, Control of smoke flow in tunnel fires, Fire Safety J. 25: 305-322 (1995)

Peters N, Turbulent Combustion, Cambridge University Press, Cambridge (2000)

Pope SB, Turbulent flows, Cambridge University Press, Cambridge (2000)

Pope SB, Ten questions concerning the large-eddy simulation of turbulent flows. New J. of Physics 6: 1–24 (2004)

Poreh M, Morgan HP, Marshall NR, Harrison R, Entrainment by Two-Dimensional Spill Plumes, Fire Safety J. 30: 1-19 (1998)

Poreh M, Marshall NR, Regev A, Entrainment by adhered two-dimensional plumes, Fire Safety J. 43: 344-350 (2008)

Quintiere JG, Fundamentals of Fire Phenomena, John Wiley and Sons, Chichester (2006)

Shi CL, Lu WZ, Chow WK, Huo R, An investigation on spill plume development and natural filling in large full-scale atrium under retail shop fire, Int. J. of Heat and Mass Transfer 50: 513-529 (2007)

Smagorinsky J, General Circulation Experiments with the Primitive Equations. I. The Basic Experiment, Monthly Weather Review 91: 99-164 (1963)

Thomas PH, Hinkley PL, Theobald CR, Simms DL, Investigations into the flow of hot gases in roof venting. Fire research technical paper no.7, London: The Stationary Office (1963)

Thomas PH, The movement of smoke in horizontal passages against an air flow, Fire Research Station Note no. 723, Fire Research Station (1968)

Thomas PH, On the Upward Movement of Smoke and Related Shopping Mall Problems, Fire Safety J. 12: 191-203 (1987)

Thomas PH, Morgan HP, Marshall N, The Spill Plume in Smoke Control Design, Fire Safety J. 30: 21-46 (1998)

Tilley N, Merci B, Relation between horizontal ventilation velocity and backlayering distance in large closed car parks, Proceedings of the Ninth International Symposium on Fire Safety Science 777-787 (2008)

Tilley N, Rauwoens P, Merci B, Verification of the accuracy of CFD simulations in small-scale tunnel and atrium fire configurations, Fire Safety J. 46: 186-193 (2011)

Tilley N, Deckers X, Merci B, CFD study of relation between ventilation velocity and smoke backlayering distance in large closed car parks, Fire Safety J, submitted

Van Maele K, Merci B, Application of RANS and LES field simulations to predict the critical ventilation velocity in longitudinally ventilated horizontal tunnels, Fire Safety J. 43: 598-609 (2008)

Vauquelin O, Caractérisation expérimentale de l'apparition d'une nappe de retour, Compte Rendus de l'Académie des Sciences, Série II b 321: 15-18 (1995)

Vauquelin O, Parametrical study of the back flow occurrence in case of a buoyant release into a rectangular channel, Experimental Thermal and Fluid Science 29: 725-731 (2005)

Viegas JC, The use of impulse ventilation for smoke control in underground car parks, Tunnelling and Underground Space Technology 25: 42-53 (2010)

Welty JR, Wicks CE, Wilson RE, Rorrer G, Fundamentals of Momentum, Heat, and Mass Transfer, John Wiley and Sons, New York NY (2001)

Wu Y, Bakar MZA, Control of smoke flow in tunnel fires using longitudinal ventilation systems – a study of the critical velocity, Fire Safety J. 35: 363-390 (2000)

Yokoi S, Study on the Prevention of Fire Spread by Hot Upward Current, Report No. 34, Building Research Institute, Japan (1960)